NASA-CR-166060
19830010565

NASA Contractor Report 166060

INITIAL '80s DEVELOPMENT OF INFLATED ANTENNAS

G. J. Friese, G. D. Bilyeu, and M. Thomas

L'GARDE, INC.
Newport Beach, California 92663

Contract NAS1-16663
January 1983

National Aeronautics and
Space Administration

Langley Research Center
Hampton, Virginia 23665

FOREWORD

This program was sponsored by the National Aeronautics and Space Administration, Langley Research Center under Contract Number NAS1-16663 for Definition and Application of Membrane Surface for Use With Inflatable Space Antenna. William F. Hinson, the NASA Technical Program Manager, monitored the program and aided in many areas including the measurement of stress, strain, and optical properties of thin films and suggestions for data reduction procedures.

At L'Garde, Gilbert J. Friese was the principal investigator. He was assisted by Gayle D. Bilyeu who was responsible for the self-rigidizing structural element development (Section 4.0) and Dr. Mitchell Thomas who calculated the paraboloid flat patterns and determined the sensitivity of the inflated antenna to off-nominal conditions (Section 8.0).

The program period of performance was from 10 June 1981 to 30 October 1982.

This Page Intentionally Left Blank

CONTENTS

This Page Intentionally Left Blank

FIGURES

FIGURES (Concluded)

1.0 INTRODUCTION

The low weight and package volume of inflatables relative to mechanical systems has long been known. While some work had been done on inflated space antennas, the concept was largely dismissed a) because meteoroids would puncture the thin film allowing the gas to escape, and b) because of an apparent lack of thermal control (Reference 1).

L'Garde showed (Reference 2) that the weight of gas needed to replace that lost through meteoroid holes was modest -- as long as the operating pressure was low. Operating for ten years in space, only about 10% of an antenna's initial weight would be replacement gas to maintain an operating pressure of 0.001 Pa.

Concerning thermal control, the radiative exchange between the sides of the inflatable can sharply reduce temperature non-uniformities. The ability of these continuous area elements making up a balloon to control temperature caused NASA to seriously consider encapsulation of satellites in balloons as a method of thermal control (Reference 3). Hughes covered an antenna with a Kapton film solely to protect the antenna dish from temperature changes (Reference 4).

With these feasibility questions answered, NASA Langley funded this initial development effort. Its objectives were (1) the definition and documentation of a membrane surface suitable for use in a space reflector system for long durations in orbit; (2) determination of requirements for a metal foil-plastic laminate structural element; (3) construction of a laboratory model of a rigidized element to test for strength characteristics; and, (4) determination of characteristics of antennas ranging from 10 to 1000 meters. The effort was limited to state-of-the-art technology.

This Page Intentionally Left Blank

2.0 SUMMARY

The basic configuration that L'Garde studied is shown in Figure 1. It consists of a) a thin film reflector, b) a thin film cone, c) a self-rigidizing structural torus at the interface of the cone and reflector, and d) an inflation system. The reflector is metallized and, when inflated, has a parabolic shape. The cone not only completes enclosure of the inflatant but also holds the antenna feed at its apex.

The torus is a structural element that keeps the inflated cone-reflector from collapsing inward; it uses technology developed for the ECHO II Program in which an aluminum-polyester-aluminum composite film becomes a rigid, smooth shell after the aluminum is yielded by gas pressure.

The lowest weight passive inflatant for the antenna body is water. The torus requires higher pressures and therefore carbon dioxide is used.

Section 4.0 describes the construction, packaging and sequence of events for the inflated antenna. The characteristics of thin films were examined and compared to existing requirements (Section 4.2). It was determined that polyester and a polyamide have the best characteristics for the inflated antenna.

A major effort was to build inflated paraboloids and to measure their accuracies (Section 5.0). A 3-meter diameter parabola was constructed from polyester thin film. It had a 3-meter design focal length, and was constructed of gores held together with 0.013 mm by 19 mm polyester tape and heat-sensitive adhesive. The paraboloid is shown in Figure 2 prior to inflation and in Figure 3 inflated to 2-3 mm H_2O differential pressure. It is constructed of 32 gores of 0.006 mm polyester film coated with about $2(10)^{-5}$ mm of vapor-deposited aluminum (VDA).

Accuracy was determined with laser test equipment. The local angles of a set of horizontal points about 680 mm below the paraboloid center were measured. The shape of this line was then determined by numerical integration. It was determined that the accuracy of these data points with respect to a best-fit parabolic shape was 0.76 mm RMS. This indicates that the inflated antenna can be possible with greater development; that is, 0.76 mm RMS was achieved with the first paraboloid. The focus according to the curve fit was 2.96 meters (instead of the 3-meter design value).

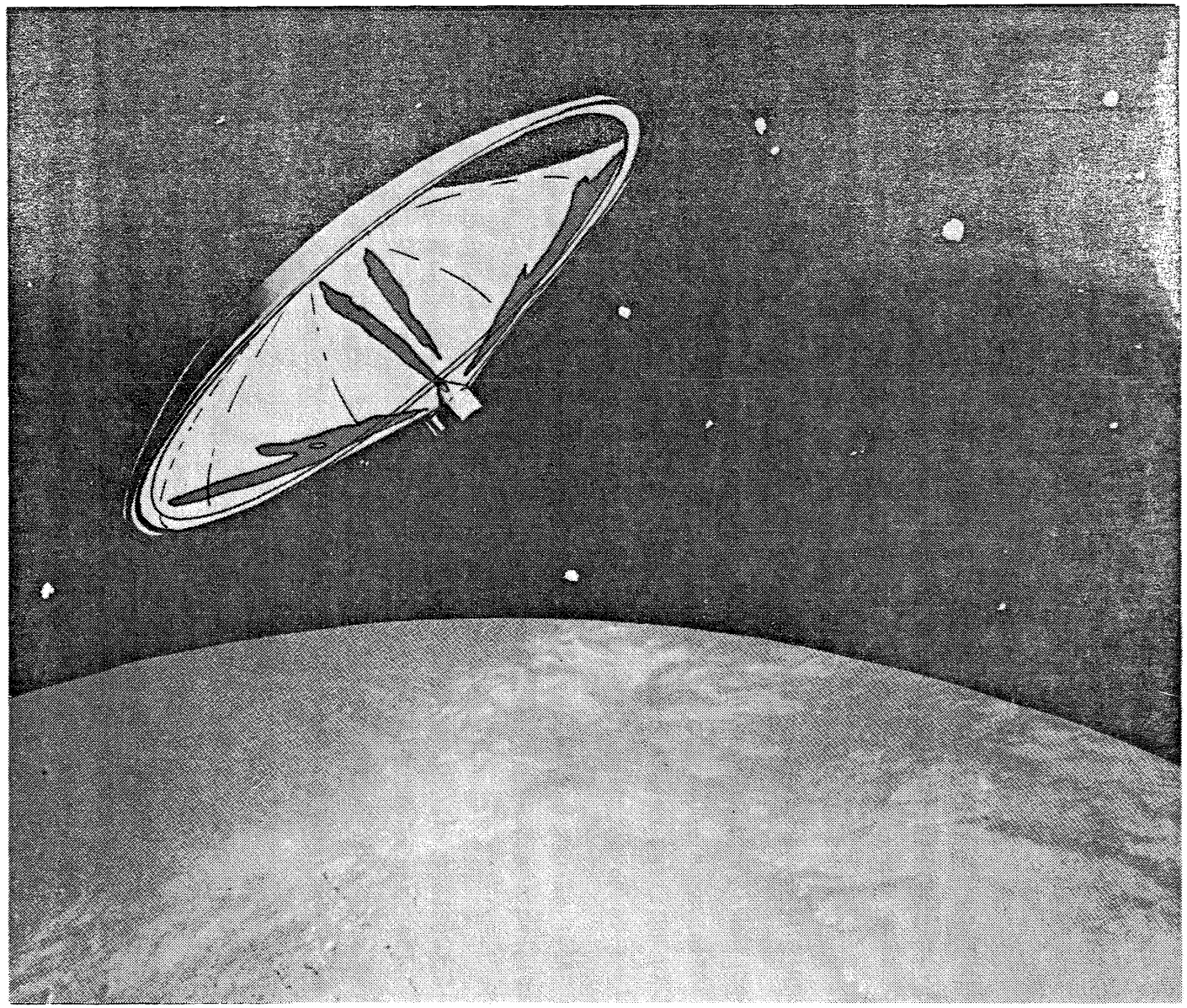

Figure 1. - Inflated antenna concept.

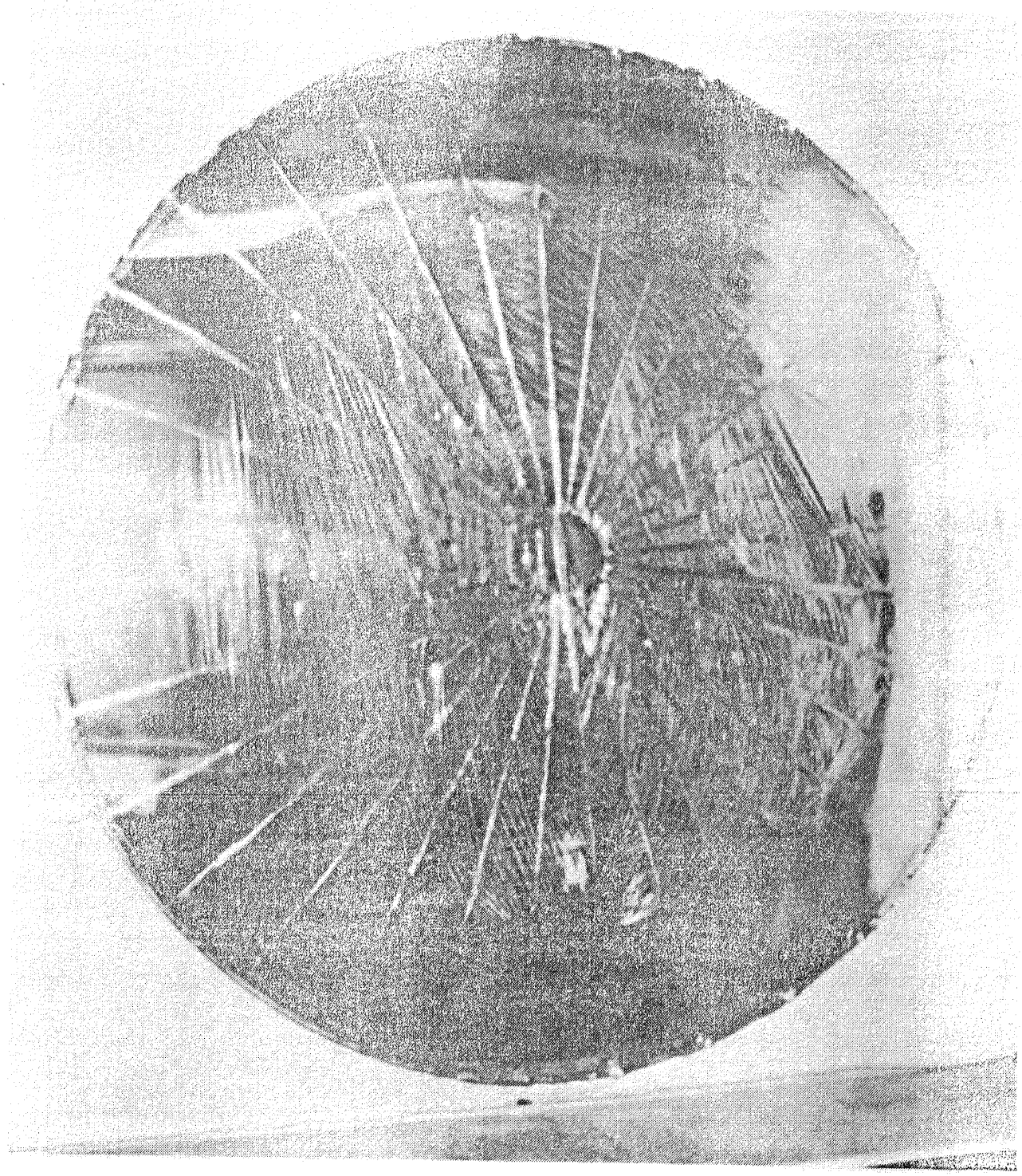

Figure 2. - Three meter diameter polyester paraboloid -- uninflated.

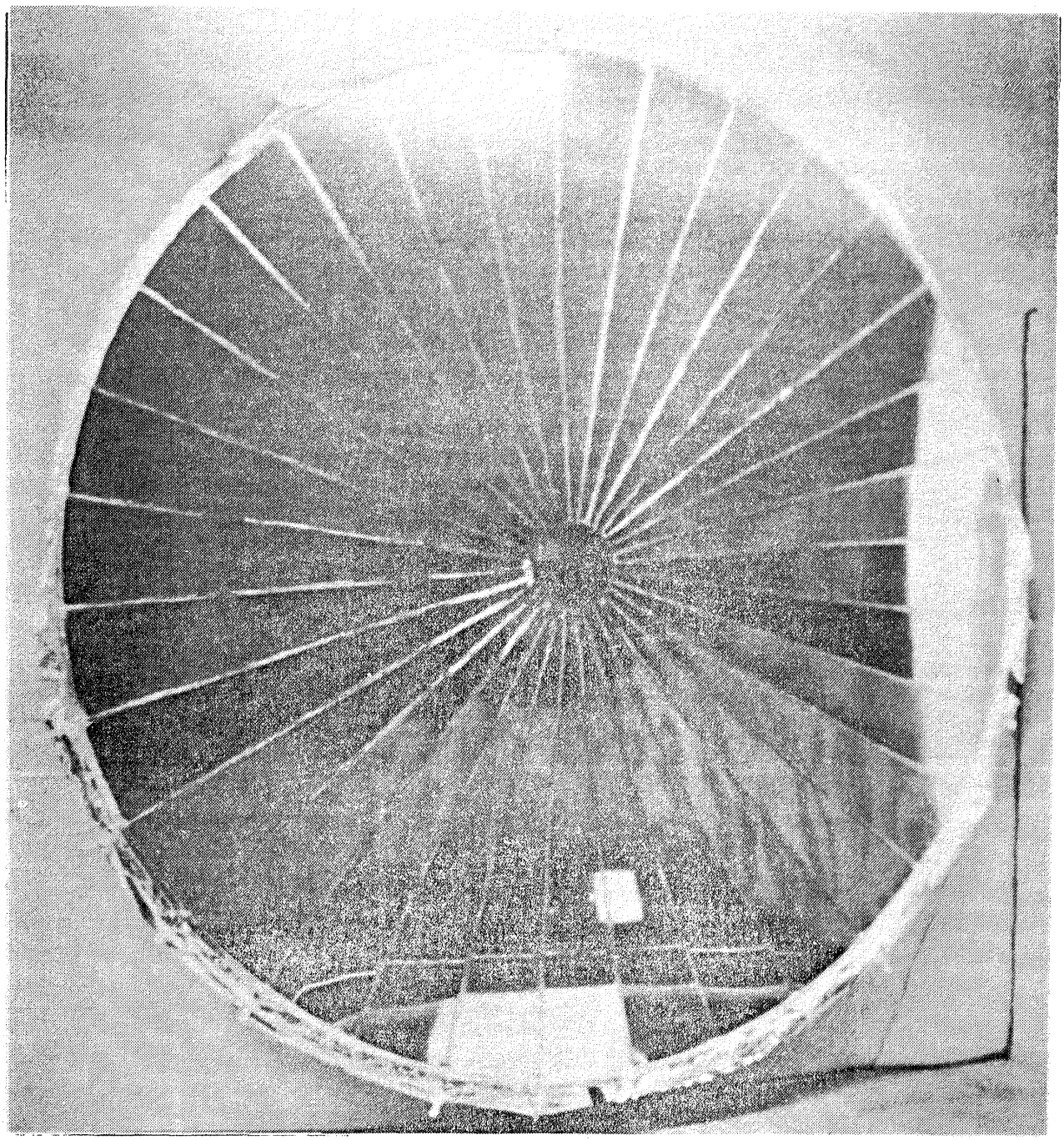

Figure 3. - Three meter diameter polyester paraboloid -- inflated to 2-3 mm H_2O pressure.

The test was repeated at about 5 mm H_2O pressure. The accuracy degraded to 0.94 mm and the focal length decreased to 2.82 meters. The changes are due to the overpressure.

Another paraboloid was made from 40 gores of 0.008 mm VDA kapton. Relative to the polyester unit, it turned out poorly. It deviated from a parabolic shape near the center. A set of horizontal measurements taken about 635 mm below the paraboloid axis resulted in a 1.64 mm RMS inaccuracy and a 3.07 meter focal length.

Another significant program effort was the initial development of the self-rigidizing structural element (Section 6.0) which would be used in a torus configuration on the antenna. The structure is made of a foil-plastic-foil composite. It is erected to a rigidized state by gas pressure; thereafter, it performs similar to an aluminum shell without internal pressure.

An analysis for this approach based upon classical buckling theory was generated. Composite material and then cylinders were made. The cylinders were inflated to stress the aluminum to just beyond the elastic limit and then depressurized. They were then loaded in compression to failure.

Figure 4 shows one such cylinder before and after pressurization, and after compressive buckling (using steel weights). This particular cylinder had two layers of 0.038 mm thick 1100-0 aluminum foil and an inner layer of 0.013 mm thick polyester. The average buckling force for the cylinders of this configuration was 136 Newtons (>30 pounds).

The tests showed that the buckling force was a function of thickness squared as expected. They were stronger than what the analysis predicted using elastic modulus data from the materials used. The effort showed that this approach would be practical to use as the structure at the collector rim.

A parametric study was performed (Section 7.0) to determine the weight and packaging volume of inflated antennas that range in diameter from 10 to 1000 meters and in focal lengths from 3.75 to 2000 meters ($3/8 < f/d < 2$). Not included were the antenna feed, telemetry, attitude control, propulsion and power supply which are mission dependent.

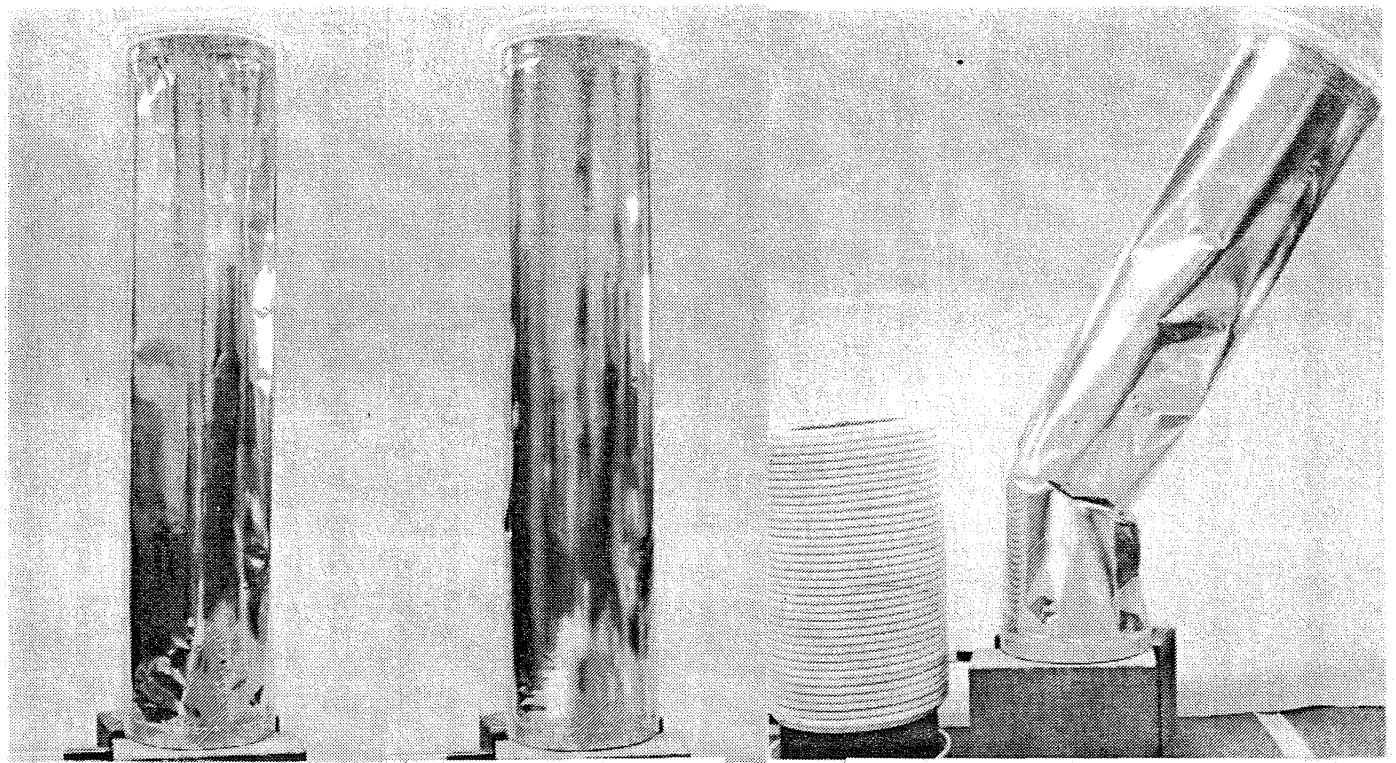

Figure 4. - Testing of a 0.076 mm aluminum cylinder.

The weight of the antenna structure and inflation system is shown in Figure 5 compared to the weights of mechanical systems according to Reference 5. The weights are for a 10-year life and a 0.001 Pa operating pressure. The space shuttle can carry a payload weighing no more than 30,000 kg. Figure 5 indicates that an antenna as large as 1000 meters in diameter could be launched. (however, some weight must be allocated for the items mentioned above that are not considered in Figure 5 and for propulsion system(s) to transfer the antenna to geosynchronous orbit.)

Figure 6 shows the package volume. The space shuttle's payload bay has a 300 cubic meter volume. A 1000-meter diameter (post-inflation) antenna will need only 10 to 27 percent of this space. The inflatable antenna will be limited by the launch vehicle's allowable payload weight rather than payload volume.

A sensitivity study was conducted (Section 8.0) which showed that internal pressure, film thickness or film elastic modulus could change by ±20% and still handle 1 cm wavelengths. Such parameters could change by ±50% and still accurately receive/transmit 3 cm wavelengths without any need to adjust the feed location.

Based on this work, it is concluded that

1. The inflated antenna is feasible.
2. Paraboloid inaccuracies will be less than 1 mm RMS.
3. Antenna accuracy is not very sensitive to internal pressure, or thin film modulus or thickness.
4. The self-rigidizing inflatable structure made from a metal-plastic laminate is practical and will be suitable for use with the antenna.
5. Weight and package volume are low relative to mechanical systems.

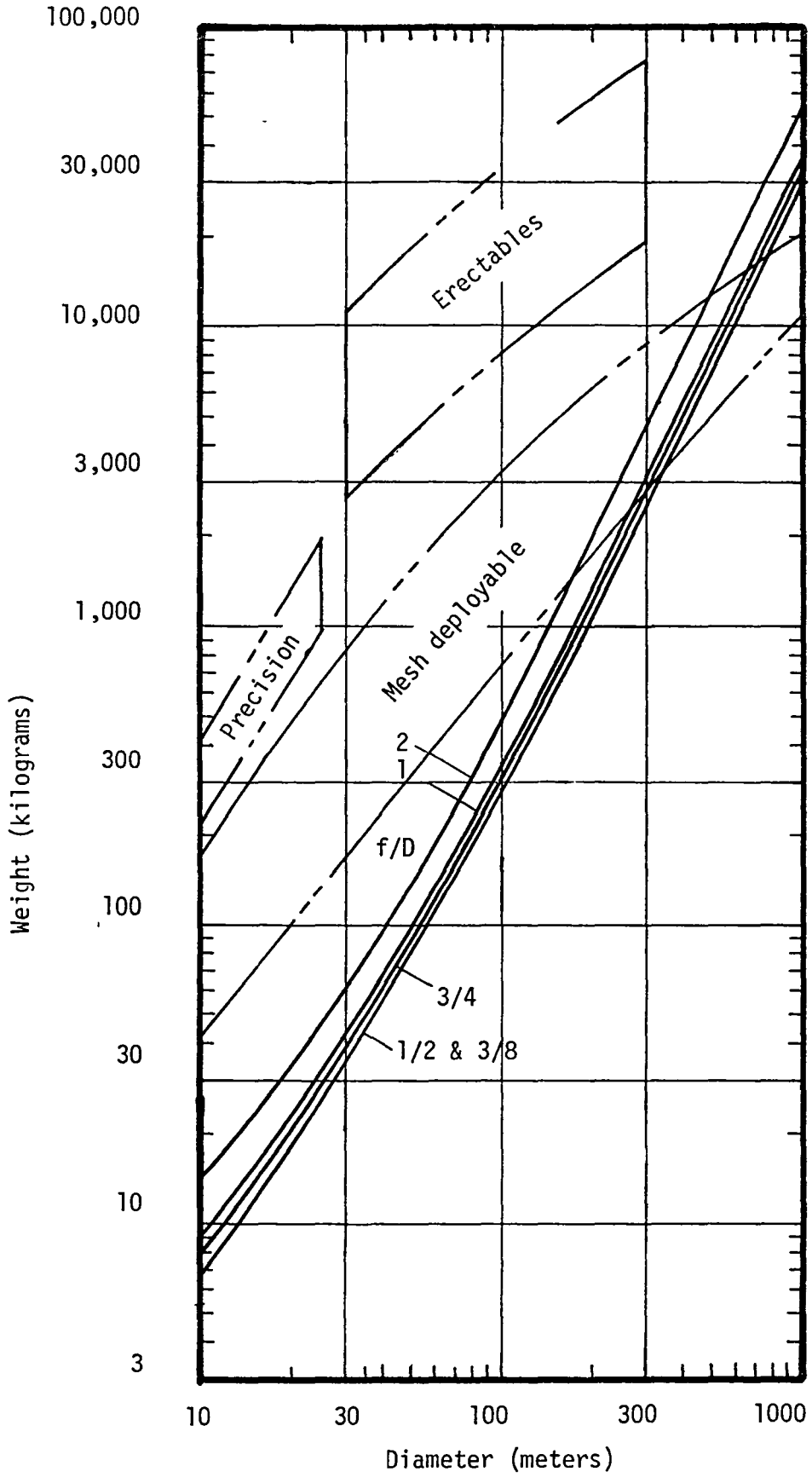

Figure 5. - Antenna weight (0.006 mm film).

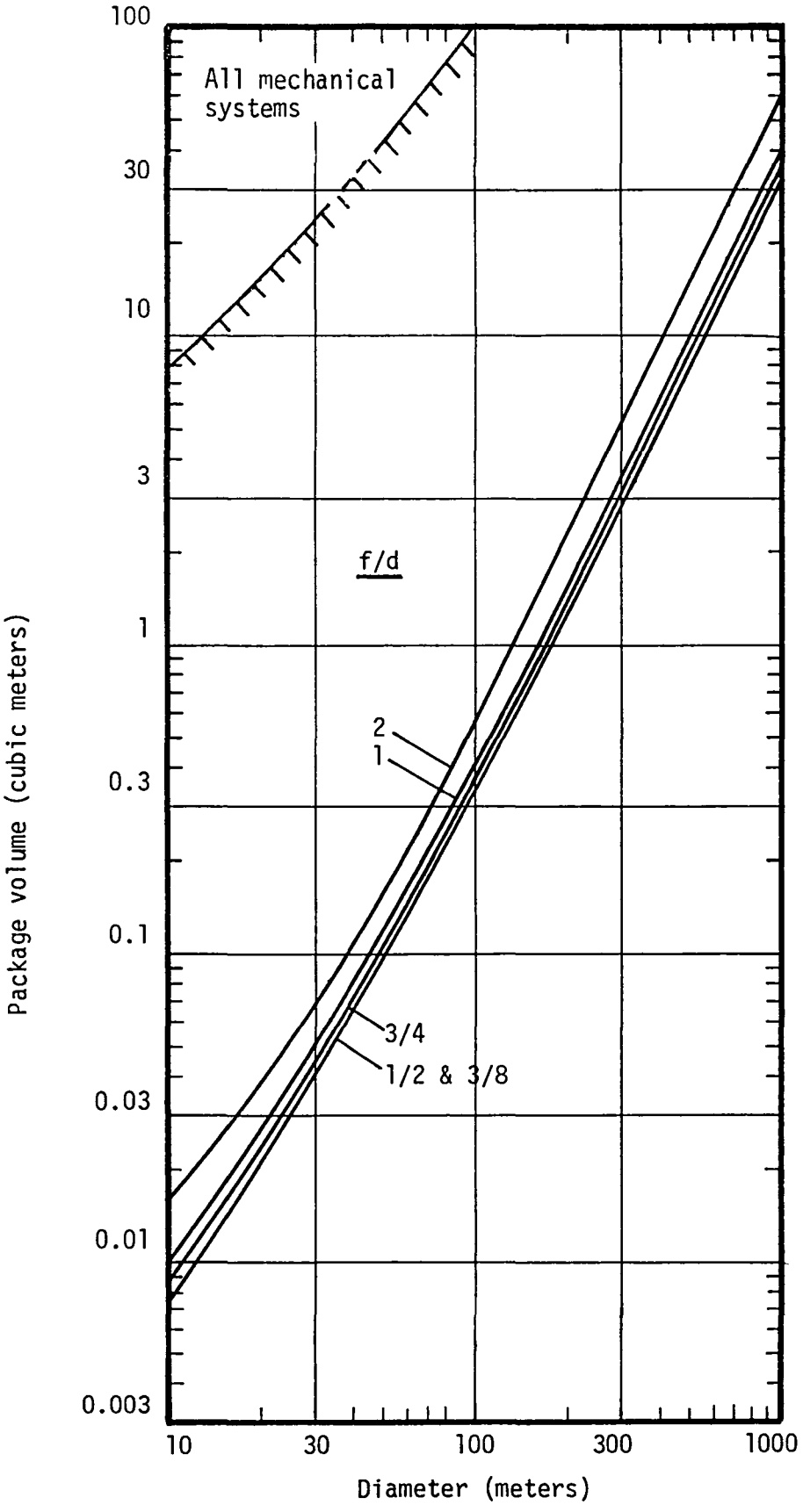

Figure 6. - Antenna package volume (0.006 mm film).

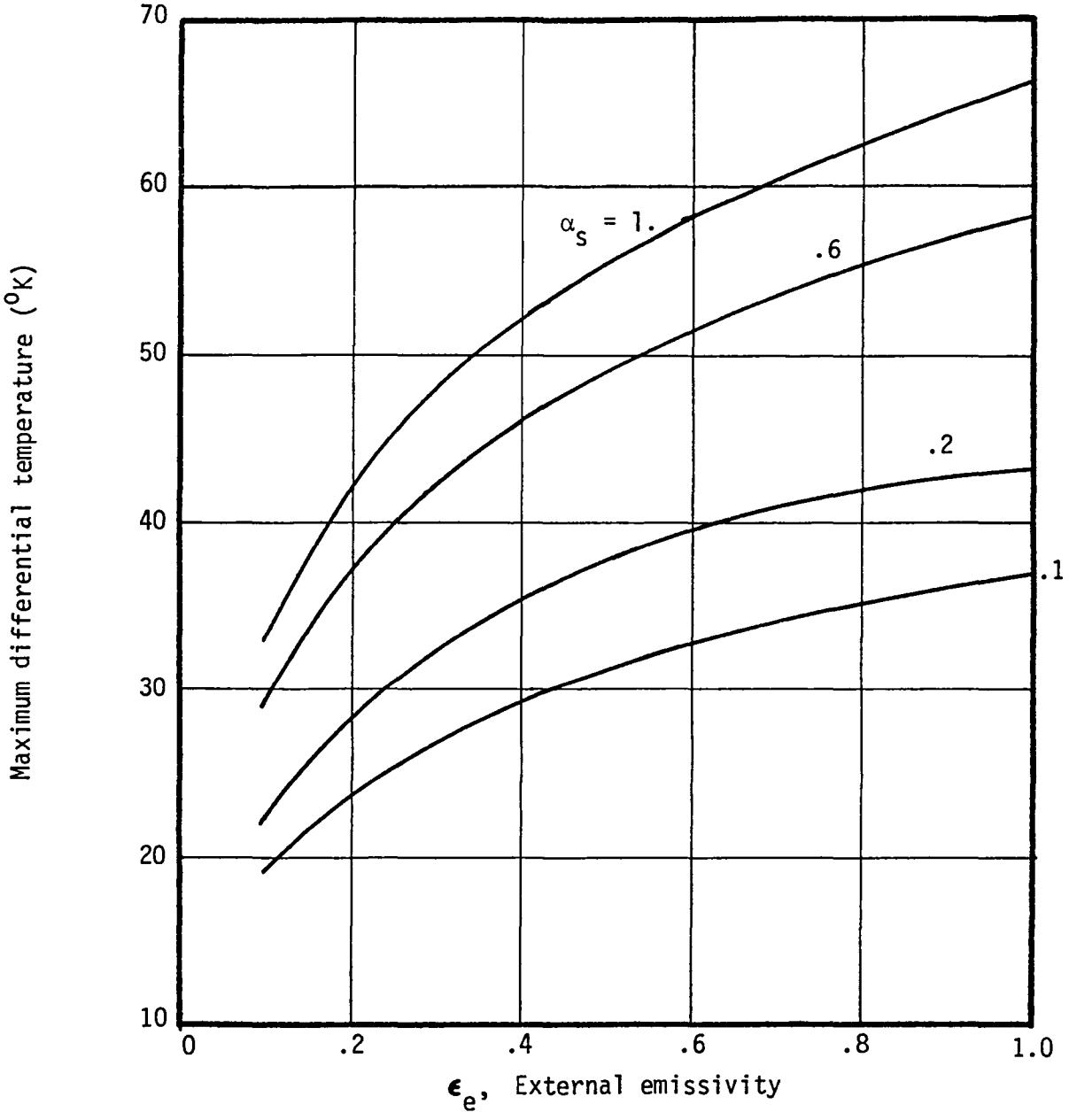

Figure 7. - Maximum temperature difference for cone-sunlit antenna, black interior (ϵ_i = 1).

3.0 SYMBOLS

A	Projected area
B	Coefficient
C	Empirical buckling coefficient
d	Torus small diameter
D	Diameter
D_t	Diameter of cone tip
E	Modulus of elasticity
E_G	Elastic modulus of gore
E_S	Secant modulus or elastic modulus of seam.
F	Force
f	Focal length
f_y	Yield stress
FS	Factor of safety
H	Height
I	Area moment of inertia
K	Fraction of load carried by aluminum or 4f/D
k_t	Thermal expansion coefficient
L	Length
M	Multiplication factor for presence of second layer
MW	Molecular weight
N	Number of gores
P	Pressure
p'	Torus running load
Q	Distributed in-plane load
R	Radius
R*	Univeral gas constant = 8314.34 J/kmol K
r	Cylinder radius
S	Yield stress
T	Temperature
t	Thickness
V	Volume
W	Maximum width of gore

w	Width of seam or weight
X	Horizontal distance from the paraboloid centerline (or focus) to the laser axis
ΔX	Horizontal distance between the laser and the vertical scale parallel to the paraboloid axis
y	Feed displacement
Z_f	Distance parallel to the paraboloid axis from the plane of the scale to the test point on the paraboloid
α_s	Solar absorptivity
ε	Strain
ε_e	External emissivity
ρ	Density
ν	Poisson's ratio
ν_p	Plastic Poisson's ratio
μ	Poisson's ratio
σ	Stress
$\overline{\sigma}$	Effective stress

Subscripts

a	Aluminum
cr	Critical
p	Plastic
1	Hoop direction
2	Longitudinal direction

4.0 OPERATIONAL SYSTEM DESIGN

The system consists of three elements: thin film cone and paraboloid, self-rigidizing torus, and the inflation system. The construction and operation of these elements will be described below following the sequence of events.

4.1 Sequence of Events

The shuttle will deliver the packaged system into low earth orbit. The antenna could be erected and then boosted into a geosynchronous orbit after inflation to the high pressure needed to yield the materials. However, it appears preferable to boost the packaged antenna to geosynchronous orbit because the booster will not have to overcome the drag on the full size object.

1. Release a small amount of water into the antenna to erect the system. Static analysis indicates 0.2 to 1000 grams are needed for 10 and 1000 meter antennas, respectively.
2. Just prior to full erection (less than a second to less than a minute depending on size), release carbon dioxide (CO_2) into the torus to bring the torus material to approximately its yield stress. This removes packaging wrinkles and will leave an aluminum structure capable of taking loads even without pressure in the torus.
3. Simultaneously, release additional water into the antenna to bring the paraboloid's thin film to approximately its yield stress. This removes packaging wrinkles from the paraboloid.
4. Propel the antenna to geosynchronous altitude or its desired orbit. Turn it to its desired initial orientation.
5. Vent the antenna's water vapor pressure down to approximately 0.001 Pa operating pressure.
6. Vent the torus' CO_2 gas to space.
7. Turn on the feed system.

8. With the antenna pointed at a known source, adjust internal pressure and feed location for maximum antenna gain.

9. As gas leaks out of the antenna, it is automatically replenished from a stored water bottle.

4.2 Collector Materials

The objective of this work was to determine which existing thin films would be best for an inflated antenna collector. Requirements were defined as they are understood from previous efforts. The properties of thin films were gathered and compared with the requirements.

Basic Requirements - Not all requirements have been defined for inflated collectors because the inflated antenna approach is relatively new. However, previous L'Garde work illustrated some basic requirements.

The film must have a low areal density because the system weight is (for larger antennas) almost directly proportional to areal density. Figure 5 was based on a film weighing 8.8 g/m^2 (0.006 mm thick). A doubling of the film thickness approximately doubles the antenna weight -- which makes the inflatable less competitive. Therefore, the film thickness must be 0.025 mm or less (0.006 mm preferred).

Temperature differentials on the paraboloid or cone will distort the configuration and reduce the antenna's gain. Such differentials on the cone are not too important because the feed could be moved to handle the distortion (as discussed in Section 7.2). However, distortions of the paraboloid can only partially be handled in this manner. Prior L'Garde work indicated what the temperature differentials are, but unknown is a quantitative impact of such differentials on antenna gain. The smallest temperature differential is considered best.

Temperature distributions in the paraboloid and cone of an f/D = 1 antenna were determined by L'Garde on another contract. Figure 7 shows differential temperature as a function of solar absorptivity and external emissivity with the

sun's rays parallel to the antenna axis. Clearly, very low solar absorptivity and external emissivity is desired. This is easy to get on the paraboloid because the surface must be aluminized, and therefore $\alpha_s \approx \varepsilon_e \leq 0.1$.

The cone must be dielectric, and therefore cannot be coated with a metal. Thin films tend to be translucent. Figure 8 contains the results of L'Garde computer thermal analyses (mostly from prior work). The upper four curves give the maximum temperature differentials on the cone, and the lower four curves provide the same information for the paraboloid. A zero degree sun angle occurs when the antenna is pointed at the sun. The temperature differentials on the cone and paraboloid are lowest for the highly reflective ($\varepsilon_e = \alpha_s = 0.1$), non-transparent cone having an internal emissivity of one (square symbol in Figure 8). Almost as good is a highly transmissive (90%) film like tinted polyester (triangular symbol in Figure 8). The latter exists in thinner films than the former, and therefore is especially attractive.

The collector film should therefore have the following optical properties:

a) External solar absorptivity of 0.1 to reject most of the heat so that the sunlit side is not much hotter than the shadowed side.

b) External emissivity of 0.1 to minimize differential temperatures.

c) Internal emissivity as high as practical to achieve reasonably even temperatures.

The collector must be RF reflective.

Low areal density, correct optical properties for thermal control, and RF reflectivity are considered to be the basic collector material requirements. They point to a black-colored film with aluminum vapor deposited on one side.

A material's coefficient of thermal expansion is important. For the optical properties previously listed and for a typical antenna, the temperatures of a collector can differ by as much as 30K. Thermal distortion could cause a problem in large antennas; therefore a low coefficient is required.

Other requirements, given below, are desirements since they don't appear to significantly affect antenna performance.

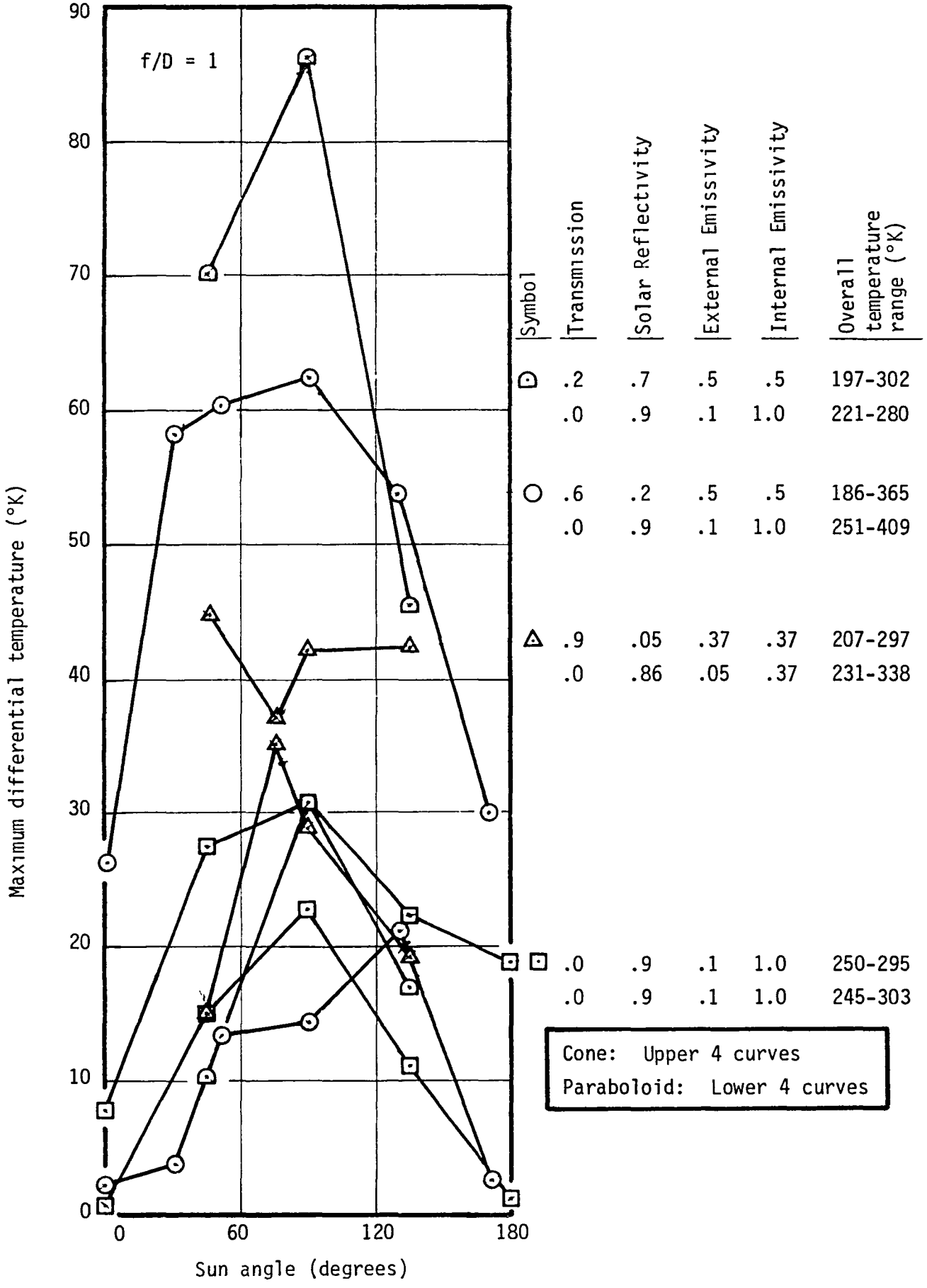

Symbol	Transmission	Solar Reflectivity	External Emissivity	Internal Emissivity	Overall temperature range (°K)
⊡	.2	.7	.5	.5	197-302
	.0	.9	.1	1.0	221-280
○	.6	.2	.5	.5	186-365
	.0	.9	.1	1.0	251-409
△	.9	.05	.37	.37	207-297
	.0	.86	.05	.37	231-338
⊡	.0	.9	.1	1.0	250-295
	.0	.9	.1	1.0	245-303

Figure 8. - Maximum temperature differences with cones of various transmittances, f/D = 1.

For an antenna with an f/D of 0.4, $D^3P \simeq 1.1W^2Et$. P must be as low as possible in order to minimize replacement gas weight; in prior studies, a P of 0.0007 Pa was selected because it is 100 times greater than solar pressure. W is limited by manufacturing; 1.6 meters widths are readily available (although wider material can be obtained without a capital investment). Thickness should be 0.013 mm or less to keep the weight down. Antenna diameters of interest go up to 1000 meters. Therefore, per the above formula, the tensile modulus of interest should be as high as 19,000 MPa (for a 1000 meter diameter antenna).

Thin film balloons have such a low areal density that they accelerate quickly under low pressure; erection must be done carefully so that the balloon does not self-destruct when the film is brought to a stop. The film's kinetic energy is converted to strain energy. A static analysis indicates that a film with a high f_y^2/E ratio will best survive erection. However, it is easier to control erection pressure than material properties so this is a minor requirement.

Another minor requirement, contrary to the one above, is that the film yield stress should be low in order to minimize initial inflation gas weight. The collector is pressurized to approximately its yield stress to eliminate packaging wrinkles.

Candidate Materials - Reinforced films were considered as well as homogeneous films. It became apparent that scrim reinforcement would create problems. A major one is that the composite effective modulus will vary considerably in different directions, for instance, a square weave does not readily elongate in the direction of the fibers, but it stretches easily at the 45° angle. There also does not appear to be any advantage to reinforcement because of an inflatable's low operating stress levels. Therefore, this research was discontinued in favor of other films.

Table I contains properties of various commercial thin films. These materials are compared to the requirements (previously discussed) in Table II.

Table II has a shortened list of candidates. The polyesters were limited to the dyed polyesters because they have higher emissivities. Polyimide Type H

TABLE I. - CANDIDATE THIN FILMS

	Polyesters				Polyimide Type H	½-mil Polyimide w/ Thin Film Black	Polyimide (FEP - Coated) Type F	2-mil Capran 80 (nylon)	½-mil Tedlar Type 20	Tedlar Type 30	5-mil Tefzel	FEP Teflon
	Mylar Type T	Mylar Type A	Melinex 329	Llumar Dyed								
Ultimate Tensile Strength (MPa)	310	172	145	172	172		117	90	110	90	52	21
Stress @ 5% Elongation (MPa)	159	103			90		62				22	13
Yield Stress @ 3% (MPa)			79		69		50	34				12
Tensile Modulus (MPa)	5520	3790		3790	5030		2210		2230	2140	965	480
Ultimate Elongation (%)	40	120	90		70		75	500	90	95	400	300
Folding Endurance (cycles)		14000			10000						85000	4000
Tear Strength - Propatating (kN/m)	8	8		8	3		5	15	6	7	>150	48
Tear Strength - Initial (kN/m)	170	310	530		200		170		130	150	>150	104
Specific Gravity	1 377	1 395	1.25		1 42		1 67		1.37	1 37	1 7	2.15
Melting Point (°K)	523	523	538		None		None				543	543
Zero Strength Temperature (°K)	521	521			1088			493	573	573		525
Coeff of Thermal Expansion ($°K^{-1}$)		$1\ 7(10)^{-5}$			$2\ 0(10)^{-5}$					$5\ 8(10)^{-5}$		$8\ 3(10)^{-5}$
Specific Heat (cal/g/°K)		28			26				0 37	26		28
Heat Sealable ?		No			No		Yes	Yes	No	Some	Yes	Yes
Emissivity (with VDA)		57			0 68	0.76						0 48
Colors ?		No	White	Black & Others	Yellow Trans-lucent	Black	No		Grey	Black & Others	Clear	No
Minimum Thickness (mm)	006	006	013	013	008		013	051	013	025	013	013

TABLE II. - COMPARISON WITH REQUIREMENTS

Requirement	Characteristic	Dyed Polyester	Polyimide Type H	Polyimide Thin Film Black	Capran 80 Nylon	Tedlar Type 20	Tefzel	Teflon FEP
Major:								
Low Weight	Minimum Thickness (mm)	0.013	0.008	0.013	0.051	0.013	0.013	0.013
	Min. Areal Den. (g/m^2)	16	11	19	~ 64	17	22	27
	Specific Gravity	1.3	1.4			1.4	1.7	2.1
High Emissivity	Emmissivity *	> 0.48	0.44	0.76				≥ 0.4
	Colors available	yes	no	black		yes	no	no
RF reflective	Plain	no	no	no	no	no	no	no
	VDA coated	yes	yes	yes	yes	yes	yes	yes
Low Coeff. of Thermal Expansion	Thermal Expansion (10^{-5}/°K)	1.7	2.0			5.8		8.3
Minor:								
E → 19000 MPa	Elastic Modulus (MPa)	3800	5030			2100	970	480
High $(f_y)^2/E$	$(f_y)^2/E$(MPa)	1.6	0.9			~0.7	0.4	0.3
Low f_y	f_y (MPa)	79	69		34	~ 40	~18	12

*Emissivities given are for clear, VDA backed film except for polyimide/thin film black.

and tedlar Type 20 were listed rather than Type F and Type 30, respectively, because of better properties.

The two best values for each requirement are underlined. Dyed polyester appears to be the best film. It has the lowest density and thermal expansion coefficient. It can be obtained in black, 0.013 mm thick film, and therefore has the potential of having a higher emissivity than VDA mylar's 0.48 (½-mil film).

The second best film would appear to be polyimide. It has the lowest areal density (because it is available in 0.008 mm thicknesses) and low thermal expansion. However, its emissivity in such a thickness (with VDA) is only 0.44.

The emissivity of 0.013 mm polyimide with thin film black is 76%. If thin film black were put on 0.008 mm polyimide, one could expect an emissivity of 76% at an areal density of 11 g/m^2. Painted polyimide could be better than dyed polyester -- however, paints tend to degrade.

Tedlar looks fair because it can be made in color. However, its emissivity is not likely to be higher than that of coated polyimide or black-dyed polyester. Also, it has a thermal expansion about three times that of the latter films.

4.3 Construction and Packaging

The paraboloid and cone are made of pie-shaped gores of thin film. Tape consisting of the same thin film plus about 0.003 mm of heat-sensitive adhesive are used to assemble the inflatable.

The gores for the paraboloid are sized and shaped such that they strain to a parabolic shape under pressure. Since the operating pressure must be low (about 0.001 Pa) to decrease the amount of replacement gas that is carried, the strain is low and the assembled uninflated paraboloid will be very close to the inflated configuration. (Section 7.0 has a complete discussion.)

The torus is made of a composite of aluminum-polyester-aluminum (discussed in Section 6.0). It, too, is made form gores held together by tape made of the same composite and a heat-sensitive adhesive.

Past experience has shown that an inflatable should be accordian-folded to minimize stresses in the material and to prevent tangling.

The inflatable is laid flat as possible with the torus on the outside, and the cone and paraboloid folded in concentric rings. Starting furthest from the pressure source, the material is accordian-folded toward the pressure source. This is continued until the pressure source is reached. At this point, the semi-packaged antenna is a "ribbon" about one antenna diameter long by the selected accordian width. The pressure source is at the middle. Accordian-folding is continued from each end toward the center.

When gas is released into this package, only a slight movement of the film exposes the entire surface, and the inflatable can open with minimal stress on the film.

4.4 Inflation System Concept

The preliminary conceptual design identifies the primary features and components of the inflation system.

The following operational requirements were assumed for the inflation system:

1. Unfold the antenna by releasing a very small portion of the inflatant (< 0.1% of that available) into the antenna.
2. Pressurize the torus to approximately yield stress and thus rigidize it.
3. Increase the pressure in the main body to bring the reflector material to approximately its yield stress. There is no minimum time restraint on this operation.
4. Reduce the antenna pressure to 10^{-3} Pa in perhaps 24 hours.

A prior L'Garde study of possible inflatants indicated that water (MW = 18) is the best passive candidate for the antenna inflatant and that ammonia, acetylene and carbon dioxide are candidates for the torus inflatant. The ammonia or acetylene could degrade the torus materials -- although this is a minor concern because the inflation gas is quickly vented. However, for this conceptual design, carbon dioxide will be used as the baseline torus inflatant.

Hydrazine, which decomposes into $N_2 + 2H_2$ (av MW = 10.7), was identified as the best active candidate. This fluid would be especially attractive for some antenna configurations because there is no freezing problem as the material is converted into gas as is the case with water. During vaporization of the water, it absorbs so much heat from the remaining liquid that the liquid can freeze prior to the antenna reaching the yield pressure. However, water will be used as the antenna inflatant for this conceptual design.

System Description - The inflation system is shown schematically in Figure 9. The system is isolated from the antenna assembly during the launch and deployment environments by two normally closed pyrotechnic valves, V1 and V2. At the completion of the canister release these two valves are opened. The first step in the deployment of the antenna is to release a small amount of water from the main storage bottle. This is accomplished by opening valve V3 for a few seconds (dependent upon configuration). This valve is a solenoid valve with a small flow control orifice diameter. Release of this water more rapidly or release of more water could result in accelerating the antenna skin to such a high velocity that it would tear itself apart when it reaches its deployed size.

In order to be assured that the proper amount of water will be injected during the time V3 is open, it is necessary to condense the total water mass in the tank and to control its location. This is accomplished with a pressurized bladder system. The pressurant could be butane (C_4H_{10}) which at 295K provides a pressure of 0.2 MPa.

Once the antenna has been unfolded and grossly deployed, the torus is pressurized. Solenoid valve V4 is opened and CO_2 is injected into the torus. In order to avoid too rapid an inflation, the CO_2 flow is controlled by a small orifice at V4, near the main storage tank. This allows the CO_2 required to pressurize the torus to be injected over a reasonable time span.

The CO_2 also must be fully condensed and the location in the tank controlled in order to provide a controlled inflation sequence. Since the vapor pressure of the CO_2 at 295K is 5.9 MPa, it is not practical to pressurize the system with another fluid; therefore a spring loaded piston is used instead of the bladder system used for the water tank. A small amount of CO_2 is on the

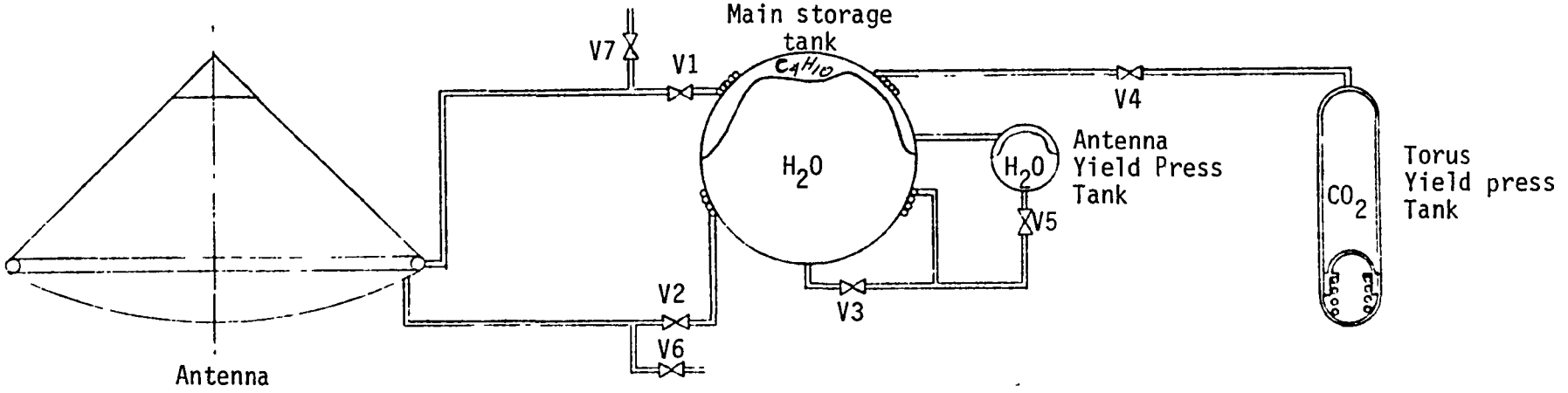

Figure 9. - Inflation system schematic

spring side of the piston also to balance the vapor pressure so that the spring needs only enough force to move the piston and hold the liquid CO_2 against the tank outlet.

As the CO_2 is released from the tank, the rapid boiling that takes place may result in the formation of CO_2 crystals. In order to avoid this problem, the plumbing is coiled around the main storage bottle. This allows the heat stored in the main water supply to be used as a heat source for vaporization.

With the torus fully rigidized and pressurized, the antenna is further pressurized so that the collector/reflector film is yielded to eliminate packaging wrinkles. This pressurization is accomplished by opening pyrotechnic valve V5 and dumping in the remaining water. Here again freezing of the vaporizing fluid is avoided by coiling the injection tubing around the main storage tank.

The antenna is now fully pressurized and is very rigid. In this condition it may be easily stabilized, oriented or propelled to another location.

After orientation and stabilization, the system pressure is reduced to operating levels. Solenoid valve V6 is opened to vent the antenna down to 0.001 Pa. When this pressure is reached as measured by the pressure sensing system, V6 is closed. The pressure is then maintained for the life of the antenna by opening and closing solenoid valve V2.

Finally solenoid valve V7 is opened to vent the CO_2 from the torus. Once the torus has been rigidized and the antenna pressure reduced to operating pressure, the torus is sufficiently rigid to maintain the antenna shape. The CO_2 is vented to space to prevent inadvertent leakage between the torus and antenna from providing excessive pressure in the antenna.

Component Description - The main storage tank will be a spherical tank for minimum weight. Since it is pressurized to only 0.2 MPa, it is made of aluminum with a wall thickness of 1.3 mm. The bladder will be reinforced rubber approximately 0.8 mm thick. The yield pressure tank will be the same as the main storage tank except the diameter and thickness will be less.

The carbon dioxide storage tank, since it incorporates a spring loaded piston, will be cylindrical in shape. The tank and the piston will be made from stainless steel.

All tubing will be stainless steel of a diameter appropriate for the flow rate required. The tubing system will be of all welded construction in order to minimize weight and reduce the chance for leaks.

The normally closed pyrotechnic valves (V1, V2, and V5) will have redundant cartridges. Solenoid valves (V3, V4, V6, and V7) will be equivalent to solenoid valves presently being used on hydrazine systems for satellite attitude control.

This Page Intentionally Left Blank

5.0 PARABOLOID FABRICATION AND ACCURACY

The objective of this task was to define a membrane surface suitable for use in a space reflector system. The results demonstrated that an inflatable thin film collector can be made with sufficient accuracy for use in space.

5.1 Polyester Paraboloid

The paraboloid was built using 0.013 mm polyester tape with heat-sensitive adhesive for seams. Its diameter was set at 3 meters. An f/D of one was selected. It was desired that the focus be far away from the paraboloid for accuracy testing.

The optimum pressure is that needed to elongate (within elastic limits) the flat gores to a circular cross section in the radial direction (Figure 10).

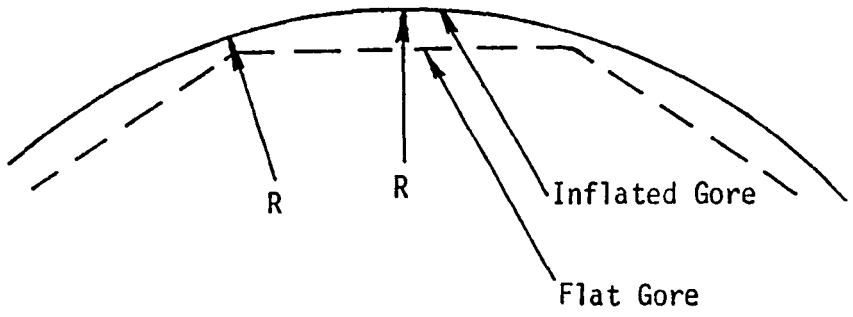

Figure 10. - Goal of optimum inflation pressure

This optimum pressure is defined (per L'Garde's modification of the analysis in Reference 6) as

$$P = (W/D)^2 E_G/1.5(1-\mu)(1-E_G/E_S)R$$

For the films and f/D given above, and for a polyester elastic modulus of 4140 MPa,

$$P = (\pi/N)^2(26300 \text{ Pa-m})/1.5(0.7)(2/3)(6.6 \text{ m})$$
$$= 56200/N^2 \text{ Pa} = 5730/N^2 \text{ mm } H_2O$$

This leaves only the number of gores for controlling optimum pressure and the gore stress (which is approximately PR/2t):

Number of Gores	Optimum Pressure (mm H_2O)	Gore Stress MPa
20	14	73
24	10	51
30	6.4	32
32	5.6	29
36	4.4	23
40	3.6	18
45	2.8	14
50	2.3	12
60	1.6	8

Because of the size (3 meters in diameter) of the paraboloid, low gore stress levels (< 6 MPa) are not practical. Rather it was decided to use a minimum number of gores and evaluate if the gores were stretching to a circular shape in the radial direction (Figure 10). A 32-gore design was selected; the gore stress is still below the proportional limit. (During testing, it was found that the optimum pressure was 2½ mm H_2O -- not 5.6 mm H_2O as indicated in the table; therefore, the stress was only about 15 MPa or 2200 psi).

The flat pattern coordinates are given in Table III.

Fabrication - A polyester template was cut to the gore's calculated dimensions. The length of the template (and gores) was extended further than indicated in Table III so that the finished paraboloid could be later mounted on the aluminum hoop. Index points were marked on the edge of the template; also the end of the paraboloid was marked on the template.

The polyester was spread on a table and smoothed out. The template was placed on top. The polyester was cut. The index marks and the paraboloid end line were transferred to each gore.

TABLE III. - POLYESTER GORE COORDINATES

Length (mm)	Width (mm)
49.5	9.8
99.0	19.5
148.6	29.3
198.1	39.0
247.7	48.8
297.2	58.5
346.8	68.3
396.5	78.0
446.1	87.8
495.8	97.5
545.5	107.3
595.2	117.1
645.0	126.8
694.9	136.6
744.8	146.3
794.7	156.1
844.7	165.8
894.7	175.6
944.8	185.3
995.0	195.1
1045.3	204.8
1095.6	214.6
1146.0	224.3
1196.4	234.1
1247.6	253.6
1348.4	263.3
1399.2	273.1
1450.1	282.8
1501.1	292.6

The gores were butt jointed and assembled with 19 mm wide tape. The index marks on adjacent gores were matched closely. The tape consisted of 0.013 mm (½-mil) polyester and 0.013 mm (½-mil) heat sensitive adhesive. A hand-held iron was used for sealing.

The support rim was assembled from 3.2 mm thick extruded and rolled aluminum angle, and 1.0 mm thick aluminum sheet. Three pieces of aluminum sheet were cut to 9.42 meters length, and then assembled (on a flat granite table) into a cylinder using rivets and doublers. Two lengths of the angle were riveted to each end of the sheet cylinder. The angles followed the cylinder edge, and were cut to fit the diameter of the cylinder.

The rim was attached to the wall with screws. The screws were not torqued down in order to maintain flatness of the cylinder. Gaps between the wall and the rim were closed with a sealant.

The paraboloid seam positions were marked on the aluminum rim. The paraboloid was attached to the hoop with 0.025 mm thick heat-sensitive, dry adhesive. The attachment sequence was done as one would torque down a circle of bolts.

Since the paraboloid would expand under inflation, the gores were assembled to the rim under approximately the same stress as it would have inflated. That is, the straight lines marked on each gore took on the curvature of the rim. This could only be done to within about ±1 mm. (In space operation, this expansion is accomplished by the inflatable, self-rigidizing rim.)

Testing - The test set-up is illustrated in Figure 11. A laser and a moveable vertical scale were set on a horizontal optical bench in front of the paraboloid. The distance between the paraboloid rim and the scale was set and measured at 2813 mm (which was the theoretical focus, i.e., 3000 mm focal length less 187 mm paraboloid depth). The bench was leveled using a machinist's level.

The laser was pointed perpendicular to the antenna rim. (A sheet of aluminized polyester was stretched across the rim, and the laser angles were

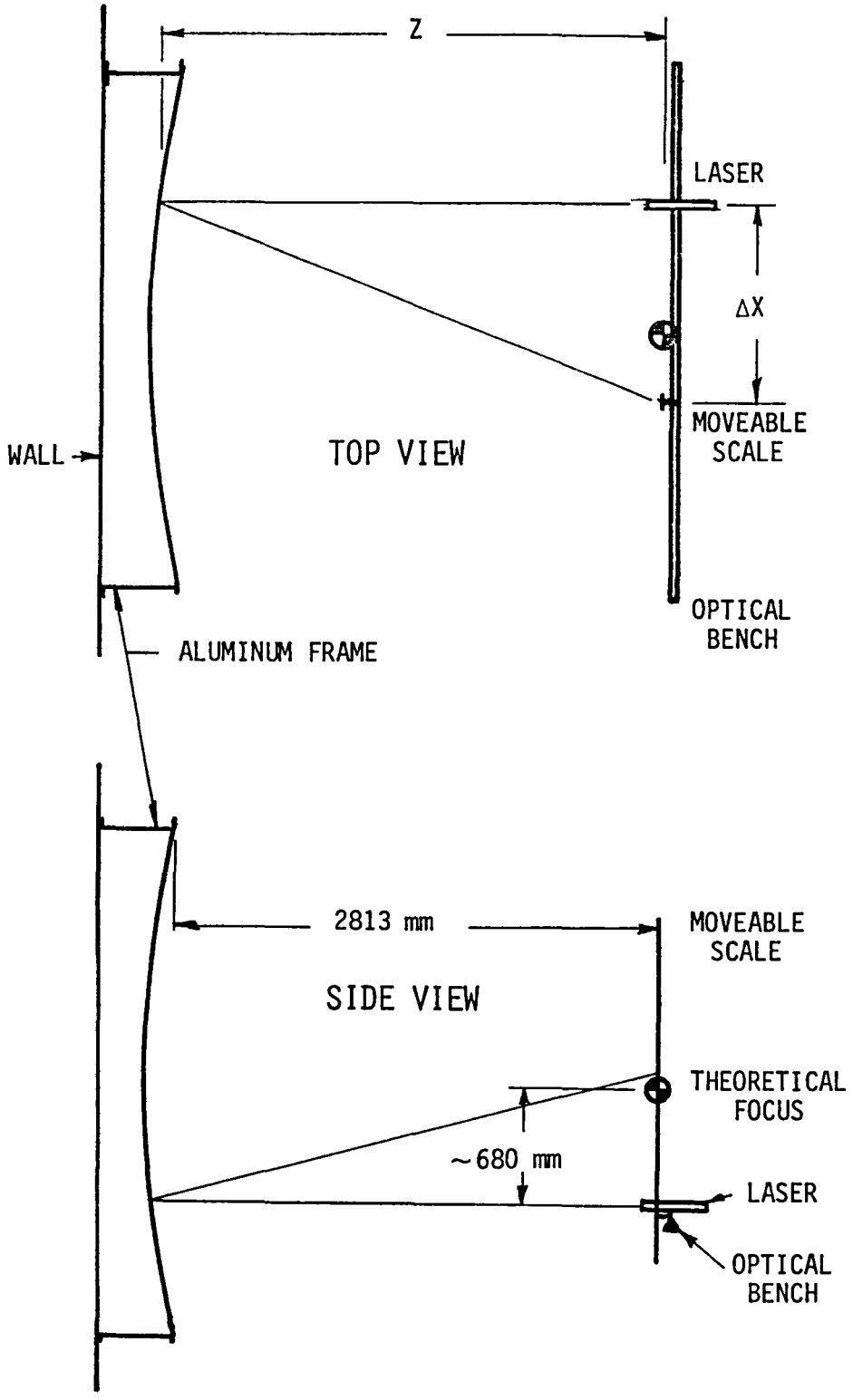

Figure 11. - Test setup.

adjusted so that its light returned to it.) Its horizontal plane was located about 680 mm below the paraboloid centerline.

A vacuum pump was connected to the aluminum frame. Needle valves in the line controlled the air flow, and were used to maintain a particular differential pressure.

It was found that a water manometer did not provide enough resolution for pressure control. Therefore, a string was stretched across the paraboloid at the rim, and the depth of the paraboloid at its center was held constant. Two tests were run:

Test No.	Paraboloid Depth (mm)	Measured Pressure (mm H_2O)	Calculated Stress (MPa)
1	187	2½	13
2	197	5	26

The laser location was read and recorded, and the vertical scale was moved to intersect the light return. The location of the scale was read and recorded. (The vertical location of the light return was also read and recorded but not used in the data reduction and analysis.) This was repeated as the laser was moved 30 mm horizontally after each reading.

The light return from the gores was sharp and clear (2-3 mm in diameter), but the return from a seam was diffuse. Therefore, only data were taken from the gores.

Data Reduction and Analysis - The local slope in the horizontal direction of the paraboloid was calculated from the test data:

$$dZ/dX = \tan \tfrac{1}{2} \left(\tan^{-1} \Delta X/Z_f\right)$$

For Test No. 1, Z_f was the theoretical:

$$Z_f(mm) = 2957.4 - X^2/(4)(3000)$$

where X is in mm. For Test No. 2 which was over-pressurized, Z_f was the following -- based upon the Test No. 1 results:

$$Z_f(mm) = 2970.8 - X^2/4(2824)$$

Figure 12 shows the results for Test No. 1. Some observations:

1. The paraboloid is not perfect; all points should be in a straight line.
2. The gores (points connected by a straight line) are curved by the pressure as desired.
3. There are discontinuities at the seams.

Figure 12 was integrated from the paraboloid rim to produce Figure 13. Integrating from the rim towards the center will result in a step at the center; in this case, that step was 1.1 mm.

The curve fit is shown on Figure 13. It is seen that the focal length is 2963 mm instead of 3000 mm so the paraboloid may still have been over-pressurized.

However, the inaccuracy relative to the curve fit (Figure 13) is 0.76 mm RMS. Actual deviations are shown in Figure 14; all points are within 1.3 mm of the curve fit.

Since the Z_f used in data reduction was that of a perfect parabola, one should now go through an iteration using

$$Z_f = 2812.5 - Z$$

where Z is taken from Figure 13. (The value, 2812.5 mm, is the distance between the paraboloid rim and the moveable scale.) This would change the data point locations and the curve fit but would not affect the RMS error.

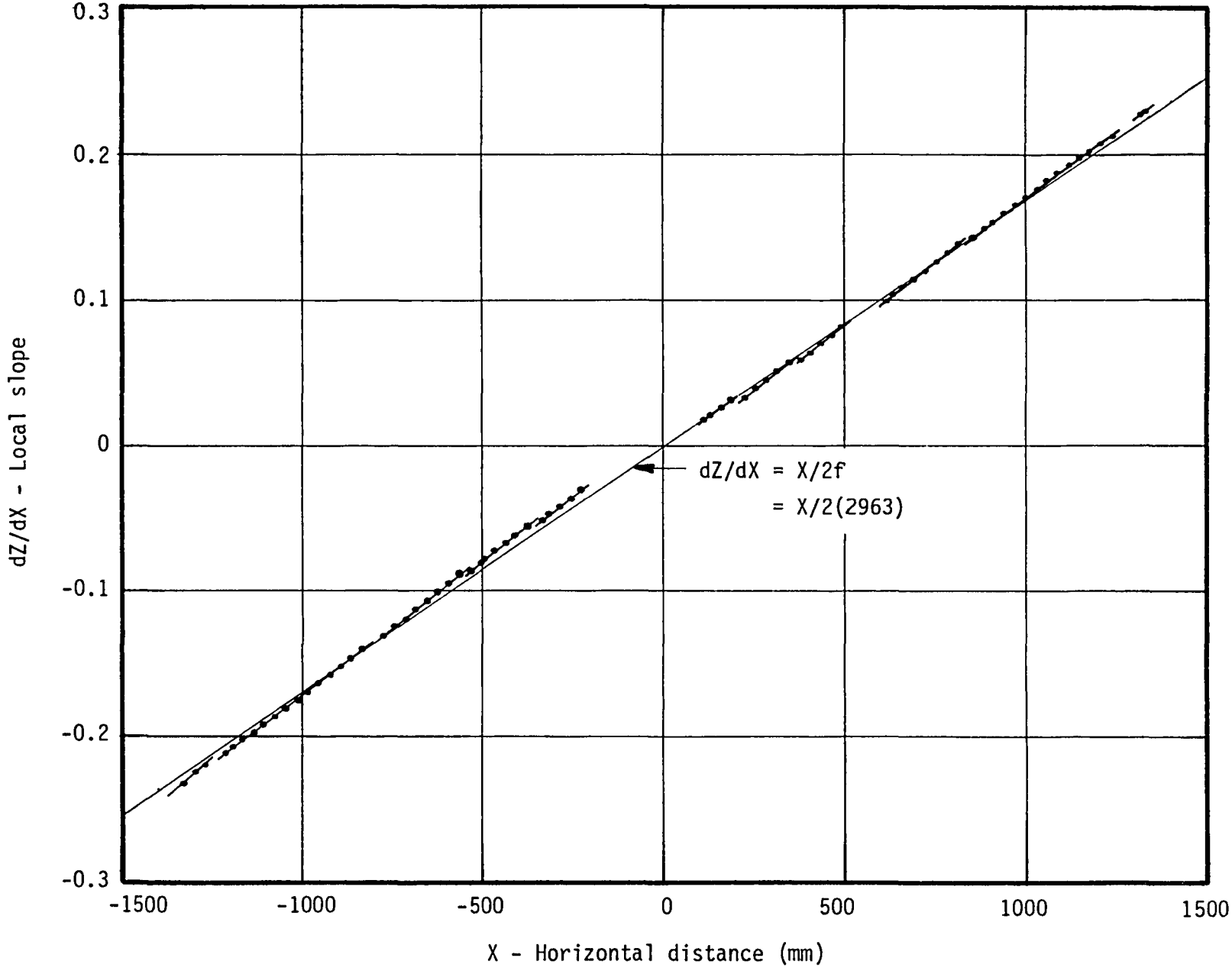

Figure 12. - Slopes of polyester paraboloid (13 MPa film stress).

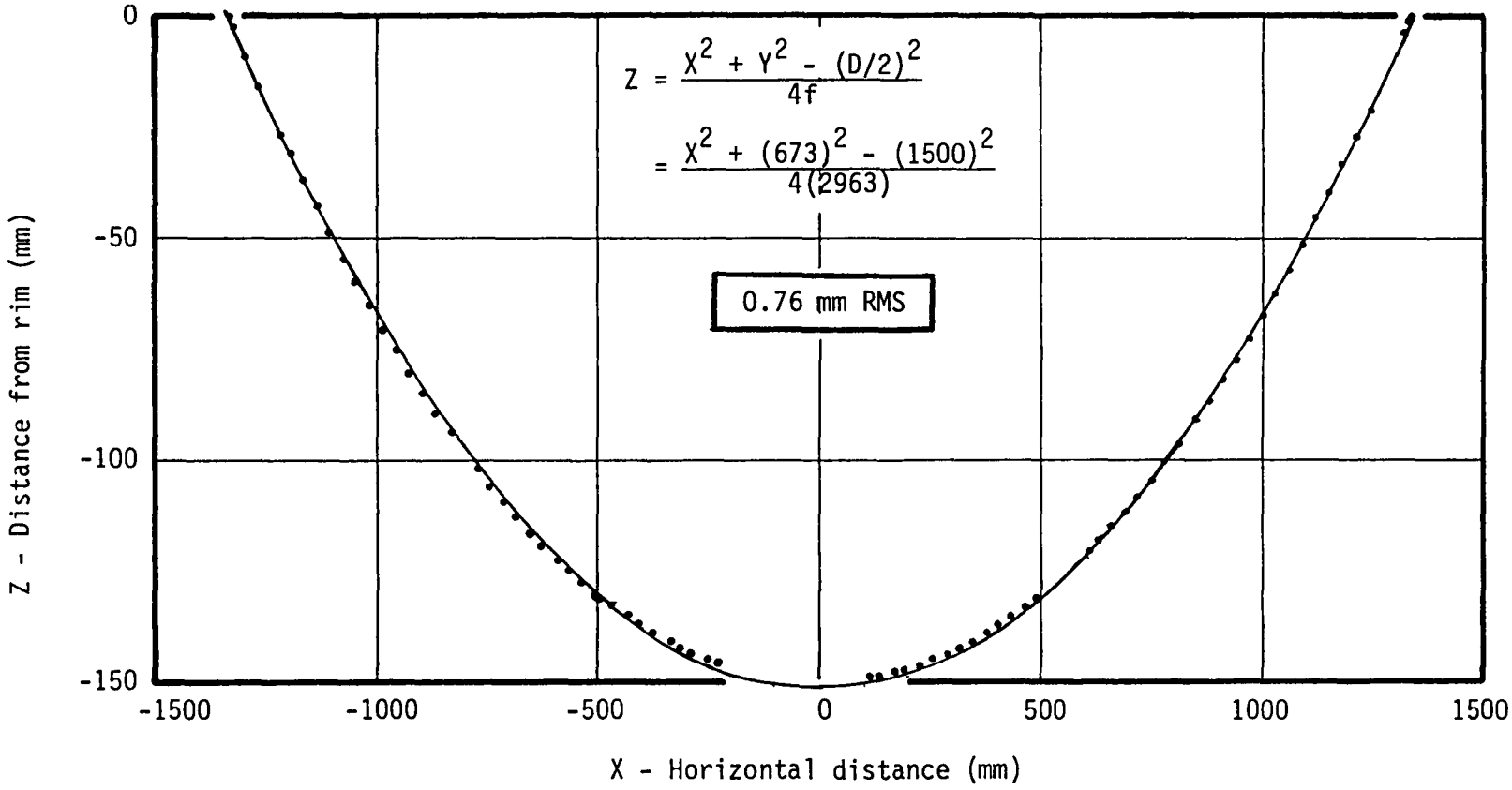

Figure 13. - Cross section of polyester paraboloid (13 MPa film stress).

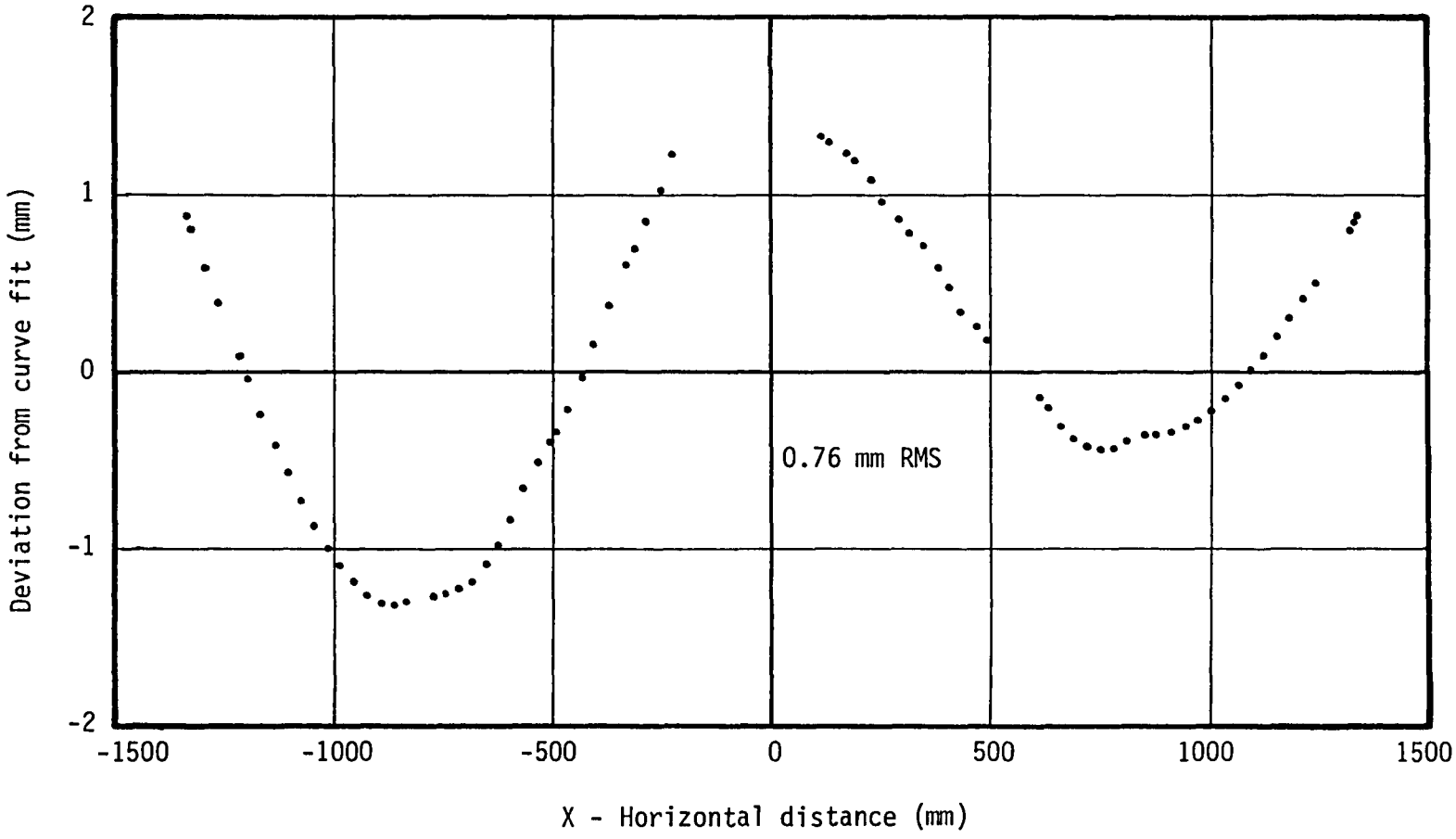

Figure 14. - Inaccuracy of polyester paraboloid (13 MPa film stress).

Consider the Figure 13 curve fit

$$Z_f = 2964.1 - X^2/11852$$

instead of

$$Z_f = 2957.4 - X^2/12000.$$

The Z_f of the former is greater than the one used by 6.7 mm to 4.8 mm (0.23% to 0.17%) for X = 0 and 1340 mm, respectively. This decreases the calculated local slopes by essentially the same percentages. Therefore, all the points and curve fit on Figure 13 would increase. The focal length would change from 2963 mm to 2969 mm -- closer to the 3000 mm design value.

The above error could be corrected by repeating the numerical integration using the inferred Z_f values. However, this is unwarranted because it won't affect the RMS value. The major real error is in the ability to read ΔX accurately. It is believed that this can be read to within $\pm\frac{1}{2}$ mm. The test equipment is located correctly in the Z direction to within ± 1 mm. These errors translate into a dZ/dX errors ranging from 0.00009 to 0.00011. Over a 1300 mm ΔX, then, ΔZ is only about 0.1 mm. This is not a complete error analysis, but does give an indication that the paraboloid stated inaccuracy of 0.76 mm RMS is valid.

The data from Test No. 2 (26 MPa film stress) were also reduced but not plotted. The curve fit from the 2-3 mm H_2O pressure test case was used to deduce a probable Z_f for data reduction:

$$Z_f = 2970.8 - X^2/(4)(2824)$$

The local slopes were calculated as before. The slopes were numerically integrated to derive Z versus X; this time, however, integration was started at the center and continued to the rim -- per the suggestion of NASA Langley. This approach eliminates the possibility of a step at the center.

The curve fit was

$$Z = \frac{X^2 + Y^2}{4f}$$

$$= \frac{X^2 - (140)^2}{4(2818)}$$

Obviously, overpressure distorts the paraboloid. The focal length of 2818 mm decreased from 2963 mm due to the added pressure also. The inaccuracy relative to this curve fit was 0.94 mm RMS; all data points were within 1.7 mm of the curve fit.

5.2 Polyimide Paraboloid

The paraboloid was built using 0.008 mm VDA polyimide film for the gores, and 0.013 mm polyester tape and heat-sensitive adhesive for the seams. The only other difference with the prior paraboloid was that it was constructed of 40 gores to reduce the gore stress and operating pressure.

Optimum pressure is, as before, calculated by

$$P = (\pi/N)^2 E_G t/1.5(1-\mu)(1-E_G/E_S)R$$

$$= (\pi/40)^2(32260 \text{ Pa-m})/1.5(0.7)(1-32260/80418)(6.6 \text{ mm})$$

$$= 47.9 \text{ Pa} = 4.9 \text{ mm } H_2O$$

The gore stress is then approximately

$$PR/2t = (47.9)(6.6)/1.524(10)^{-5} = 21 \text{ MPa}$$

The flat pattern coordinates are given in Table IV.

TABLE IV. - POLYIMIDE GORE COORDINATES

Length (mm)	Width (mm)
49.7	7.8
99.4	15.6
149.1	23.5
198.8	31.3
248.5	39.1
298.2	46.9
348.0	54.7
397.8	62.6
447.6	70.4
497.4	78.2
547.3	86.0
597.2	93.8
647.1	101.7
697.1	109.5
747.2	117.3
797.3	125.1
847.4	132.9
897.7	140.8
947.9	148.6
998.3	156.4
1048.7	164.2
1099.2	172.0
1149.7	179.9
1200.3	187.7
1251.1	195.5
1301.9	203.3
1352.7	211.1
1403.7	218.9
1454.8	226.8
1506.0	234.6

Fabrication. - The polyimide paraboloid was made in the same manner as the polyester paraboloid.

When the paraboloid was assembled to the rim, the gores near their centerlines had to be pulled to place the line on the gore on the rim. Unlike the polyester case, however, the seams at the rim ended up at zero stress and buckled.

The paraboloid, inflated to approximately 1 mm H_2O, is shown in Figure 15. Its imperfections are evident upon inspection. Even under pressure, the seams near the rim are under nearly zero stress, and the surface in each of these forty areas is poor. More evident is the poor center section. It is recessed more than desired for about 0.3 meter from the center.

Close inspection showed that there was a gap of about ½ mm between each set of adjacent gores. Since there are forty seams, this results in about 30 mm excess material. The technician could not close up this gap while working on a flat table. The paraboloid should have been made with a mandrel that created the proper angle between gores.

Testing. - The test set-up was identical to that described in Section 5.1 except that the horizontal test plane was about 635 mm below the paraboloid centerline (instead of about 680 mm).

The paraboloid was held at a fixed pressure by using the laser test set-up to determine any change in pressure. The laser was pointed at the paraboloid near its edge. The ΔX distance was read and recorded. The laser was returned several times during the testing to this reference point to determine if ΔX changed, and the air flow rate was changed as necessary to keep ΔX constant. The pressure was measured at 1 mm H_2O, and the film stress was 4 MPa (calculated).

Data Reduction and Analysis. - Z_f was

$$Z_f = 2964.0 - X^2/(4)(3000).$$

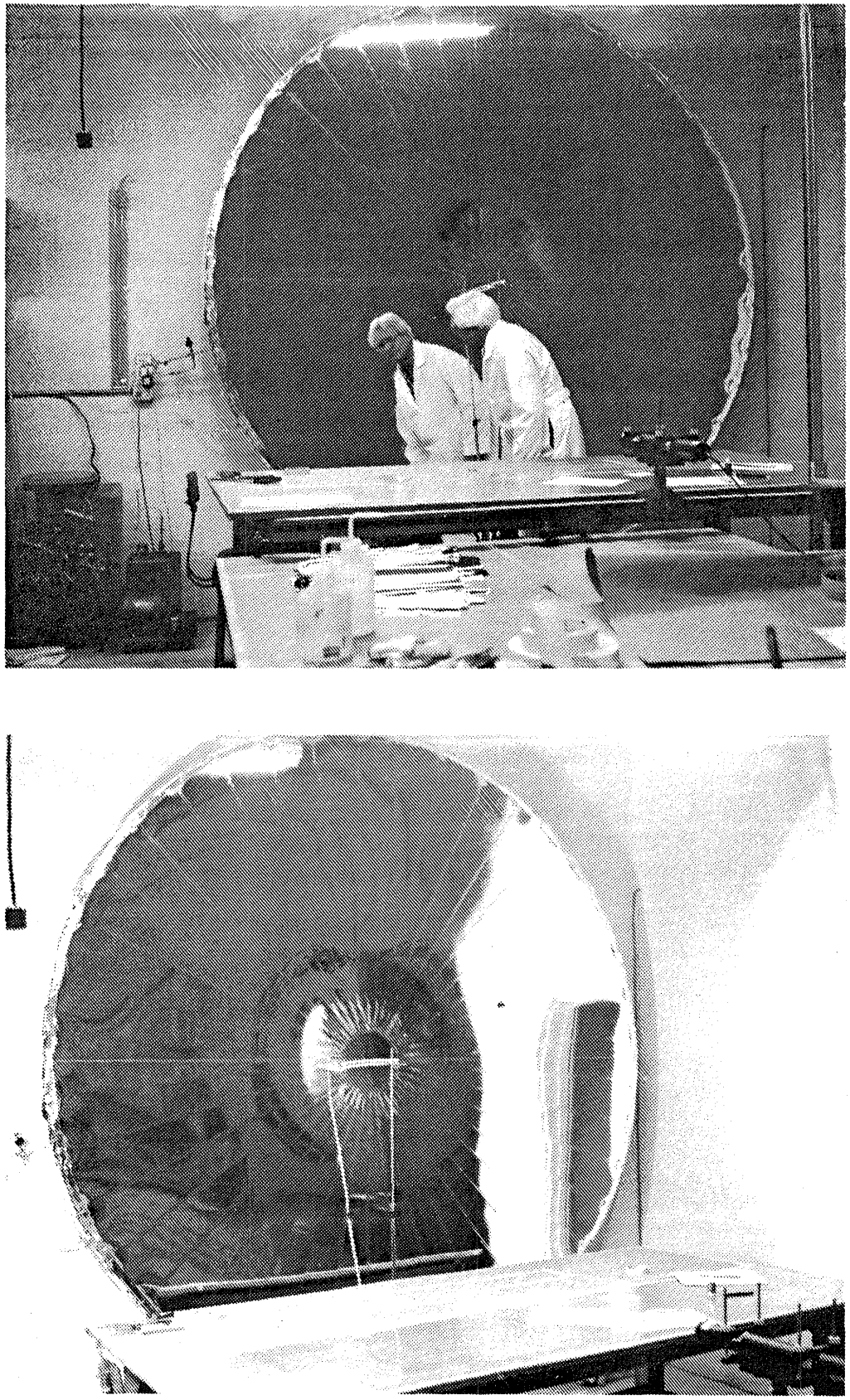

Figure 15. - Inflated polyimide paraboloid.

Figure 16 shows the local slopes of the gores. The polyimide paraboloid is not as good as the polyester one (Figure 12). All points should lie on a straight line. The two gores near the rim are poor -- probably adversely affected by the low stress seams previously mentioned. The slopes of the two gores in the -500 to -1000 mm region appear to create a curved line which is inconsistent with the definition of a parabola.

The data shown in Figure 16 was integrated starting at the center, and working outward towards the rim. The result is shown in Figure 17. One immediately sees that a better curve fit would be available for a more general equation of a parabola. The data indicate that the curve fit should be shifted to the left and perhaps tilted.

The horizontal cut has an inaccuracy of 1.64 mm RMS. The surface deviates from the curve fit by ±2.5 mm as shown in Figure 18.

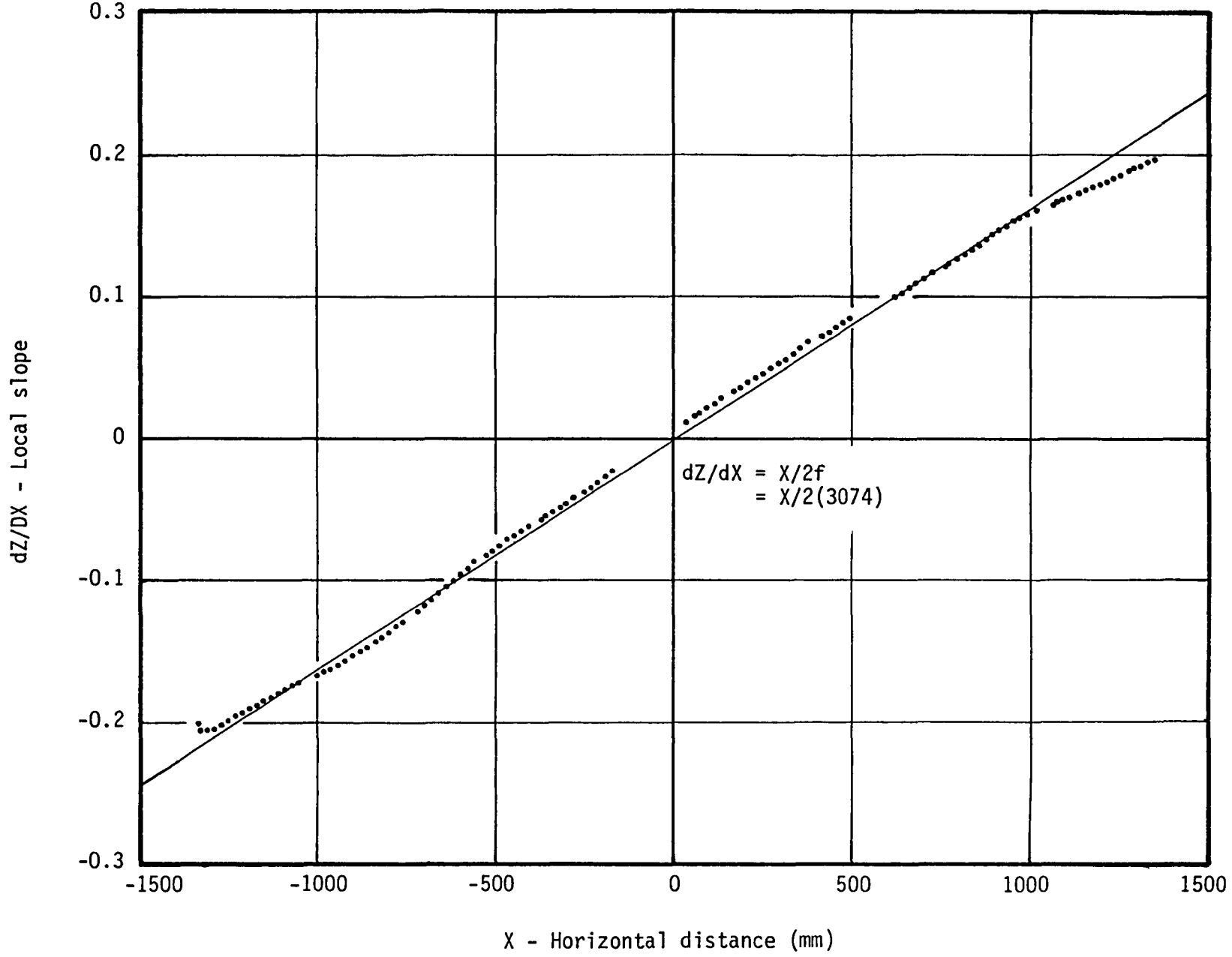

Figure 16. - Slopes of polyimide paraboloid (4 MPa film stress).

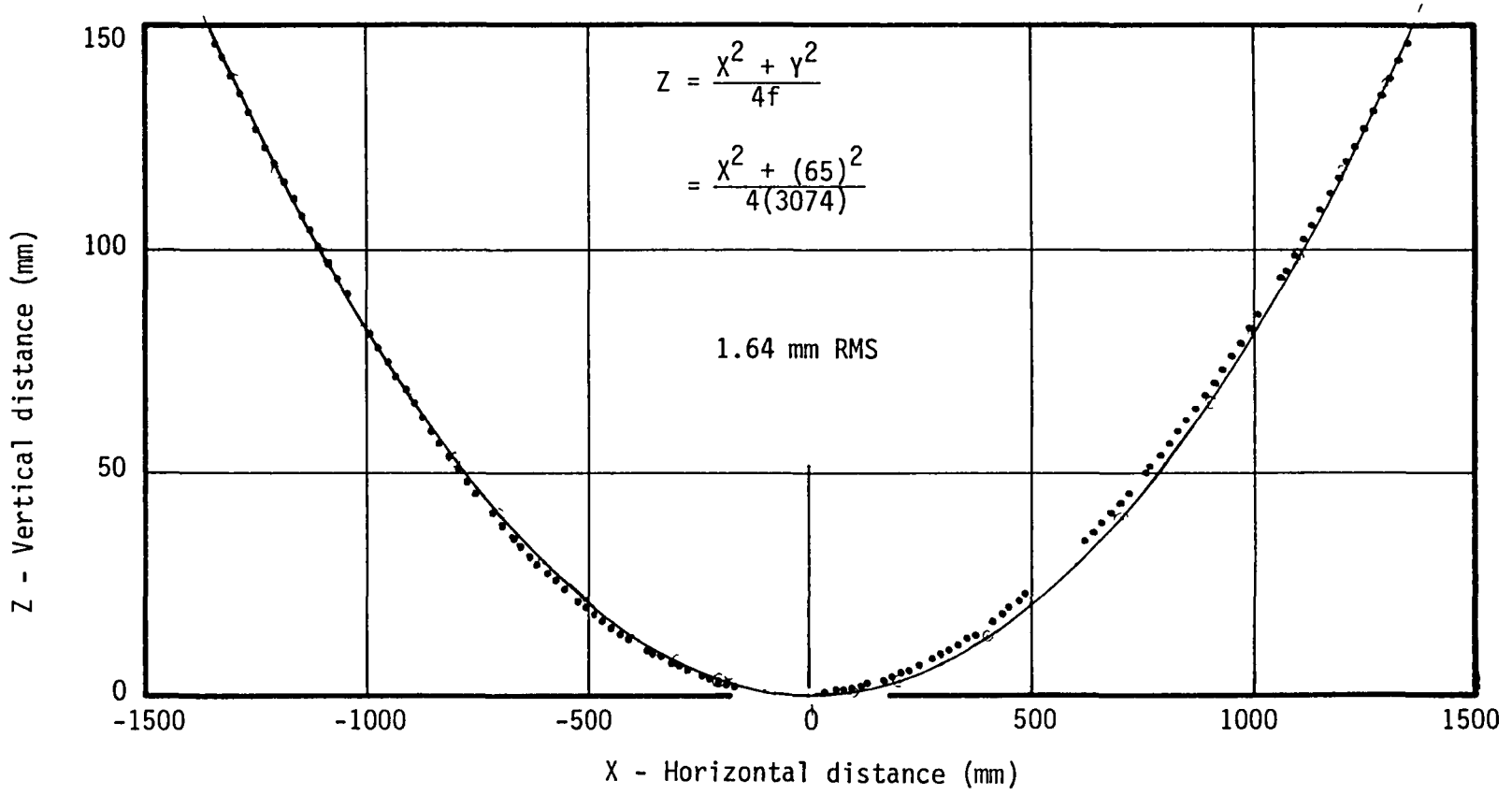

Figure 17. - Cross section of polyimide paraboloid (4 MPa film stress).

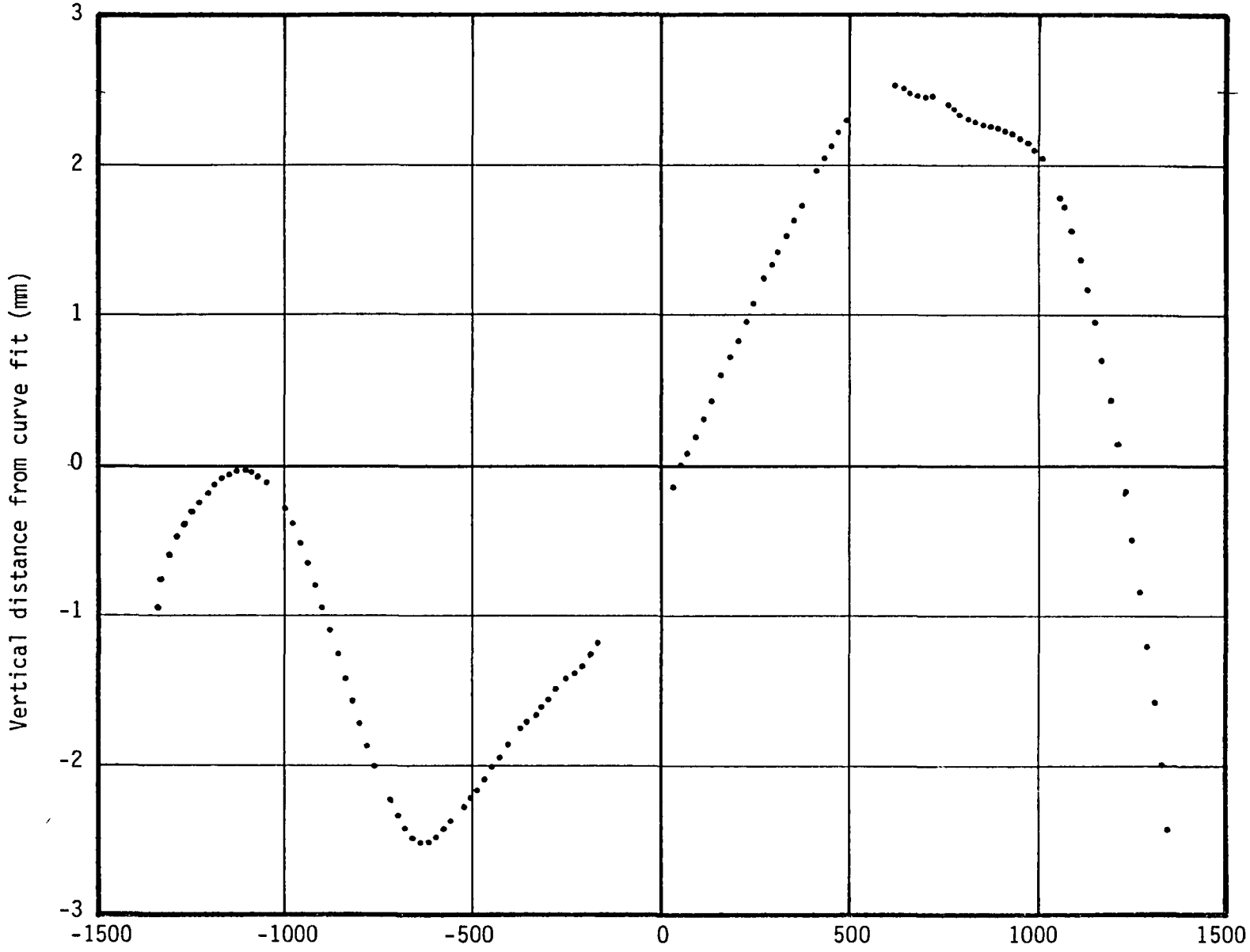

Figure 18. - Inaccuracy of polyimide parabola (4 MPa film stress).

This Page Intentionally Left Blank

6.0 SELF-RIGIDIZING STRUCTURAL ELEMENT

The torus at the interface between the cone and paraboloid keeps the inflated cone-paraboloid from collapsing. A pressurized plastic torus is not feasible because the pressure requirements are too high -- the weight of replacement gas is prohibitive. Therefore, the rim must be rigid without pressure.

The technology developed for NASA's ECHO II appears to be ideal for this application. ECHO II was a large sphere made of an aluminum foil-polyester-aluminum foil composite. This material could be folded into a small package volume. In space, the balloon was pressurized back into its spherical configuration. The film stresses caused by the pressure removed the packaging wrinkles. Remaining was a thin aluminum composite sphere that could withstand the atmospheric drag loads.

For the collector torus application, loads are much higher (but still small -- 0.03 to 3.3 Pa/meter for diameters of 10 and 1000 meters, respectively), and the configuration may be more difficult (since stress levels in the hoop direction are twice that in the longitudinal direction).

In this initial development, this type of structure was analyzed (Section 6.1). A set of nine cylinders was constructed (Section 6.2) and tested (Section 6.3). Section 6.4 evaluates the results.

It was found that the cylinders were considerably stronger than the analysis predicted using measured aluminum foil elastic moduli. More analysis and testing are required before a correlation can be confidently made.

6.1 Analysis

The self-rigidizing structural element has three operational phases:

1. Pressurizing the cylinder to approximately yield the aluminum but not the polyester.
2. Releasing the gas; this action can result in a residual compressive stress in the aluminum balanced by a residual tensile stress in the polyester.

3. Placing a compressive load on the cylinder. At the critical load, the compressive load stresses plus the residual stresses will result in buckling failure.

Pressurization. - The cylinder geometry is shown in Figure 19. Assumptions follow:

1. r/t is large. For r = 51 mm and 0.050 mm $\leq$ t $\leq$ 0.102 mm, 1020 $\geq$ r/t $\geq$ 500.
2. Membrane shell theory applies; $N_1 = pr$ and $N_2 = pr/2$. N_i is the distributed inplane load (N/m).
3. The aluminum is stressed significantly beyond the yield point.
4. The polyester deformation is linearly elastic.
5. The deformation theory of plasticity (Reference 7, page 190) is valid for the aluminum layers.

$$\bar{\sigma} = \sqrt{[(\sigma_1-\sigma_2)^2+(\sigma_1-\sigma_3)^2+(\sigma_2-\sigma_3)^2]/2}$$

where σ_i is a principal stress.

The strains are:

$$\varepsilon_1 = (\sigma_1-\nu_p\sigma_2-\nu_p\sigma_3)/E_s$$

$$\varepsilon_2 = (\sigma_2-\nu_p\sigma_1-\nu_p\sigma_3)/E_s$$

$$\varepsilon_3 = (\sigma_3-\nu_p\sigma_1-\nu\ \sigma_2)/E_s$$

The stresses in the aluminum are:

$$\left.\begin{aligned} \sigma_1 &= K_1Q/t = K_1\ pr/t_a \\ \sigma_2 &= K_2Q/ta = K_2\ pr/2t_a \end{aligned}\right\} \quad (1)$$

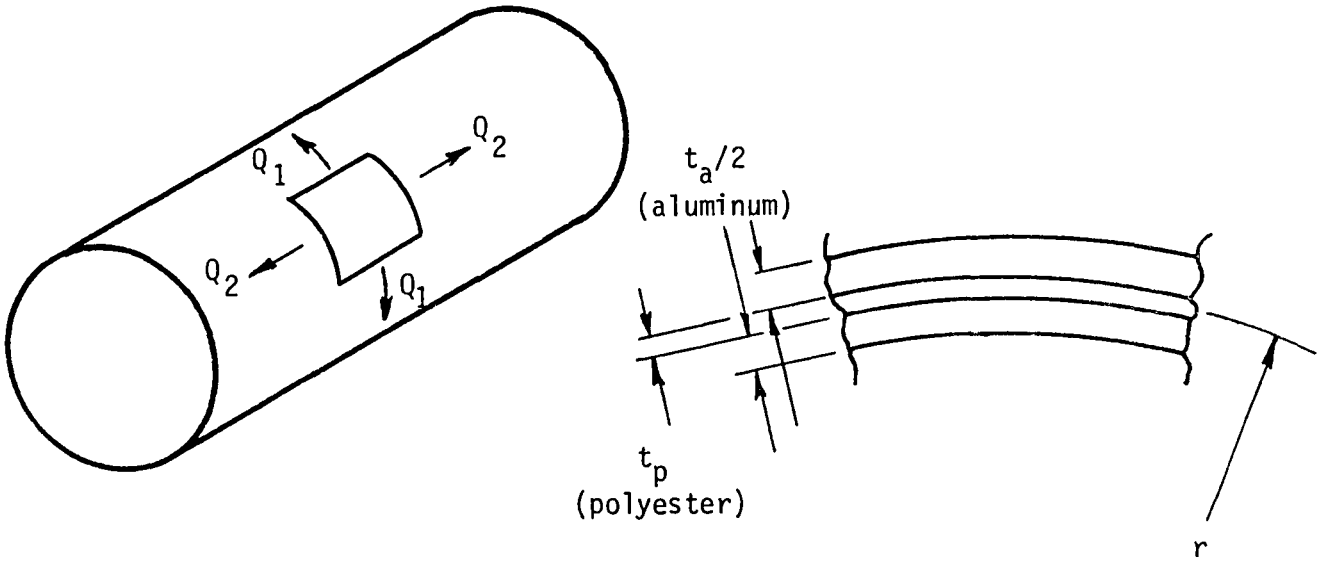

Figure 19. - Cylinder geometry.

The effective stress becomes

$$\bar{\sigma} = \sqrt{[(K_1-K_2/2)^2+(K_1-0)^2+(K_2/2-0)^2]/2}\ pr/t_a$$

$$= \sqrt{K_1^2-K_1K_2/2+K_2^2/4}\ pr/t_a \qquad (2)$$

Alternately

$$p = \bar{\sigma}\ t_a/r\sqrt{K_1^2-K_1K_2/2+K_2^2/4} \qquad (3)$$

Ignoring elastic strain in the aluminum, the plastic strains are, for $\nu_p = 0.5$,

$$\varepsilon_1 = (K_1-K_2/4)\ pr/E_s t_a \qquad (4)$$

$$\varepsilon_2 = (K_2-K_1)\ pr/2E_s t_a \qquad (5)$$

Similarly, the stresses and strains in the polyester are

$$\left.\begin{aligned}\sigma_1 &= (1-K_1)\ pr/t_p \\ \sigma_2 &= (1-K_2)\ pr/2t_p\end{aligned}\right\} \qquad (6)$$

$$\varepsilon_1 = (1-\nu/2-K_1+\nu K_2/2)\ pr/E_p t_p \qquad (7)$$

$$\varepsilon_2 = (\tfrac{1}{2}-\nu+\nu K_1-K_2/2)\ pr/E_p t_p \qquad (8)$$

The strains in the aluminum are equal to the strains in the polyester. Therefore, Equations (4) and (7) are equated, and Equations (5) and (8) are equated to produce

$$K_1(1+E_p t_p/E_s t_a)-K_2(\nu/2+E_p t_p/4E_s t_a)-1+\nu/2=0$$

$$K_1(\nu+E_p t_p/2E_s t_a)-K_2(\tfrac{1}{2}+E_p t_p/2E_s t_a)+\tfrac{1}{2}-\nu=0$$

Solving the above two equations simultaneously yields

$$K_1 = \frac{1-\nu^2-\nu C+1.25C}{1-\nu^2-\nu C+2C+0.75C^2} \tag{9}$$

$$K_2 = \frac{1-\nu^2-2.5\nu C+2C}{1-\nu^2-\nu C+2C+0.75C^2} \tag{10}$$

where $C = E_p t_p/E_s t_a$

For any $\bar{\sigma}$ and its corresponding E_s, the load distributions, stresses and strains in the aluminum and polyester, and the pressure can be obtained.

Depressurization. - When the pressure is removed, the aluminum was assumed to unload elastically. Therefore, the changes in stress can be calculated by applying an equal and opposite pressure.

The strains in the aluminum, per Equations (4) and (5) are

$$\Delta\varepsilon_1 = (K_1-\nu K_2/2)\Delta pr/E_a t_a$$

$$\Delta\varepsilon_2 = (K_2/2-\nu K_1)\Delta pr/E_a t_a$$

and the strains in the polyester per Equations (7) and (8) are

$$\Delta\varepsilon_1 = (1-\nu/2-K_1+\nu K_2/2)\Delta pr/E_p t_p$$

$$\Delta\varepsilon_2 = (\tfrac{1}{2}-\nu+\nu K_1-K_2/2)\Delta pr/E_p t_p$$

The strains must be equal in both the polyester and aluminum:

$$K_1-\nu K_2/2=(1-\nu/2)/(1+E_p t_p/E_a t_a) \tag{11}$$

$$K_2/2-\nu K_1=(\tfrac{1}{2}-\nu)/(1+E_p t_p/E_a t_a) \tag{12}$$

Solving Equations (11) and (12) simultaneously yields

$$K_1=K_2=\frac{(Et)_a}{(Et)_a+(Et)_p} \tag{13}$$

Equations (1) and (13) are then used to calculate the delta stresses:

$$(\Delta\sigma_1)_a = \frac{pr}{t_a+E_p t_p/E_a}$$

$$= pr/\left(t_a+E_p t_p/E_a\right)$$

$$(\Delta\sigma_2)_a = (\Delta\sigma_1)_a/2$$

$\Delta\sigma_1$ and $\Delta\sigma_2$ are subtracted from the σ_1 and σ_2 calculated in Section 6.1 for aluminum to obtain the residual compressive stress in the aluminum. The effective stress or equivalent uniaxial stress is then:

$$\sigma = \sqrt{\sigma_1^{\,2}-\sigma_1\sigma_2+\sigma_2^{\,2}}$$

This compressive stress was subtracted from the critical buckling stress.

Critical Buckling Stress. - Per Reference 8, the critical buckling stress for an isotropic cylinder under axial compression is

$$f_{cr} = CE_a t_a / r\sqrt{3(1-\nu^2)} \qquad (14)$$

where C, obtained empirically for cylinders having an r/t < 1500, is

$$C = 1-0.901\left[1-\exp(-\sqrt{r/256t_a})\right] \qquad (15)$$

Because of the polyester and the bond lines, the test cylinders are not isotropic. The plastic inner layer reduces the critical buckling stress because it places a residual compressive stress in the aluminum as discussed in Section 6.1. It also tends to increase the critical buckling stress because a) it separates the aluminum faces like a honeycomb construction, or b) it adds both thickness and stiffness.

Douglas Aircraft in 1961 determined by analysis and test the increase in strength that a second layer provides. The quantity, M, of Figure 20 represents the increase in strength of the two-layer cylinder under axial compression over the single layer shell. Equation (14) therefore needs to be multiplied by M to obtain the final critical buckling stress.

The critical buckling load is obtained by multiplying the critical buckling stress by the cross sectional area of the aluminum:

$$P_{cr} = 2\pi CME_a t_a^2/\sqrt{3(1-\nu^2)} \qquad (16)$$

where C and M are obtained from Equation (15) and Figure 20, respectively.

6.2 Cylinder Construction

The composite was made by laying up the materials in the following order and bonding them together using a hot iron:

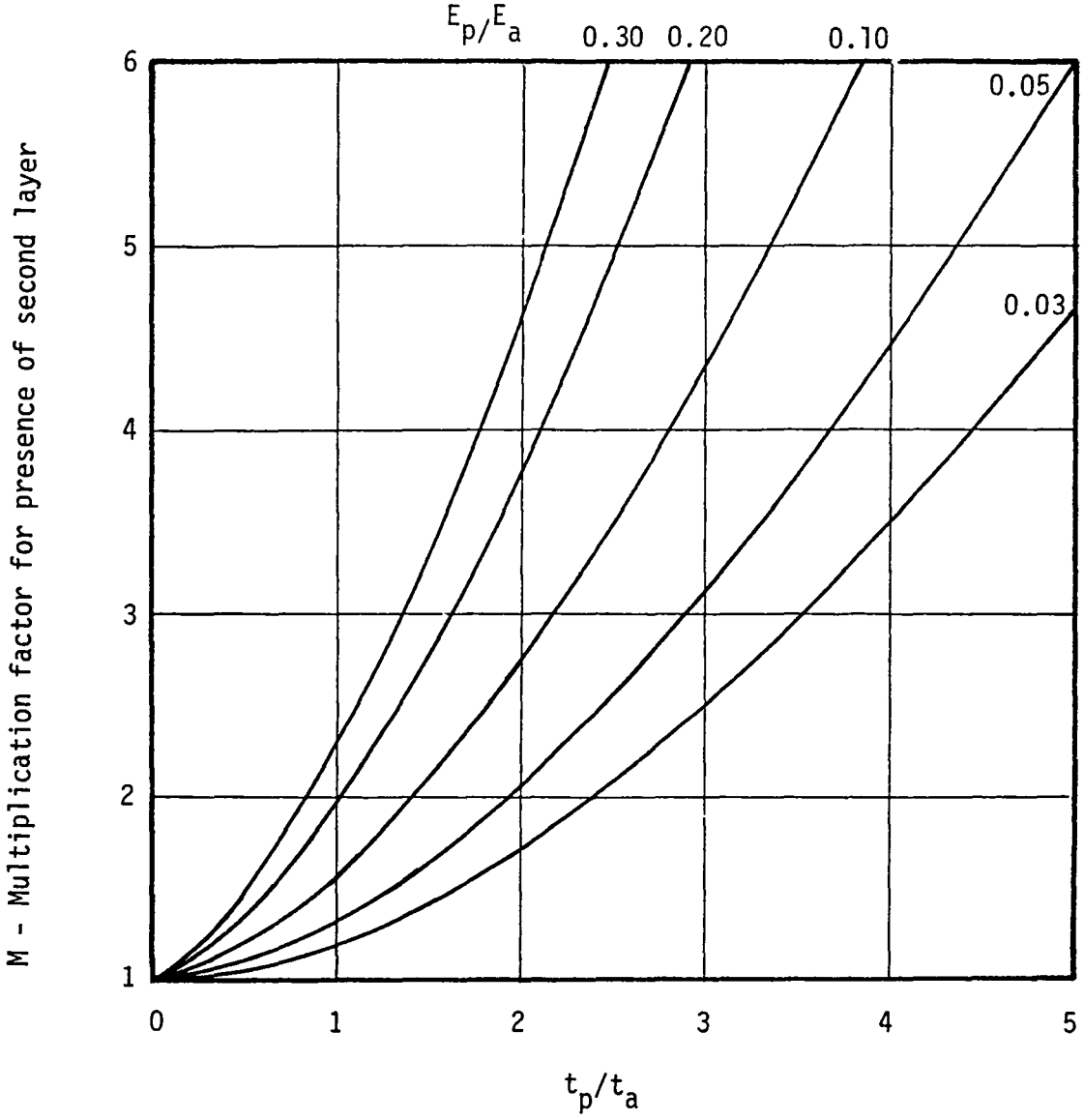

Figure 20. - Buckling of two-layer cylindrical shells under axial compression.

t mm 1100-0 aluminum foil
0.025 mm T-100 dry film adhesive
0.013 mm polyester
0.025 mm T-100 dry film adhesive
t mm 1100-0 aluminum foil

The thicknesses of the aluminum foil were 0.025, 0.038, and 0.051 mm. Gores, 160 mm by about 500 mm, were cut from the composite.

For assemblying the gores, 25 mm wide tape was made from the following layup:

0.013 mm polyester
0.025 mm T-100 dry film adhesive
0.025 mm 1100-0 aluminum foil
0.025 mm T-100 dry film adhesive

Two gores were butt-jointed and held together with the tape on both sides of the composite. The ends were attached to rigid plastic 102 mm in diameter.

The result were cylinders 102 mm in diameter by 460 mm long. Three cylinders were made from each of the three thicknesses for a total of nine cylinders. Figure 21 shows one cylinder of each thickness as built and prior to inflation.

6.3 Testing

Stress-Strain. - Five specimens of each aluminum thickness were tested per ASTM E345 "Tension Test of Metallic Foil" and referenced ASTM E8 "Tension Testing of Metallic Materials". A CRE Scott Tester was used. Specimen widths were 12.7 mm wide; gage length was 127 mm. Crosshead speed was 1.1 mm/second.

The average results are shown in Figure 22 compared with typical values according to Reference 9. The big surprise was that the elastic modulus of our test data was only about 10% of that of typical aluminum.

The results were spot checked on a different machine by different people, and the data appear to be correct.

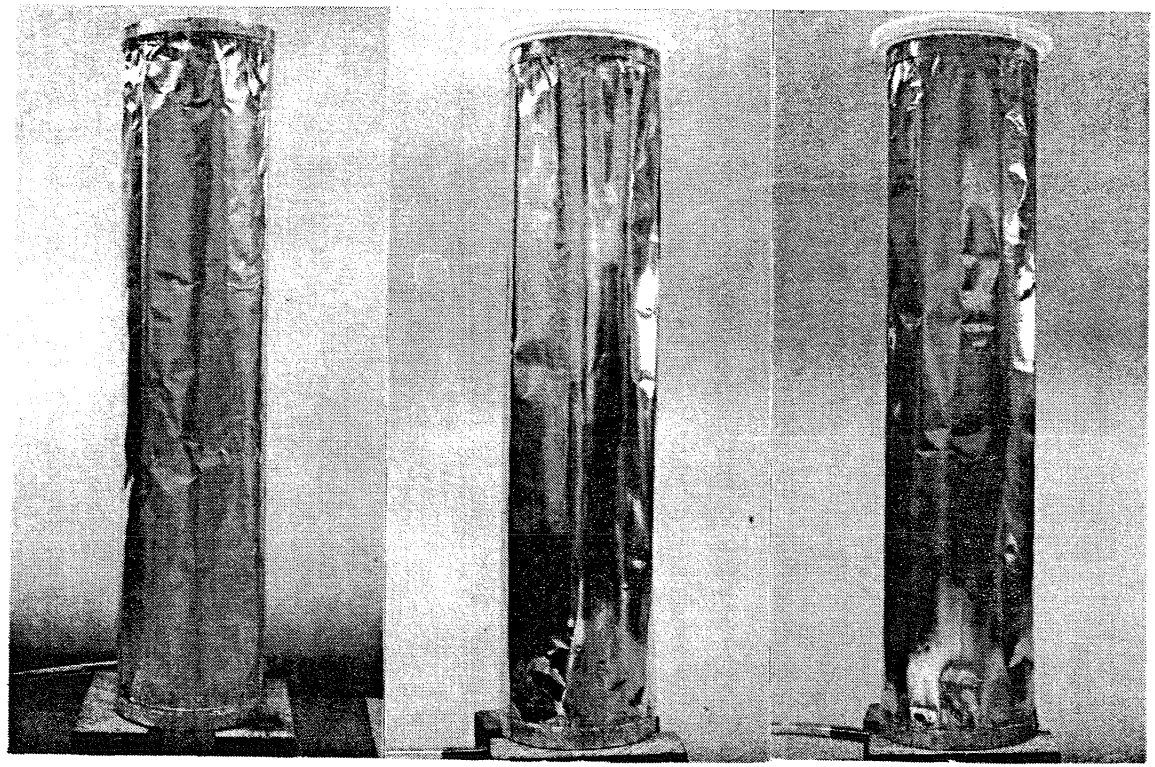

t_a = 0.050 mm t_a = 0.076 mm t_a = 0.102 mm

Figure 21. - As-built cylinders.

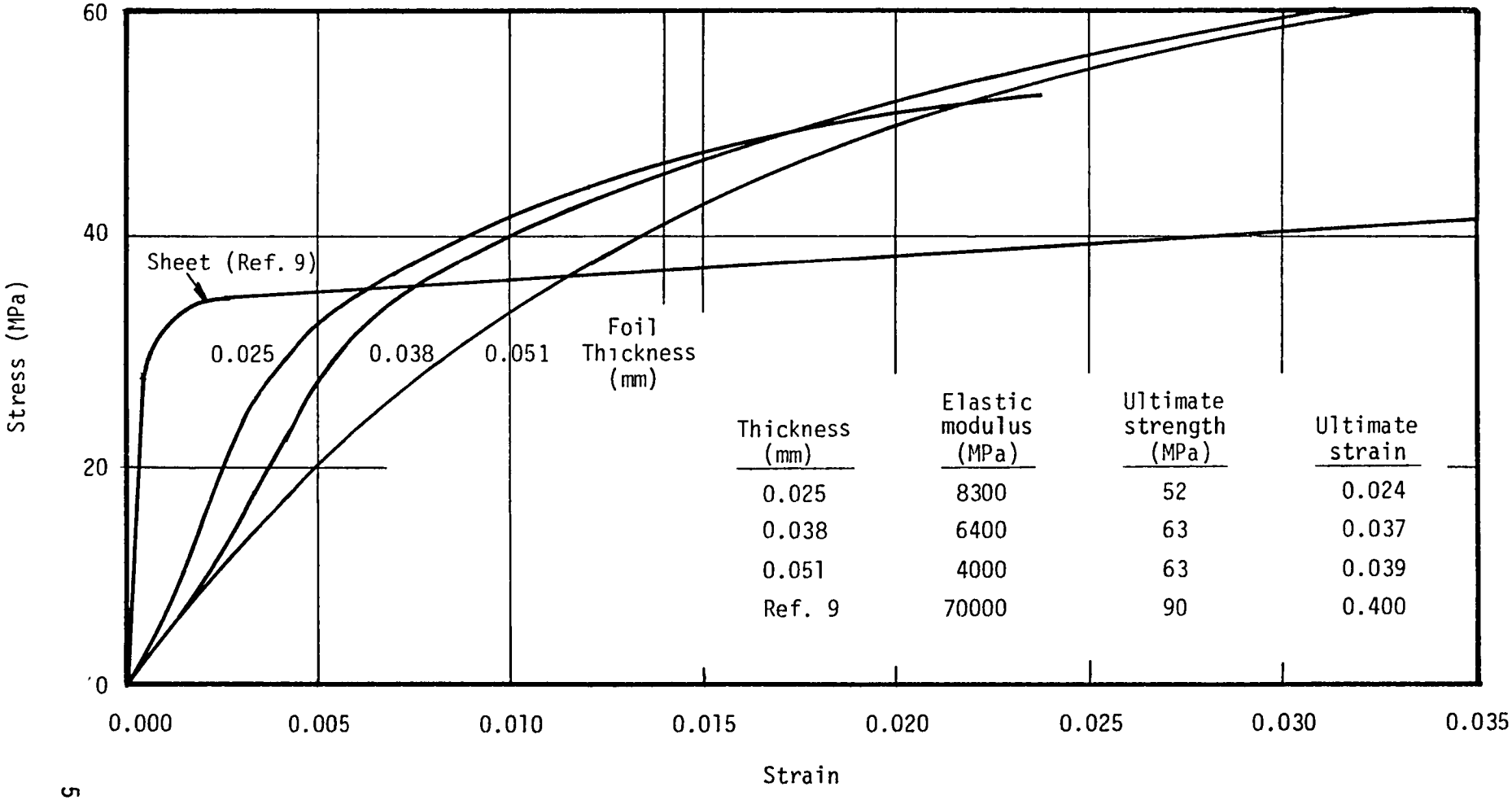

Figure 22. - 1100-0 aluminum foil tensile data

The results of testing the 0.013 mm polyester film per ASTM 0882 are shown in Figure 23. These appear to be reasonable.

Cylinders. - In prior work, stressing the aluminum well into the yield range did result in local failures (pinholes in the aluminum) and cylinder buckling did appear to occur in such weak areas. Therefore, for this set of cylinders, it was decided to stress the aluminum just above the elastic limit. From the four curves of Figure 21, the stress level, $\bar{\sigma}$, of 28.5 MPa was selected. Corresponding strains for the different thickness aluminums were then taken from the curves.

These and other values (E_p = 760 MPa, t_p = 0.013 mm, ν = 0.3, and r = 51 mm) were used in Equations (9), (10), and (3) to obtain pressure values:

t_a(mm)	Strain	E_a(MPa)	K_1	K_2	P(MPa)
0.050	0.0040	7120	0.978	0.986	0.033
0.076	0.0054	5280	0.980	0.988	0.050
0.102	0.0080	3560	0.978	0.987	0.067

The nine cylinders were tested one at a time. Each was first slowly pressurized to the above level and held at pressure for five minutes. Figure 20 shows three of the cylinders under pressure.

Most of the wrinkles were removed. (Compare Figures 24 and 21 -- which are photos of the same cylinders.) It appeared that only manufacturing defects remained. Slightly higher pressures may have been beneficial to remove some of these.

A slightly higher pressure would not have been beneficial to the cylinders containing 0.102 mm of aluminum thickness. The tape at the seams contained only 0.051 mm thick aluminum. Two of these cylinders exploded shortly after reaching 0.067 MPa pressure (Figure 25). The third cylinder (Figure 24) started leaking at a seam at 0.067 MPa, pressure was not maintained, and the cylinder survived.

Pressure was then released from the cylinders. Surface appearance did not change significantly.

The cylinders were then loaded in compression. Two cylinders were loaded to failure by placing steel weights on top as seen in Figure 26. It was felt

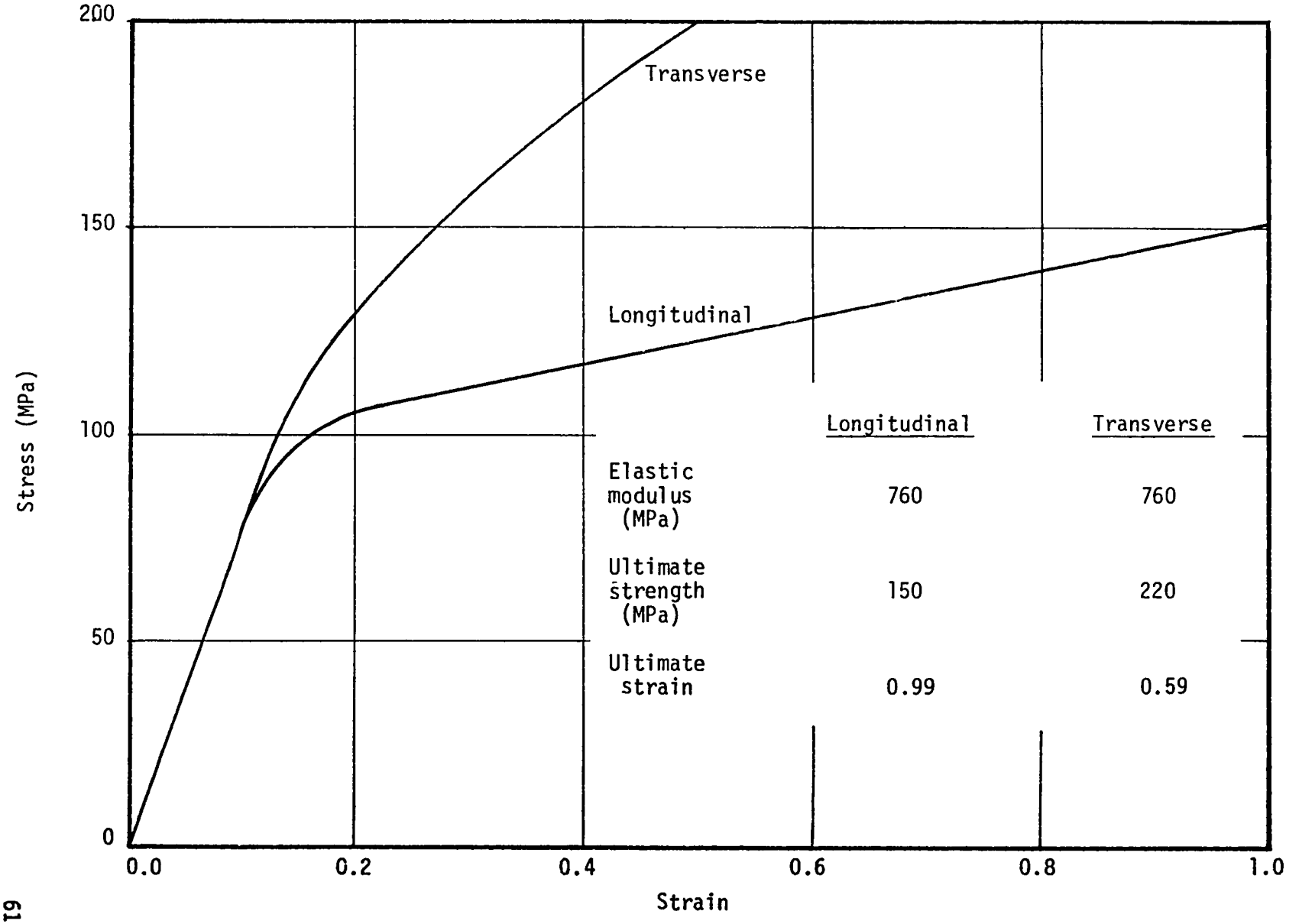

Figure 23. - 0.013 mm polyester tensile data.

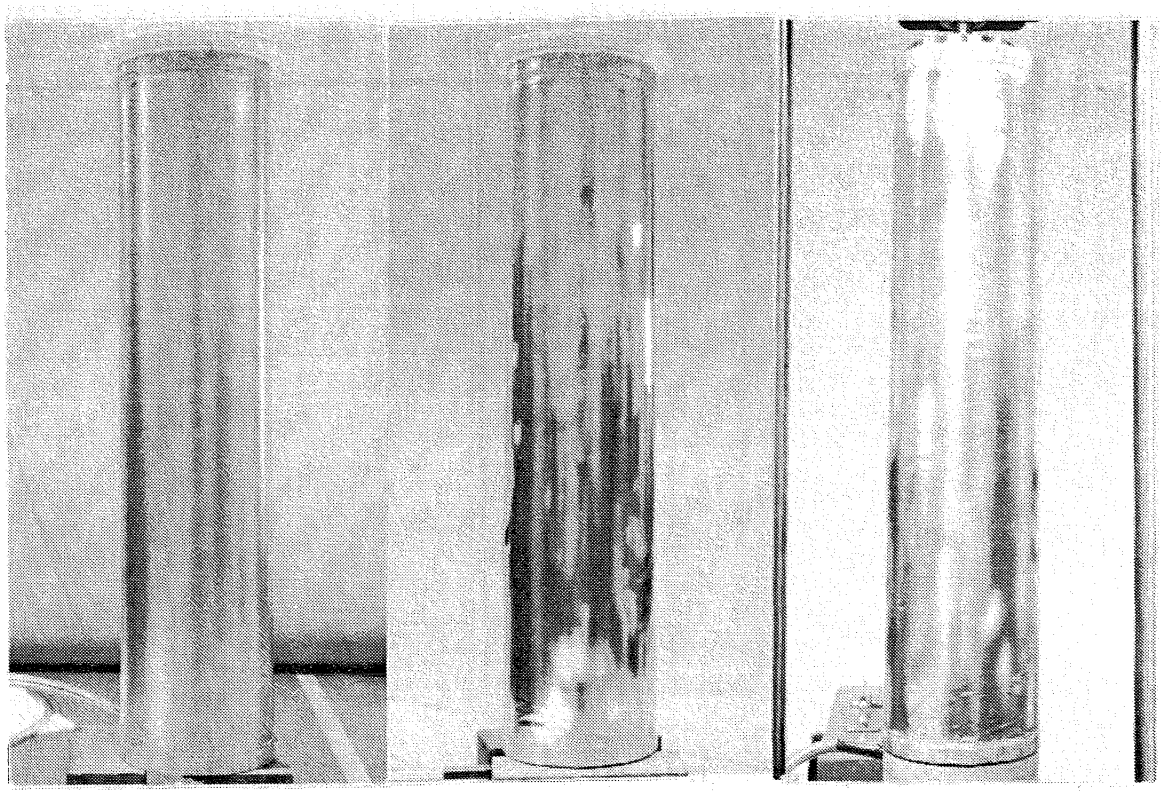

Figure 24. - Pressurized test cylinders.

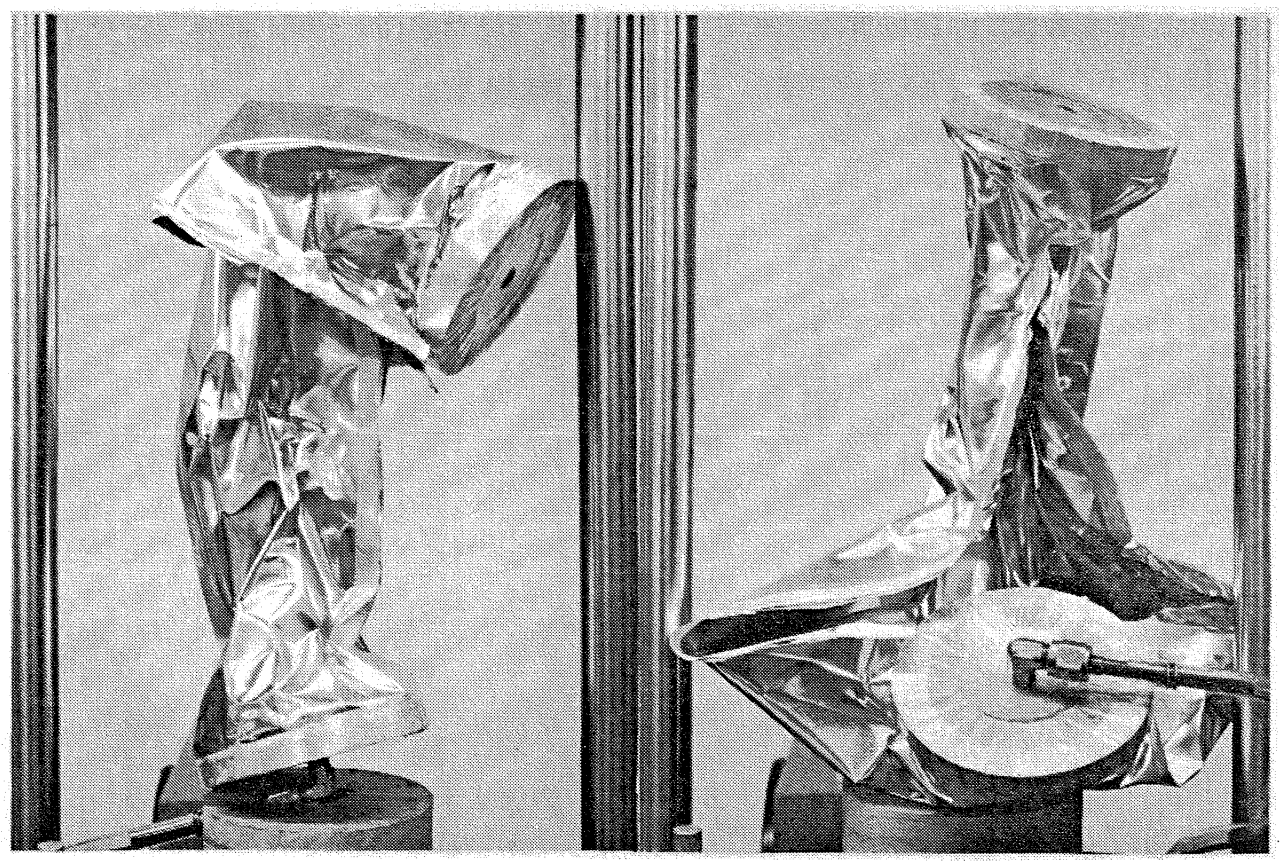

Figure 25. - Test cylinders exploded due to insufficient aluminum at the seams.

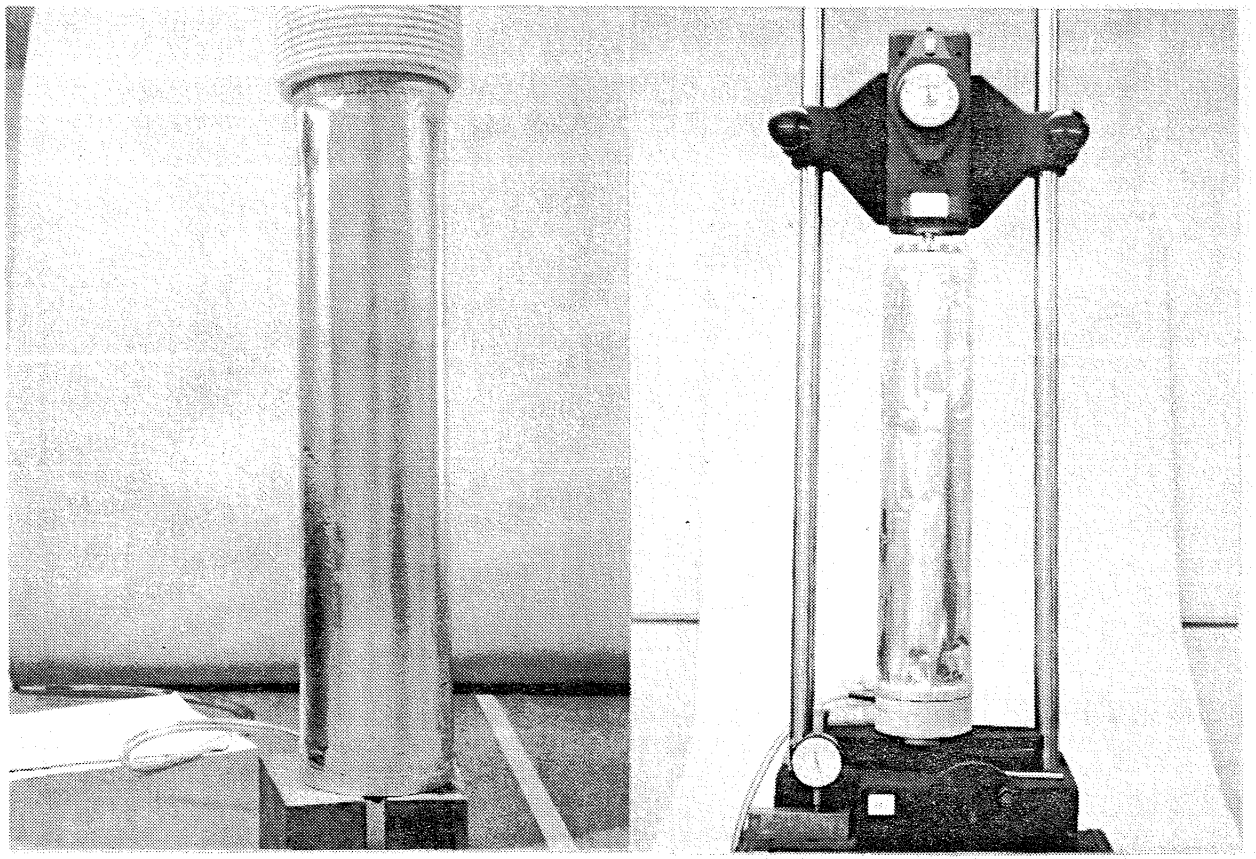

a) With steel weights.

b) With Ametek tester.

Figure 26. - Cylinder loading methods.

that this lacked some control, so the remaining five were tested in an Ametek tensile tester (also Figure 26). With the latter, bending moments were less. Also, the buckling load could be determined with greater precision since the compressive force cannot increase when buckling occurs.

Failures of the cylinders having 0.050 mm thick aluminum are shown in Figure 27. All three failed at the ends where the manufacturing defects were most severe.

Failures of the cylinders having 0.076 mm thick aluminum are shown in Figure 28. Again failure occurred at the ends except for the first cylinder.

Failure of the 0.102 mm thick aluminum shell is shown in Figure 29. Failure occurred at the center right at the place where the seam leaked during pressurization. Figure 29 clearly shows the classical diamond pattern that should occur at buckling failure.

The buckling loads were as follows:

Aluminum Thickness (mm)	Buckling Load (Newtons) for Cylinder No.1	No.2	No.3
0.050	53	45	56
0.076	114	134	148
0.102	232	---	---

6.4 Evaluation

When the cylinders are pressurized significantly into the plastic area of the aluminum, the polyester is still operating in its elastic region. Therefore, when the pressure is removed, the polyester will force the aluminum into compression and the cylinder will have reduced compressive strength. (In testing prior to this program, one cylinder was made in which the polyester and aluminum thicknesses were equal. The cylinder buckled as soon as pressure was removed.)

The analysis for this pre-stress was provided in Section 6.1. Since the test cylinders were stressed to just above the proportional limit by pressure, the pre-stress was insignificant and the analysis of Section 6.1 was not used.

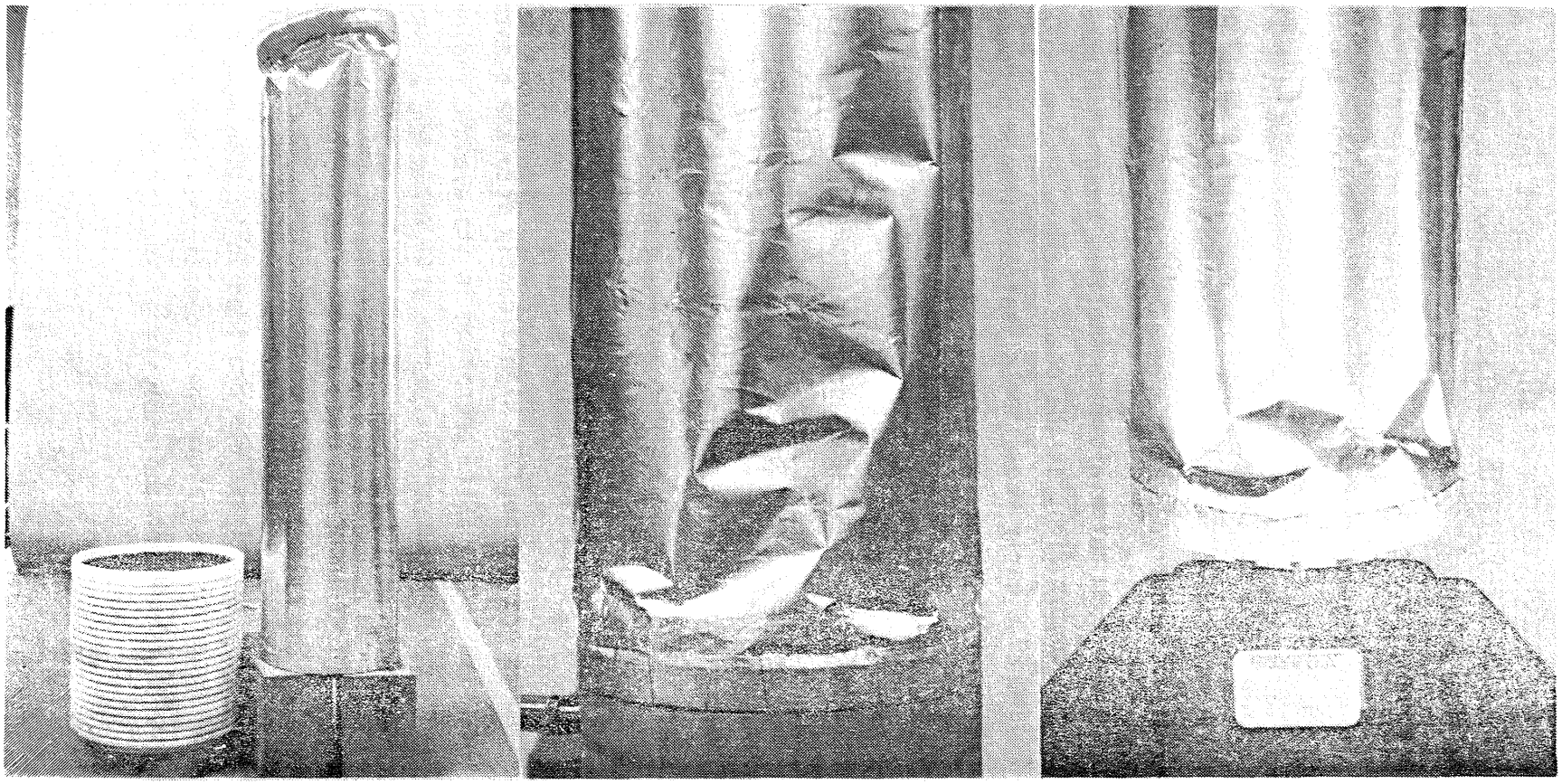

Figure 27. - Buckling failure of 0.050 mm aluminum cylinders.

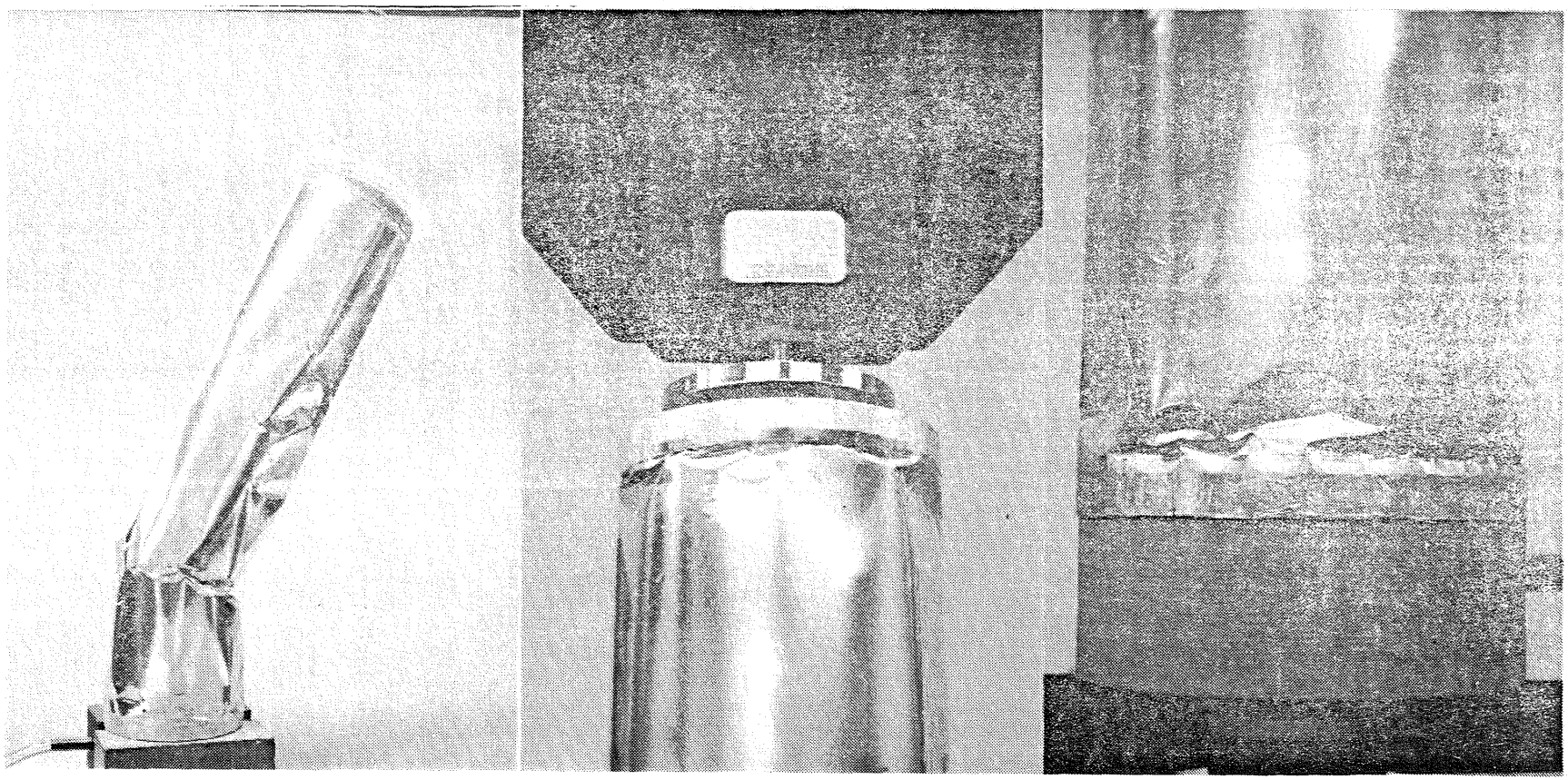

Figure 28. - Buckling failure of 0.076 mm aluminum cylinders.

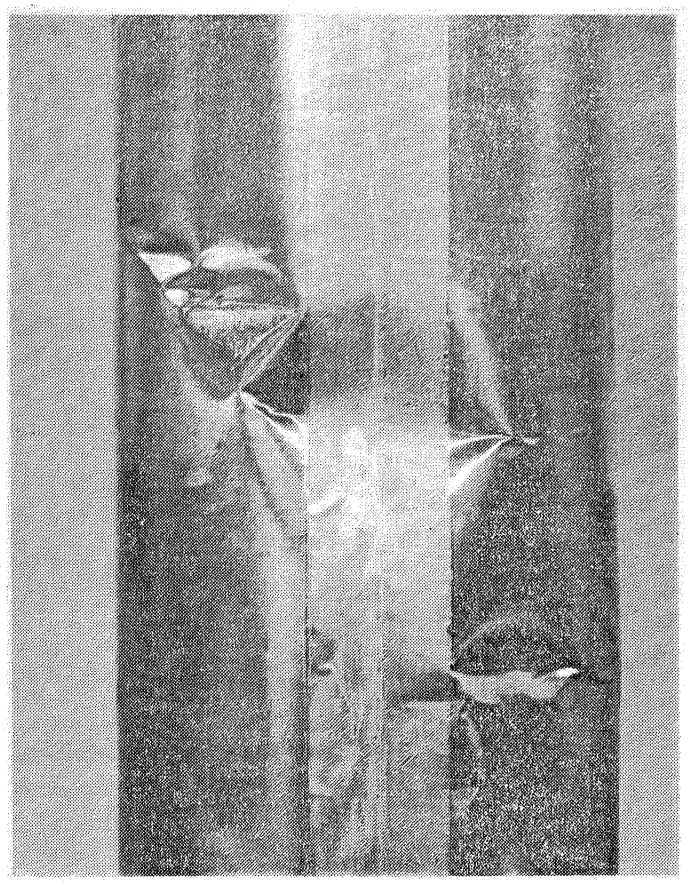

Figure 29. - Buckling failure of 0.102 mm aluminum cylinder.

Critical buckling load was calculated per Section 6.1, Equation (16). The results are plotted in Figure 30 for three aluminum modulus values:

70000 MPa - typical aluminum
17000 MPa - curve fit of the cylinder test data
8300 MPa - test data for 0.025 mm aluminum foil

Figure 30 shows that the critical buckling load is a function of t^2 as classical buckling theory for long ($L^2 > 42tr$) cylinders states. This is encouraging but expected.

The semi-empirical curves indicate that either the test modulus values of Figure 22 are too low or the coefficient C of Equation (16) is too pessimistic. Let us calculate coefficients (B) using the cylinder and the tensile test data, and the formula

$$P_{cr} = 2\pi B E_a t_a^2 / \sqrt{3(1-\nu^2)}.$$

Aluminum Thickness (mm)	Elastic Modulus (MPa)	Average Compressive Load (Newtons)	B	CK
0.050	8300	51	0.65	0.39
0.076	6400	132	0.94	0.42
0.102	4000	232	1.47	0.47

The coefficient, C, is empirical and accounts for imperfections in shells. It is always less than one. The coefficient, B, should also be less than unity. Something is incorrect, and the elastic modulus values are suspect.

The elastic modulus of 0.051 mm aluminum was measured again -- this time in the Ametek tensile tester previously shown in Figure 26. The foil was loaded in steps up to 35 MPa, then to zero and back to 35 MPa. The results are shown in Figure 31 along with the data generated per ASTM E345.

The elastic modulus was 3400 MPa initially -- essentially confirming the 4000 MPa value obtained per ASTM E345. However, after work hardening, the

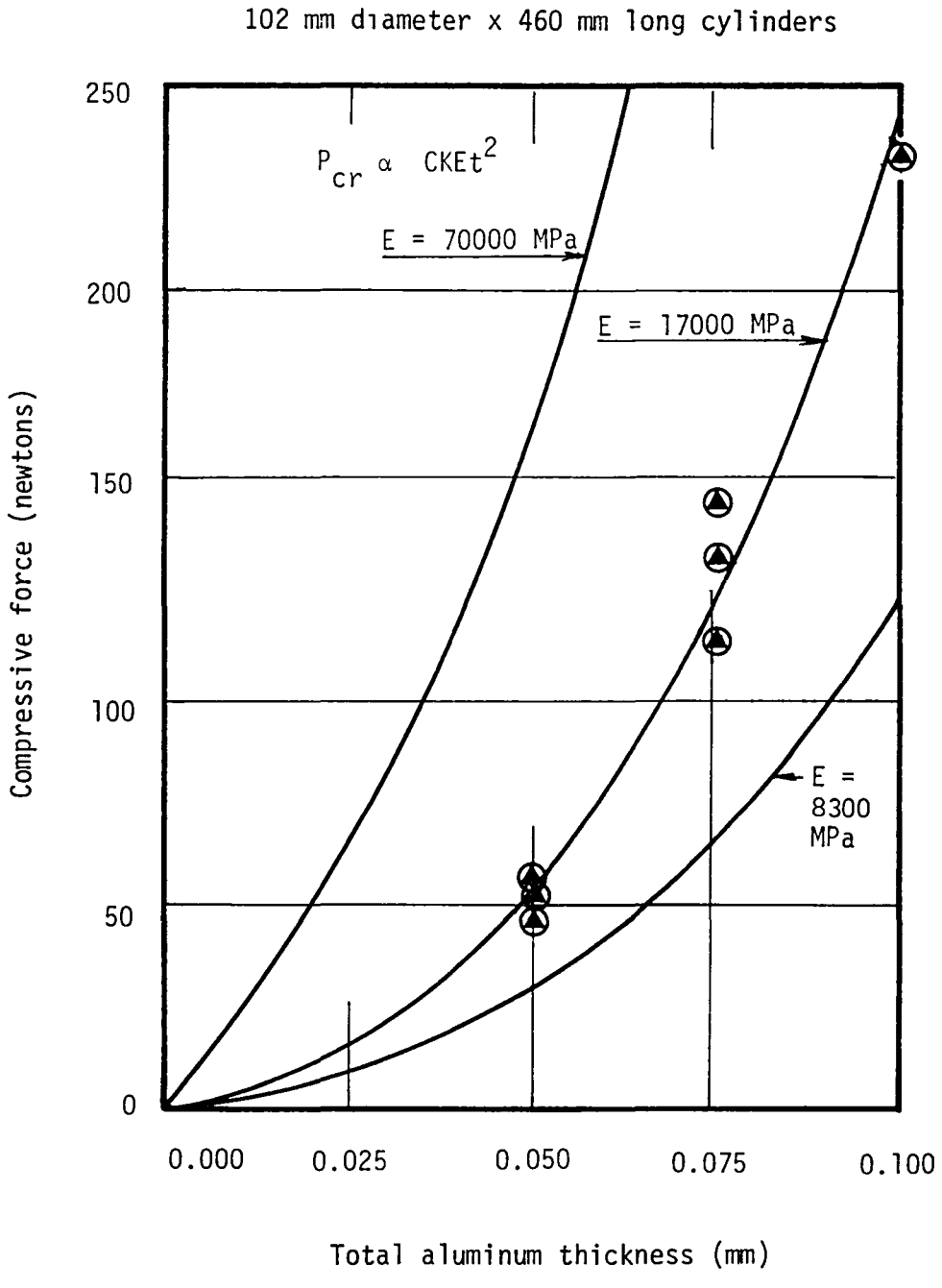

Figure 30. - Buckling strength of 102 mm diameter x 460 mm long.

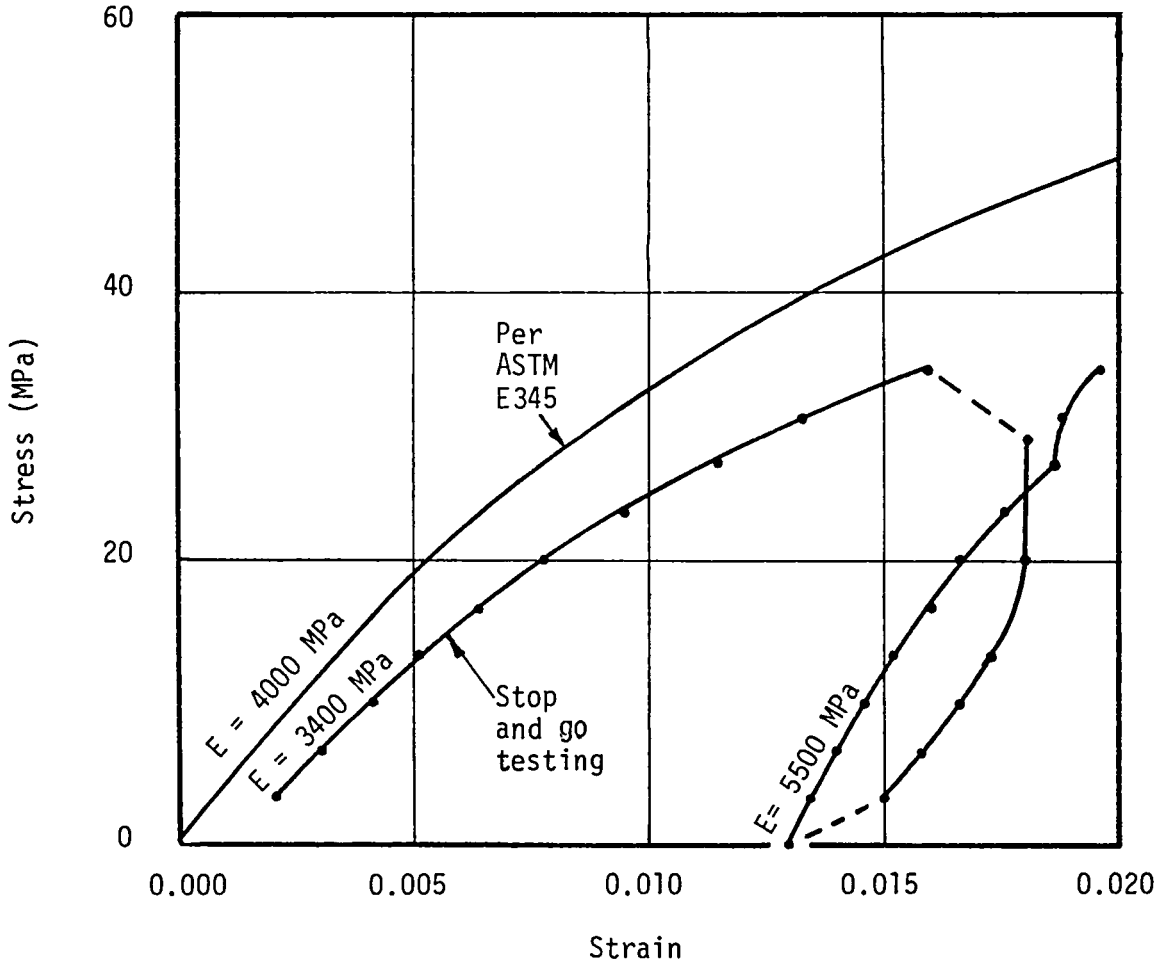

Figure 31. - Effect of initially yielding aluminum foil (0.051 mm 1100-0).

elastic modulus was 5500 MPa -- an increase of 37%. This percentage increase decreases B in the prior table to 1.07.

In retrospect, what is needed is extensive tensile data. Data needs to be gathered for the various composites as well as the basic materials. These specimens need to be taken to various plastic stress levels, then to zero, and finally to ultimate.

More cylinder fabrication and testing must also be done. The cylinders actually failed prematurely because the ends were poorly made -- resulting in failure at the ends. Also the aluminum in the seams was of improper thickness for the two heavier sets of cylinders. Finally, pressurization needs to be done to a variety of levels to achieve the optimum.

This work proves the practicality of the approach. Despite the belief that the cylinders failed prematurely, they still were stronger than the earlier analysis indicates.

7.0 WEIGHT AND PACKAGE VOLUME

A parametric study was performed to determine the weight and packaging volume of inflated antennas that range in diameter from 10 to 1000 meters and in focal lengths from 3.75 to 2000 meters ($3/8 < f/d < 2$).

The configuration is shown in Figure 32. The paraboloid and cone are constructed from gores of thin film and assembled with tape of essentially the same material. The paraboloid is aluminized to reflect radiation.

The torus is made from a composite of 0.025 mm aluminum/0.013 mm polyester/ 0.025 mm aluminum. It is erected by carbon dioxide and yielded such that it maintains structural integrity after the CO_2 is vented or lost.

The main body of the antenna is erected by water vapor. Initially the paraboloid is stressed to approximately yield to eliminate packaging wrinkles. Then the pressure is reduced to operate at 0.001 Pa.

The inflation system also contains a water supply to replace gas lost through holes in the thin film. These holes will be mainly the result of meteoroid penetration. Enough water is aboard to keep the antenna inflated for at least ten years.

Not included in this study or in the weights and package volumes are such items as the:

a) the feed
b) telemetry
c) attitude control
d) propulsion, and
e) power supply

The weight and volume of the antenna structure and inflation system were shown in Figures 5 and 6.

Weight breakdowns are given as a function of f/d for antenna diameters of 10, 100 and 1000 meters in Figures 33 through 35. The torus and carbon dioxide weights are at a minimum at $f/d = 0.515$ because that's where the torus load is at a minimum. (At f/d of $\frac{1}{4}$, the torus load becomes infinity as the cone becomes a flat plate.)

The following sections provide the formulas used to derive Figures 5, 6, 33, 34, and 35.

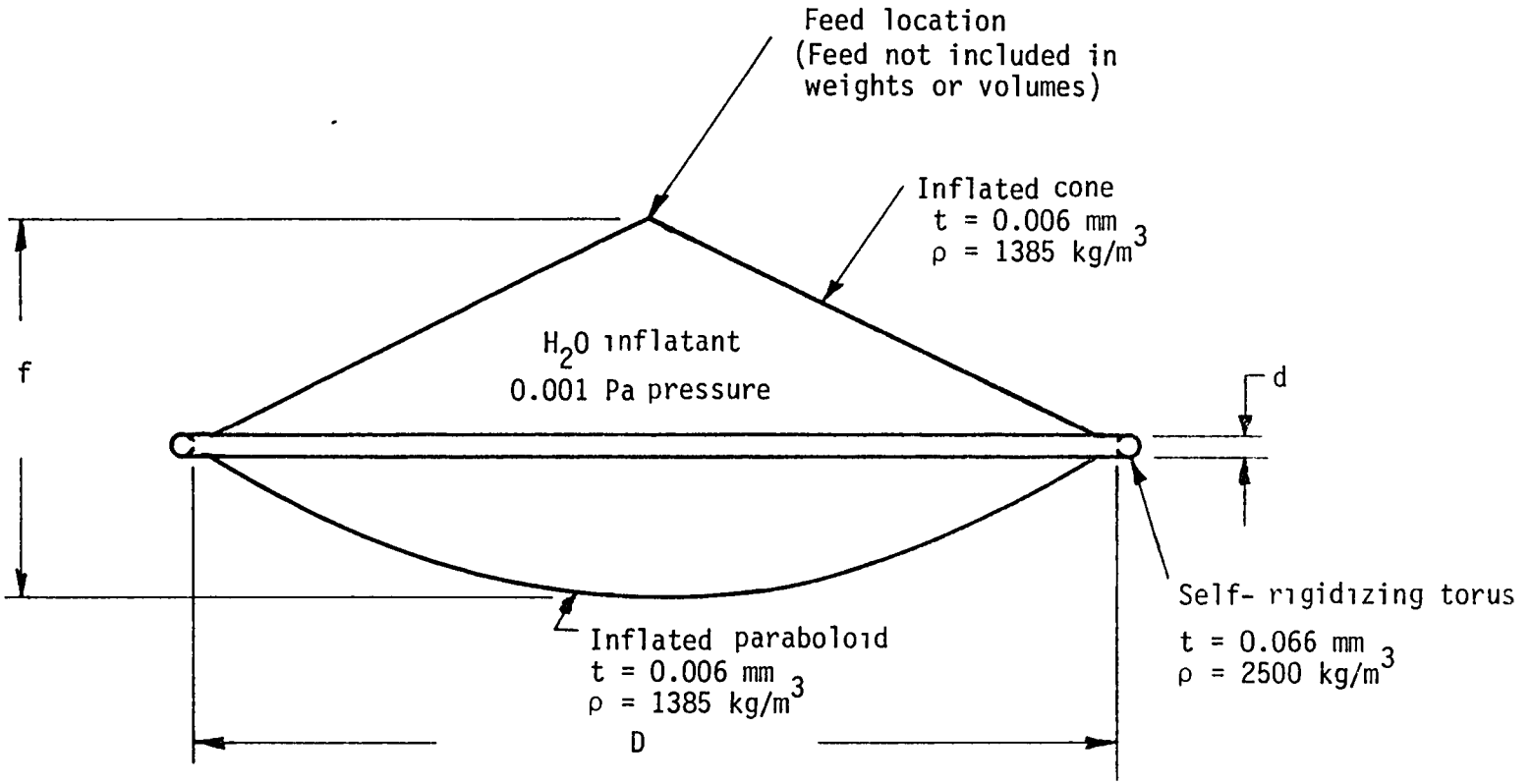

Figure 32. - Antenna configuration.

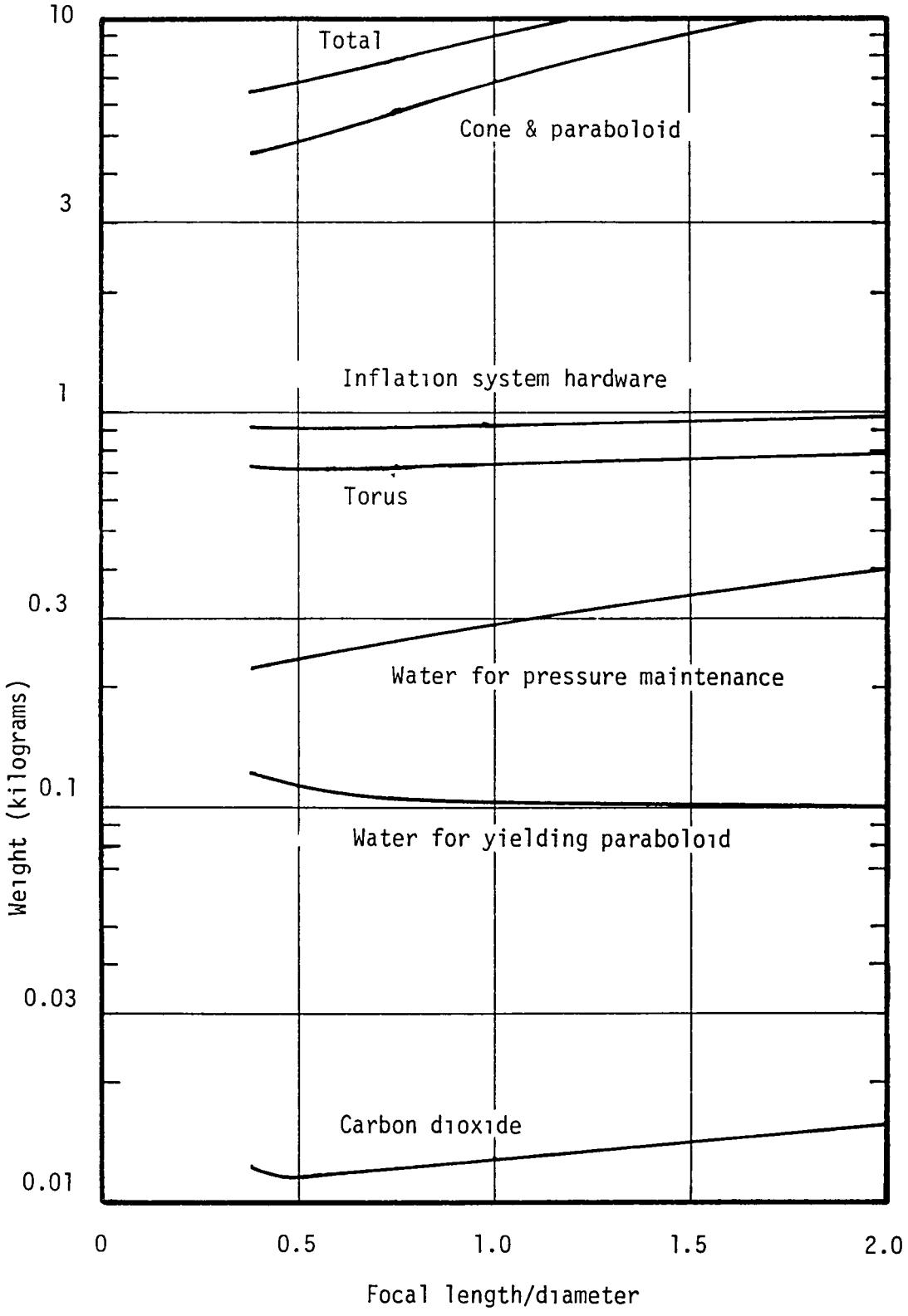

Figure 33. - Weight breakdown for 10-meter diameter reflector.

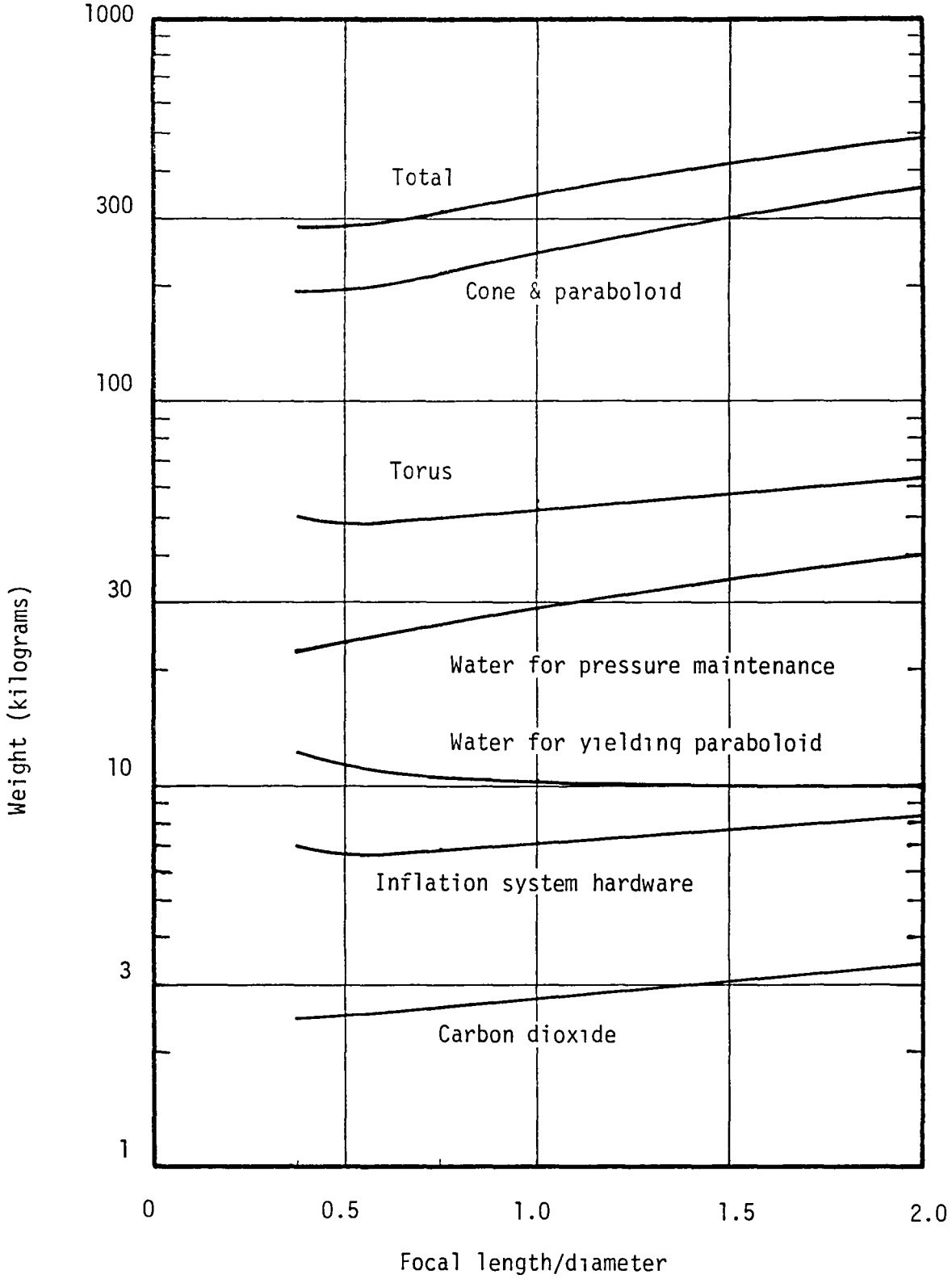

Figure 34. - Weight breakdown for 100-meter diameter reflector

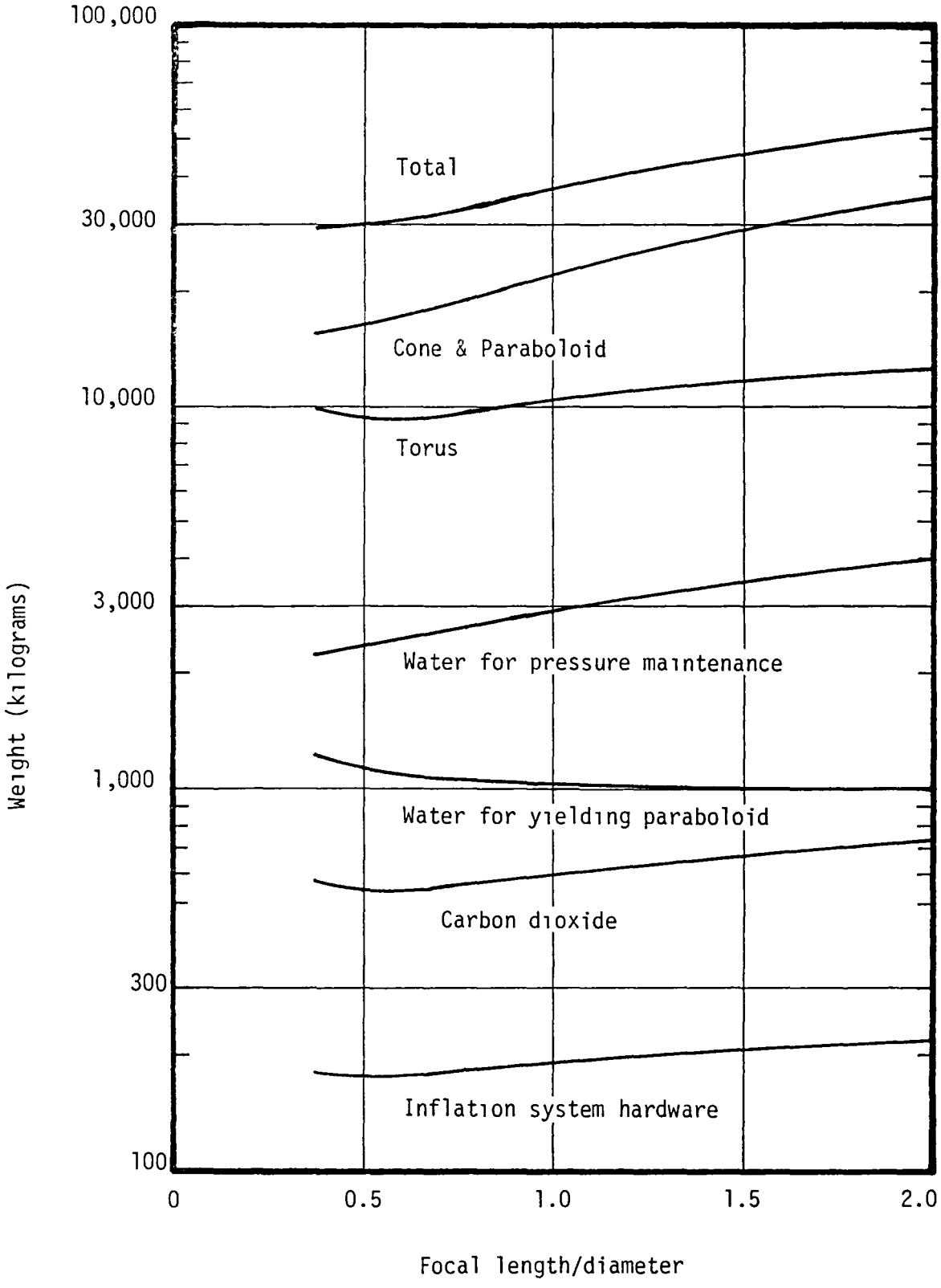

Figure 35. - Weight breakdown for 1000-meter diameter reflector.

7.1 Cone

The feed will normally be located at the cone tip. Because of the feed weight and because the stresses at the tip are near zero, a rigid cone is necessary at the tip so that the feed will move with the antenna during a maneuver. In this parametric study, the maneuver loads are unknown so it was assumed that the rigid cone would be 4.2 meters in base diameter for any size antenna. A rigid cone of this diameter will fit in the space shuttle cargo bay.

The allowable force on the feed would then be:

$$F = pA = (0.001)\pi(4.2)^2/4$$

$$= 0.014 \text{ Newtons}$$

which is likely to be satisfactory for most space antenna since accelerations tend to be very low.

The material volume in a thin cone is:

$$V = \pi RT\sqrt{R^2 + H^2}$$

where

$$R = D_T/2, \text{ and}$$

$$H = f\text{-}D_T^2/16f = (K\text{-}K^{-1})D_T/4.$$

Therefore

$$V = (K+K^{-1})\ \pi\ D_T^2\ t/8. \qquad (1)$$

It was assumed that the cone tip was made of 0.1 mm thick polyester with a density of 1385 kg/m^3. A cone tip for f/d = 1 would therefore weigh four kilograms. Between the cone tip and antenna torus is a thin film cone. The volume of the thin film cones is:

$$V = (K+K^{-1})\ \pi\ D^2 t/8. \qquad (2)$$

For this study, t = 0.00635 mm (¼ mil) and ρ = 1385 kg/m^3.

Gores of thin film must be held together by tape at the seams because thin film cannot be obtained in "infinite" widths. The gore and seam pattern used in the study is shown in Figure 36. This approach is used to reduce seam weight slightly. If the gore were continuous from the 1000 meter maximum diameter to the 4.2 meter diameter cone tip, the cone would be mostly seam near the tip.

For calculating weight and volume of the cone seams, the following were used:

$$W = 1.6 \text{ m}$$
$$w = 0.020 \text{ m}$$
$$t = 9(10)^{-6} \text{ m}$$
$$\rho = 1385 \text{ kg/m}^3$$

7.2 Paraboloid

The volume of a solid paraboloid of revolution is:

$$V = \pi R^2 H/2$$

where $R = D/2$ and $H = D^2/16f = D/4K$ for the outer surface of the thin film paraboloid, and where $R = D/2\text{-}t/\sin\theta = D/2\text{-}tK\sqrt{1+K^{-2}}$ and $H = D/4K\text{-}t$ for the inner surface. Subtracting the smaller volume from the larger and dropping terms containing t^2 and t^3 in the numerator yields:

$$V = (1 + \sqrt{1 + K^{-2}})\ \pi D2\ t/8 \qquad (3)$$

For this study, $t = 0.00635$ mm (¼ mil) and $\rho = 1385$ kg/m^3.

Uninflated, the gores are flat. There is an optimum pressure that strains the material in the hoop direction to approximately a circular cross section as previously shown in Figure 10. Analytically, this pressure is:

$$p = WEt/1.5(1\text{-}\mu)RD^2 \qquad (4)$$

where R in this case is the radius of curvature and E and t are properties of the gore.

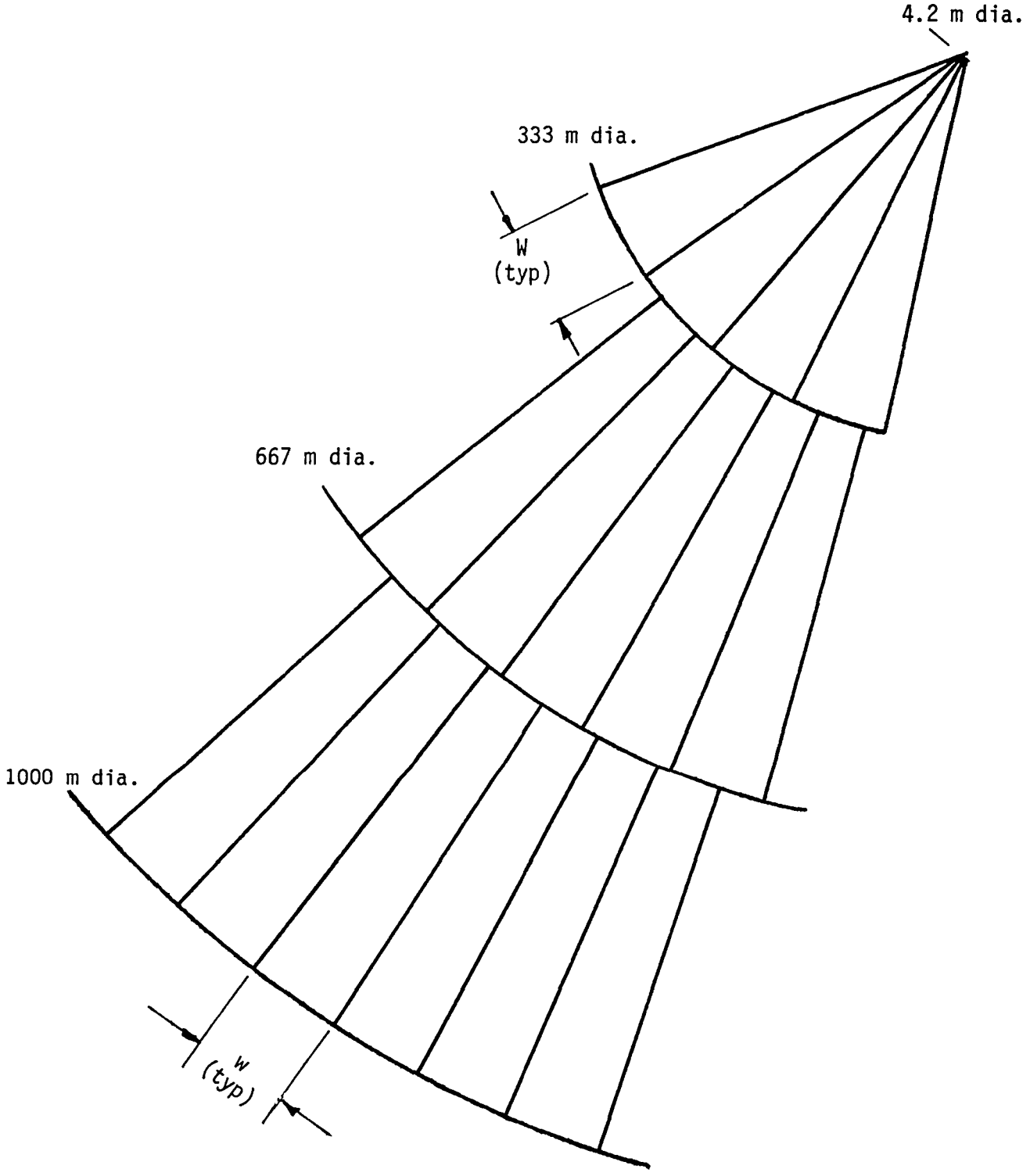

Figure 36. - Gore and seam pattern.

It is necessary to keep this optimum pressure as low as possible because meteoroids will puncture the antenna, and the replacement gas weight is proportional to operational pressure (Reference 2). Therefore, a pressure of 0.001 Pa was selected; this is at least 100 times solar pressure.

A paraboloid is nearly spherical in shape. By curve-fitting, it was determined that R for $0.25 < f/d < 2$ is:

$$R = (0.48\ K + 0.11)\ D \tag{5}$$

Substituting Equation (5) and $p = 0.001$ Pa, $E = 4.8(10)^9$ Pa, $t = 0.00635$ mm ($\frac{1}{4}$ mil), and $\mu = 0.3$ into Equation (4) yields:

$$W^2 = 1.654(10)^{-8}\ D^3\ (K + 0.23) \tag{6}$$

where W and D are in meters.

For diameters of approximately 30 meters or less, W is 50 mm or less. This is close to the normal seam tape width of 20 mm; therefore, it makes sense to produce 100 percent seam configurations that are constructed to the final parabolic surface. This is a (high labor) job of cutting small, thin film pieces and patching them together on a mandrel. For this parametric study, Equation (3) was used -- with $t = 0.009$ mm (adhesive included) and $\rho = 1385$ kg/m^3.

For larger diameter reflectors, Equation (6) was used to determine gore width. This value or 1.6 meters, whichever was smaller, was used in producing a seam and gore pattern like that previously shown in Figure 36. The length of a seam from the paraboloid center to its edge was derived by integrating:

$$L = \int \sqrt{(1 + K^2/4f^2)}\ dx$$

to arrive at

$$4L/D = \sqrt{1+K^{-2}} + K \ln(K^{-1} + \sqrt{1+K^{-2}}) \tag{7}$$

L varies only from 0.535 to 0.500 for $0.375 < f/d < \infty$.

7.3 Torus

The torus is loaded as shown in Figure 37. The internal pressure between the cone and paraboloid produces a force of $p\pi D^2/4$ and, therefore, a running load of $pD/4$. Normal to the plane of the torus, the loads are equal and opposite. In the plane of the torus, there is a running load that tries to collapse the torus. This load, derived from the geometry, is:

$$p' = (FS)pK(K^2+1)/4(K^2-1) \tag{8}$$

There will be occasional forces on the torus caused by orientation or translation of the antenna. These are generally small and mission dependent. For the purposes of this study, Equation (8) includes a factor of safety (FS), which has been set at four.

This thin-walled torus will fail due to buckling. According to Reference 10, such a ring can take:

$$p' = 24\ EI/D^3 \tag{9}$$

$$\text{where } I = (\pi + 2/3)d^3t/8$$

for the configuration shown in Figure 37. This doesn't include the overlapping seams which will increase the area moment of inertia of the torus cross section by 300 percent, 20 percent and 1 percent for diameters of 10, 100 and 1000 meters respectively.

The material volume of the Figure 37 torus is:

$$V = \pi\ Ddt(\pi + 1) \tag{10}$$

Combining Equations (8), (9) and (10) yields:

$$V^3 = 192.8\ pD^7t^2K(K^2+1)/(K^2-1)E \tag{11}$$

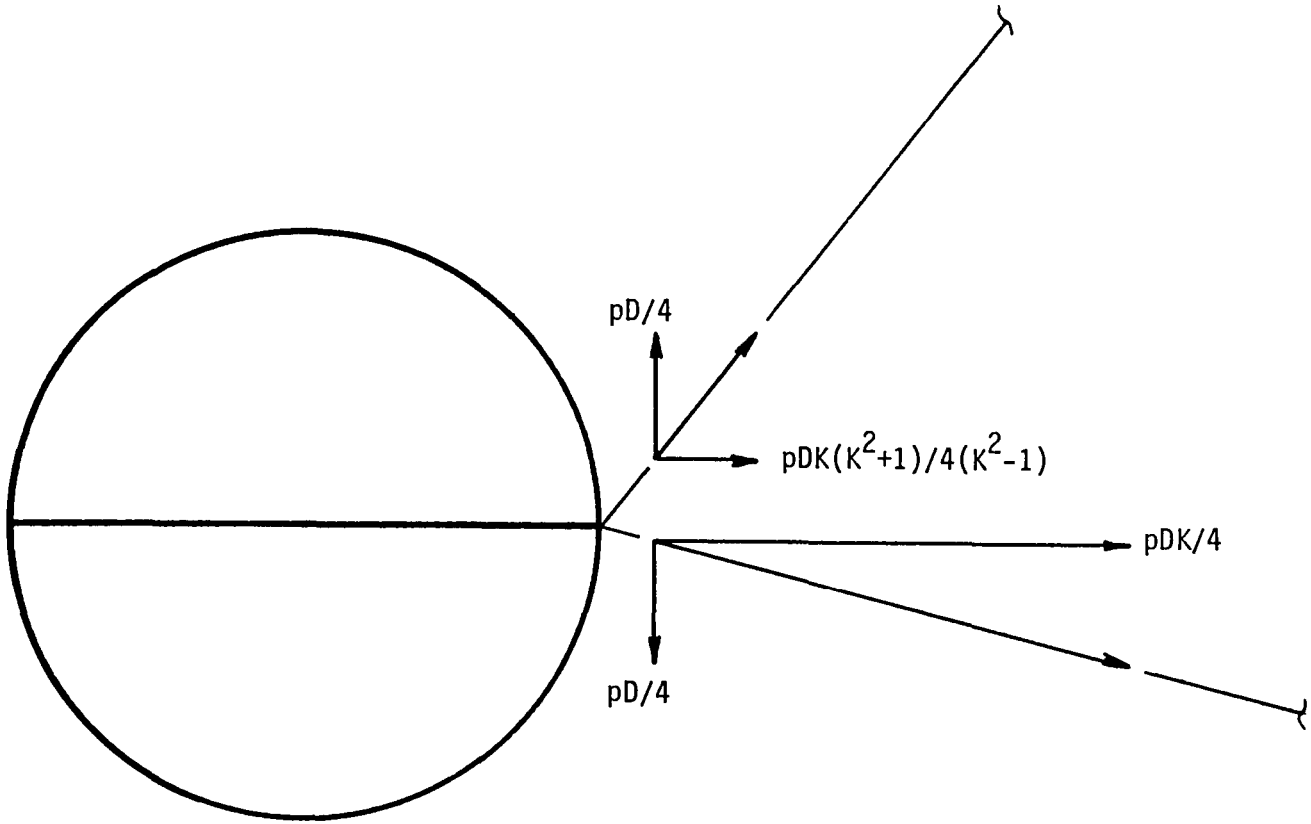

Figure 37. - Torus loads.

The torus is glued together using the same material as shown in Figure 38. By adding in this material it can be shown that Equation (11) becomes:

$$V = (1+1.185\ w/W)\left[\ 192.8\ pD^7t^2K(K^2+1)/(K^2-1)E\right]^{1/3}+4\pi wtD \qquad (12)$$

In this study, the following values were used:

$$w = 0.02\ m$$
$$W = 1.6\ m$$
$$P = 0.001\ Pa$$
$$t = 0.063\ mm$$
$$E = 5.86(10)^{19}\ Pa$$

The cross-sectional diameter (d) is calculated by equating Equations (8) and (9):

$$d^3 = D^4pK(K^2+1)/(K^2-1)3Et(\pi+2/3) \qquad (13)$$

For p = 0.001 Pa, E = $5.86(10)^{10}$ Pa and t = 0.063 mm, d is as follows:

	d(m) for f/d of		
Diameter (m)	3.8	1	2
10	0.0096	0.010	0.012
100	0.21	0.22	0.27
1000	4.5	4.7	5.7

A torus with a 0.01 m diameter could be impractical to build. However, Equation (13) doesn't include the stiffening effect of the torus seams (Figure 38) although the seam volumes (and weights) are included in Equation (12). Therefore, tori for small antenna can be significantly larger than indicated above without an additional weight penalty.

All parts made of 0.025 mm aluminum, 0.013 mm polyester, 0.025 mm aluminum composite. Heat sensitive adhesive film used to bond the five pieces together.

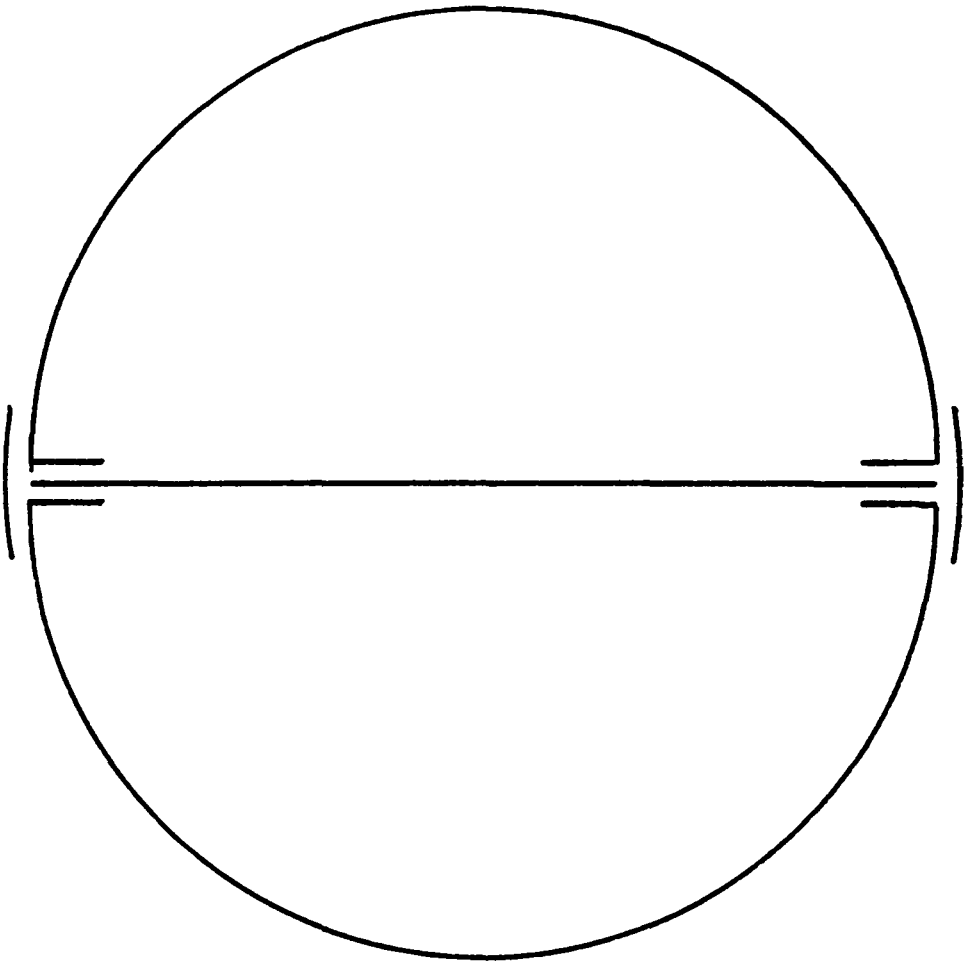

Figure 38. - Torus construction

7.4 Inflatant for Yielding the Paraboloid

Previous studies showed that water was the lowest weight, passive inflatant because of its low molecular weight and storage pressure. An active hydrazine system is likely to produce a lower weight system because hydrazine converts into molecules lower in weight than water. For conservatism, this study uses water as an inflatant.

The internal volume of the antenna is that within the paraboloid and cone:

$$V_{paraboloid} = R^2H/2 = \pi D^3/32K$$

$$V_{cone} = \pi R^2H/3 = \pi D^3(K-K^{-1})/48$$

Combining these yields:

$$V = \pi D^3(2K+K^{-1})/96 \tag{14}$$

The pressure is:

$$p = 2\ St/R \tag{15}$$

Where $R = D(.48K+.11) \approx 0.52DK$ for $.375 < f/d < 2$. (Water has a vapor pressure of 128 Pa at 0°C -- more than required by Equation (15) for the smallest K and D of interest.) The gas weight is:

$$w = p\ MV/R^*\ T \tag{16}$$

Substituting Equations (14) and (15) into (16) yields:

$$w = .126MStD^2(2K+K^{-1})/KR^*\ T \tag{17}$$

For this study,

$$MW = 18$$
$$S = 775(10)^5 Pa$$
$$t = 0.00635 \text{ mm}$$
$$R^* = 8314.34 \text{ J/kmol K}$$
$$T = 270K$$

The water's volume is: $V = w/\rho$ (18)

where $\rho = 1000 \text{ kg/m}^3$.

7.5 Inflatant for Maintaining Pressure

Reference 2 shows that the amount of inflatant required to replace gas lost through meteoroid holes is:

$$w = \sqrt{MW}\, pA\, Y^2/127.6 \quad (19)$$

where the units are kg for w, Pa for p, m^2 for A and years for Y.

The projected area, A, should be an average for all lines of sight since the meteoroids can come from any direction. For simplicity, what is used in this study is the average of the projected areas along and normal to the antenna axis:

$$A = (\pi + K/2 + 5/6K)D^2/8 \quad (20)$$

For this study, MW = 18, p = 0.001 Pa, and Y = 10 years. Also, the inflatant weight was increased by one-third to account for other leaks.

7.6 Inflatant for Erecting the Torus

Combining Equations (13) and (16) with

$$p = 2St/d$$

and $V = \pi^2 d^2 D/4$ yields

$$w = \left[10.5pD^7t^2K(K^2+1)/K^2-1)E\right]^{1/3} SM/R*T \qquad (21)$$

For this study,

$p = 0.001$ Pa

$t = 0.063$ mm

$E = 5.86(10)^{10}$ Pa

$S = 2(10)^7$ PA

$MW = 44$

$R = 8314$ J/kmol K

$T = 270$K

and $\rho = 933$ kg/m^3

7.7 Inflation System Hardware

The inflation system consists of that previously shown in Figure 9 plus an operating pressure sensor and control logic. Erection signals and wiring will be charged to the electronic system (feed and power supply).

Water has insignificant pressure (100-200 Pa). The water required to yield the paraboloid will be contained in an aluminum sphere having a wall thickness of 0.76 mm. An additional 20 percent of metal is added for support hardware, 10 percent is added for valves and tubing, and 10 percent is added for contingency. Therefore, these items weigh 45% of the basic sphere.

The material in this sphere has a volume of:

$$V = \pi d^2 t$$

The sphere diameter is:

$$d^3 = 6V_{H_2O}/\pi$$

Therefore, the total metal volume in the sphere, support hardware, valves, tubing and contingency is:

$$V = 4.84tV_{H_2O}^{2/3} \qquad (22)$$

V_{H_2O} is obtained from Equations (17) and (18).

Bottle weight is the product of V of Equation (22) and the density of aluminum, 2770 kg/m^3.

The water needed to maintain pressure will also be held in an aluminum sphere. The volume of aluminum is that of equation (22) with V_{H_2O} coming from Equations (18), (19) and (20). Weight is obtained by multiplying volume by density (of 2770 kg/m^3 for aluminum).

The bottle holding the CO_2 will be a steel cylinder with an internal piston. Based upon prior L'Garde work, the weight of this tank is:

$$w = 1.9\, w_{CO_2}^{2/3}$$

where weight is in kg. Steel volume was obtained by dividing the above weight by the density of steel, 7840 kg/m^3.

The pressure sensor is viewed as a large, thin diaphram that deflects under the low pressure. This and other contingent items weigh 0.7 kg and occupy 0.00025 m^3.

7.8 Packaging Volume

In the prior sections, equations for material volume were generated. However, material volume is not packaging volume.

In L'Garde's prior work with inflatables, complex structures made of thick cloth and/or rubber could be packaged with an efficiency of 50 percent. (Packaging efficiency is defined as material volume divided by package volume.) On the other hand, thin film inflatables with a minimum of seams (such as a pillow-case configuration) can be packaged with about 90 percent efficiency.

It is believed that these antennas will be packaged with 60 percent efficiency. The efficiency will be better for large antennas (having a low seam to gore area ratio) than for small antennas -- but this is insignificant for the purposes of this study.

Most of the inflation system consists of liquid-filled spheres. For launch hardware, cylinders can be installed more efficiently. One could assess the inflation system packaging efficiency at:

$$V \text{ sphere}/V \text{ cylinder} = 4 \pi D^3/6 \pi D^3 = 2/3$$

It was decided to estimate the total antenna's packaging efficiency at 60 percent. Therefore, the material volumes derived in the previous sections were divided by 0.6 to obtain the packaging volumes previously shown in Figure 6.

8.0 SENSITIVITY TO OFF-NOMINAL CONDITIONS

The sensitivity of the configurations to changes in film elastic modulus, thickness, optical properties and antenna internal pressure was evaluated. Not considered are items such as irregular distortions and random roughness.

8.1 Mechanical Properties and Internal Pressure

For the very large antennas, where the inflation pressure is significantly stretching the antenna gores into the parabolic shape, variations in pressure, elastic modulus, or film thickness can cause shape distortions. The shape of the antenna is determined by the value of the parameter, P/Et (m^{-1}). Therefore, shape changes due to uncertainties in the value of any of these three parameters can be studied by looking at the shape variation caused by variations in η.

The L'Garde FLATE code solves for the shape of inflatable paraboloid antennas given design parameters. The case of the axisymmetric paraboloid is solved including rigorous treatment of the longitudinal and hoop stresses in the film. Furthermore, the effect of off-design values of the parameter η can be studied using FLATE.

The effects of off-design conditions will be accented by looking at an antenna at the large end of the size spectrum. For smaller antennas, the effects are less pronounced, as verified by FLATE calculations for a 15-m diameter antenna. For a 1000-meter diameter system with F/D = 1, FLATE results for the blur circle radius are presented in Figure 39.

The blur circle is computed using classical geometric optics. FLATE performs ray tracing sufficient to obtain the energy density across the focal plane of a uniformily illuminated antenna. The blur circle radius (R) is that radius where the spot intensity has fallen to one-half of its maximum (center) value. FLATE can find these data both at the nominal antenna focal plane and also at the "best fit" new focal plane after the antenna has been distorted.

The data in Figure 39 show the blur circle radius as a function of the design parameter, η. The effects are more pronounced for values of η greater than the nominal. The range of the curves here show the effect of pressures, elastic moduli, or film thicknesses off by as much as a factor of ten from the design value. The maximum case creates a blur circle radius of about 580 mm. If the antenna is refocused by moving the feed or receiver to the best new focal plane,

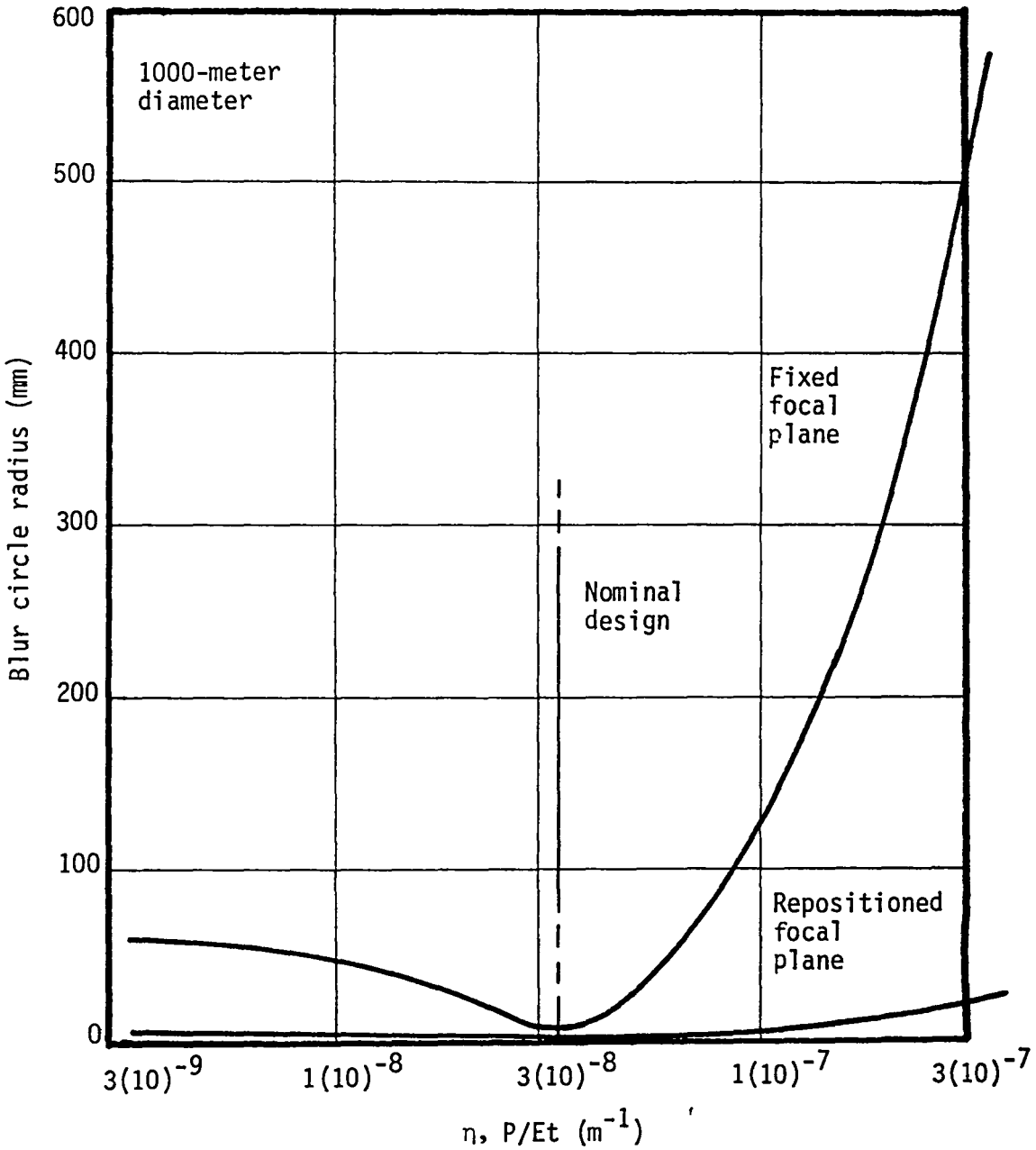

Figure 39. - Classical optics blur circle due to paraboloid shape change (1000 m diameter).

the blur circle error drops to the lower curve in Figure 39. The movement of the focal plane is also given approximately by the upper curve in Figure 39 for F/D = 1.

For a uniformily-illuminated circular aperture, the half-power beam width, θ_H, per Reference 11 is given by

$$\theta_H = 1.028\lambda/D$$

The fall off in energy given above is a result of the coherent wave nature of the radiation and cannot be substantially improved by variation of antenna design. The radius of the blur circle pattern for a F/D = 1 antenna is then given by

$$R = D\theta_H = 1.028\lambda$$

Thus a "perfect" antenna would have a blur circle radius about equal to λ. Blur circles of this same order caused by antenna distortion would not significantly affect gain. In other words, with no readjustment of the focal plane, the 1000-m diameter antenna with the maximum distortion as computed above, will operate with negligible gain loss for λ greater than 580 mm. With readjustment of the focal plane, this antenna will show no degradation for λ greater than 23 mm.

Since the Figure 39 curve is unsymmetrical, an alternate approach to readjusting the focal plane would be to operate the antenna at a lower nominal pressure. The required tolerances on P/Et for various operating wavelengths can be determined from the curve:

Wavelength (cm)	Allowable Change in P/Et
1	±20%
2	±35%
3	±50%
4	±65%
5	±75%
6	±90%

Therefore, if P/Et can be held to ±20%, a one-centimeter wavelength, 1000 meter diameter antenna is feasible. A ± 65% variation in P/Et is allowable for a four-centimeter wave, 1000-meter diameter antenna. For smaller antennas, variations in P/Et are of little importance for centimeter wave antennas.

8.2 Thermal

Figure 40 shows the effect of changing solar absorptivity (α_s) and external emissivity (ε_e) for an antenna having an internal emissivity and an f/D ratio of one. The antenna is sunlit along its axis, and all energy exchange is by radiation.

The curves show that both emissivity and solar absorptivity should be low for minimum temperature differences across the collector. If the design values for both these parameters were 0.1, Figure 40 shows that maximum temperature differential is 19K. If emissivity and solar absorptivity double (to 0.2) for any reason, the maximum temperature difference increases to 28K, only a 50% increase.

Unfortunately, the effect of temperature differences on the shape of the paraboloid could not be determined within the scope of this study. Therefore, it is unknown whether such variations are significant.

The effect of temperature differences between one side of the cone and the other can be calculated reasonably well; however, Figure 41 shows the case that was evaluated. The material on the left side of the cone is hotter than that on the right side. It therefore becomes longer and the feed (apex) moves off axis.

The geometry works out such that

$$y/D = K_t(\Delta T)(4f/D+D/4f)^2/8$$

where ΔT = Temperature difference between hot and cold sides or cone

Figure 40 showed that temperature differences can be as high as 45K. For a polyester thermal expansion coefficient of $17(10)^{-6}K^{-1}$:

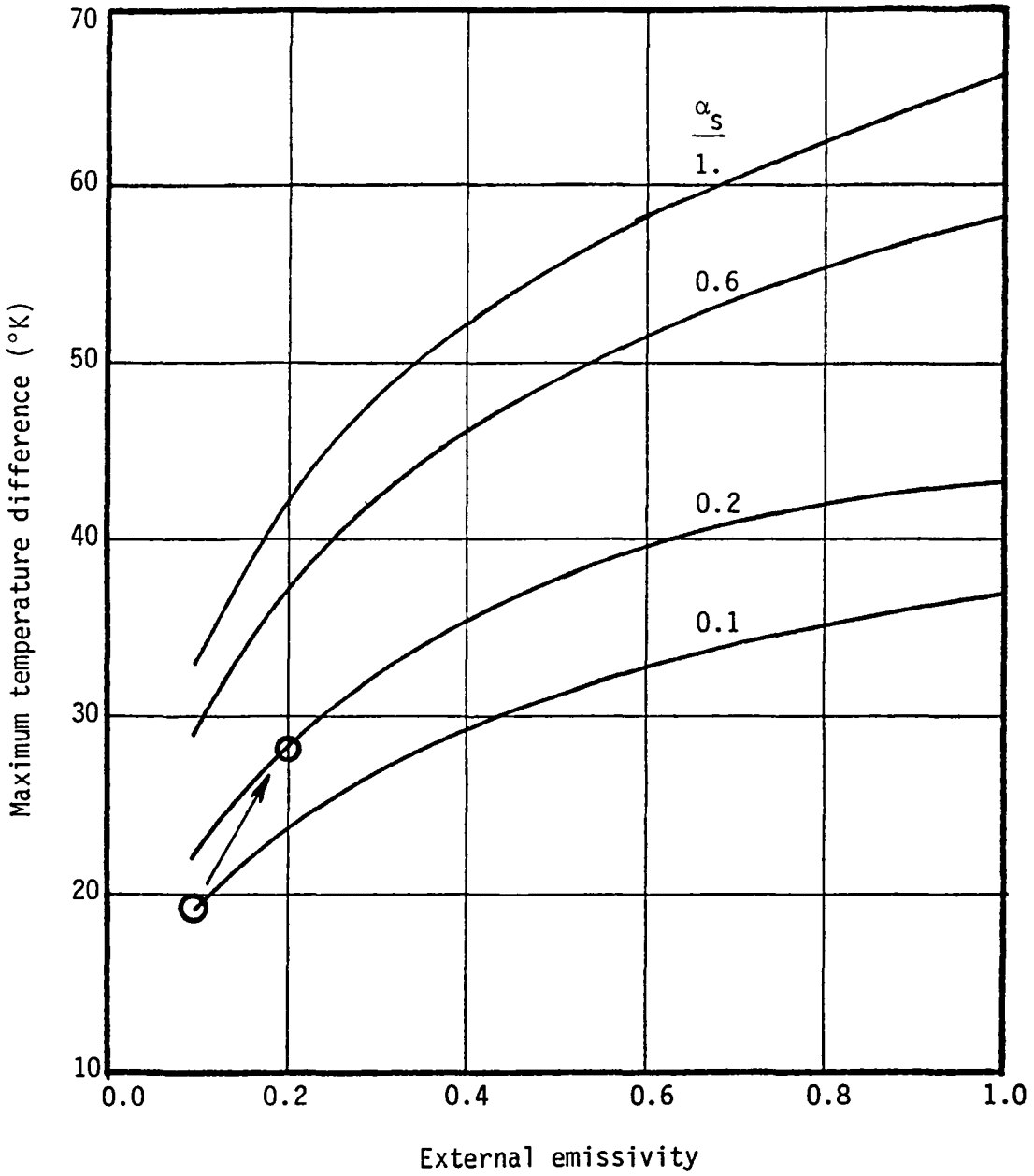

Figure 40. - Effect of changing thin film optical properties (internal emissivity = 1).

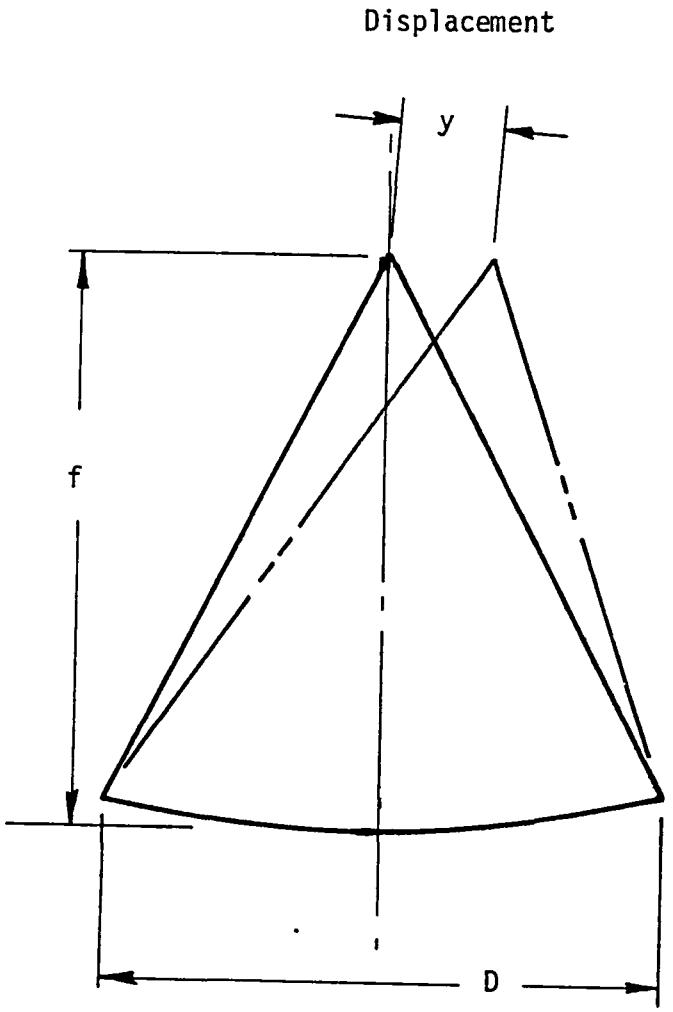

Figure 41. - Displacement of feed location due to broadside sun.

Diameter (m)	Maximum Feed Displacement (m) for f/D = 0.5	0.75	1.0
10	0.01	0.01	0.2
100	0.06	0.11	0.17
1000	0.60	1.1	1.7

For most antenna designs, differential temperatures on the cone will not be of concern because as the focal point moves, the feed dimensions are large compared to the displacement -- except for cases of large f/D.

REFERENCES

1. Wendt, A. J. and Surber, L. D., "Unfurlable Antennas", Transactions of the Third Aerospace Expandable and Modular Structures Conference, AFAPL TR-68-17, May 16-18, 1967.

2. Thomas, M. and Friese, G., "Pressurized Antennas for Space Radars", Paper No. 80-19280CP from AIAA Sensor Systems for the 80's Conference, AIAA Publication CP807, December 1980.

3. Sweet, George E., An Experimental and Analytical Investigation of Balloon-Type Enclosures for Thermal Control of Satellites, NASA TN D-5230, June 1969.

4. Hughes News Release "Science/Scope", Aviation Week & Space Technology, February 18, 1980, p. 70.

5. Freeland, R. E., Industry Capability for Large Space Antenna Structures, Report 710-12, Jet Propulsion Laboratory, May 25, 1978.

6. Investigation of a 15-KW Solar Dynamic Power System for Space Application, Contract AF-33(615)-7128, Sunstrand Aviation-Denver, Report Number AFAPL TR-64-156, February 28, 1965.

7. Shanley, F. R., Strength of Materials, McGraw-Hill, 1957.

8. "Buckling of Thin-Walled Circular Cylinders", NASA SP-8007, August 1968.

9. Aluminum Standards and Data, The Aluminum Association, Inc., March 1979.

10. Roark, Raymond J., Formulas for Stress and Strain, McGraw-Hill Book Company, 1954.

11. Microwave Performance Characterization of Large Space Antenna, edited by D. A. Bathker, Jet Propulsion Laboratory Report 77-21, May 1977, p. 4-5.

1 Report No	2 Government Accession No	3. Recipient's Catalog No
NASA CR-166060		

4 Title and Subtitle	5 Report Date
INITIAL '80s DEVELOPMENT OF INFLATED ANTENNAS	January 1983
	6 Performing Organization Code

7 Author(s)	8 Performing Organization Report No
G. J. Friese, G. D. Bilyeu, and M. Thomas	LTR-82-GF-107
	10 Work Unit No

9 Performing Organization Name and Address	11 Contract or Grant No
L'Garde, Inc. 1555 Placentia Avenue Newport Beach, California 92663	NAS1-16663
	13 Type of Report and Period Covered
12 Sponsoring Agency Name and Address	Contractor Report
National Aeronautics and Space Administration Washington, DC 20546	14 Sponsoring Agency Code

15 Supplementary Notes

Langley Technical Monitor: William Hinson
Final Report

16 Abstract

The purpose of this work was the definition and documentation of a thin membrane surface suitable for use in an inflatable space antenna concept.

A three-meter diameter paraboloid was fabricated from 0.006 mm polyester. Its inaccuracy with respect to a perfect paraboloid was measured with the aid of a laser test system at 0.76 mm RMS. A similar paraboloid was constructed from 0.008 mm polyimide; inaccuracy was 1.6 mm RMS.

Laboratory tests were conducted to determine the buckling strength of a self-rigidizing structural element made of a foil-plastic-foil laminate. The cylinders were stronger than that predicted by semi-empirical theory. This self-rigidizing approach appears practical for use in inflated antennas.

Weight and package volume calculations showed that the inflated antenna were lighter and much smaller than competitive mechanical systems. The inflated antenna accuracy was also found to be relatively insensitive to off-nominal conditions.

This effort indicates that large inflated antenna can be built for operation at wavelengths of 1 cm or greater.

17 Key Words (Suggested by Author(s))	18 Distribution Statement
Inflatable Antenna Concept Surface Accuracy Thin Membranes Rigidized Structural Cylinder	Unclassified - Unlimited Subject Category 18

19 Security Classif (of this report)	20 Security Classif (of this page)	21 No of Pages	22 Price
Unclassified	Unclassified	105	A06

For sale by the National Technical Information Service, Springfield, Virginia 22161